Aus dem Institut für Anatomie und Zellbiologie
Geschäftsführender Direktor: Prof. Dr. Ralf Kinscherf
Abteilung Medizinische Zellbiologie
des Fachbereichs Medizin der Philipps-Universität Marburg

Effects of novelly synthesized nucleolipides on different tumor cell lines (HT29, HepG2, Panc-1, RenCa) with special respect to glioma cell lines (BT4Ca, GOS3, G28, G112, U251, U87) of human or other species

Inaugural-Dissertation zur Erlangung des
akademischen Doktorgrades der Naturwissenschaften
dem Fachbereich Medizin der Philipps-Universität Marburg
vorgelegt von

Katharina Hammerbacher aus New Bern, N.C., USA

Marburg, November 2020

Angenommen vom Fachbereich Medizin
der Philipps-Universität Marburg
am: 17.03.2020

Gedruckt mit Genehmigung des Fachbereichs
Medizin

Dekan: Herr Prof. Dr. H. Schäfer

Referent: Herr Prof. Dr. R. Kinscherf

1. Korreferent: Herr PD Dr. M. Wanzel

Phantasie ist wichtiger als Wissen,
denn Wissen ist begrenzt.

Albert Einstein

Foreword and acknowledgments

This dissertation originates from the cooperation of the working groups of:

apl. Prof. Dr. Rosemeyer, Institute of Chemistry and Materials, University of Osnabrück and

Prof. Dr. Kinscherf, Institute of Anatomy and Cell Biology, University of Marburg.

Based on the former dissertations of Dr. Anisa Farhat "Überprüfung des Drug Delivery Konzepts von „Lipid-Nucleosid- und Polysaccharid-Konjugaten von 5-Fluorouracil"(2016) and Dr. Christine Knies "Nucleolipide: Synthese und Bio-medizinische Aspekte"(2017), this study perpetuates and expands the research of my master thesis "Cytotoxic/cytostatic effects of novel nucleolipides of uridine, 5-Methyluridine and Inosine with O-2', 3'-ketalic lipidgroups and/or N(3)/N(1)-positioned prenylgroups (terpenoids) on human glioma (GOS3) and rat glioma (BT4Ca) cells" (2015) and is supported by the Bachelor thesis of Katharina Görtemaker „Synthese und cancerostatische in-vitro-Aktivität neuer Nucleosid-O-2',3'-Ketale" (2017) and bachelor thesis of Vanessa Schneider "Zytotoxische und Zytostatische Effekte neuer Guanosin-Nukleolipide auf humane Gliomzellen (GOS3), Ratten Gliomzellen (BT4Ca) und humane PMA-differenzierte Makrophagen (THP1)" (2018) .

The presented data are also partly published in:

1. Knies C, Bonaterra GA, **Hammerbacher K**, Cordes A, Kinscherf R, Rosemeyer H. (2015a). Ameliorated or Acquired Cytostatic/Cytotoxic Properties of Nucleosides by Lipophilization. Chemistry & Biodiversity 12(12):1902–1944.

2. Knies C, **Hammerbacher K**, Bonaterra GA, Kinscherf R, Rosemeyer H. (2015b). Nucleolipids of Canonical Purine ß-d-Ribo-Nucleosides: Synthesis and Cytostatic/Cytotoxic Activities toward Human and Rat Glioblastoma Cells. ChemistryOpen 5 (2):129-141.

3. Knies C, **Hammerbacher K**, Bonaterra GA, Kinscherf R, Rosemeyer H. (2016). Novel Nucleolipids of Pyrimidine β-D-Ribonucleosides: Combinatorial Synthesis, Spectroscopic Characterization, and Cytostatic/Cytotoxic Activities. Chemistry & Biodiversity 13(2):160-80.

4. **Hammerbacher K**, Görtemaker K, Knies C, Bender E, Bonaterra GA, Rosemeyer H, Kinscherf R. (2018). Combinatorial Synthesis of New Pyrimidine- and Purine-ß-D-Ribonucleoside Nucleolipids: Their Distribution Between Aqueous and Organic Phases and Their in vitro Activity Against Human- and Rat Glioblastoma Cells in vitro. Chem Biodivers. 2018 Jun 21. doi: 10.1002/cbdv.201800173; PMID: 29928783

5. Knies C, Reuter H, **Hammerbacher K**, Bender E, Bonaterra GA, Kinscherf R, Rosemeyer H. (2018). Synthesis of New Potential Lipophilic Co-Drugs of 2-Chloro-2'-deoxyadenosine (Cladribine, 2CdA, Mavenclad®, Leustatin®) and 6-Azauridine (z6U) with Valproic Acid. Chem Biodivers. 2018 Dec 21. doi: 10.1002/cbdv.201800497; PMID: 30614625

6. Rosemeyer H, Knies C, **Hammerbacher K**, Bender E, Bonaterra GA, Hannen R, Bartsch JW, Nimsky C, Kinscherf R. (2019). Nucleolipids of the Nucleoside Antibiotics Formycin A and B: Synthesis and Biomedical Characterization particularly using Glioblastoma Cells. Chem Biodivers Volume16, Issue4 April 2019. doi: 10.1002/cbdv.201900012; PMID: 30773842

7. Reuter H, Van Bodegraven A.M, Bender E, Knies C, Diek N, Beginn U, **Hammerbacher K**, Schneider V, Kinscherf R, Bonaterra GA, Svajda R, Rosemeyer H. (2019). Guanosine Nucleolipids: Synthesis, Characterization, Aggregation and X-Ray Crystallographic Identification of Electricity-Conducting G-ribbons. Chem Biodivers. 2019 Feb. 22. doi: 10.1002/cbdv.201900024; PMID: 30793846

Table of contents

List of abbreviations

5-FU	5-Fluorouracil
5-FUrd	5-Fluoruridine
Ab	Antibody
Act. Casp. 3	Active Caspase 3
BCA	bicinchoninic acid
Campto.	Camptothecin
DCF	2', 7' –dichlorofluorescein
DCFDA	2', 7' –dichlorofluorescin diacetate
DMSO	Dimethyl sulfoxide
dTMP	desoxythymidine monophosphate
dUMP	desoxyuridine monophosphate
dUTP	desoxyuridine triphosphate
FdUMP	fluorodesoxyuridine monophosphate
FdUTP	fluorodesoxyuridine triphosphate
FUMP	fluorouridine monophosphate
FUTP	fluorouridine triphosphate
Mϕ	Macrophage
NL	Nucelolipid
PI	Propidium iodine
PMA	Phorbol 12-myristate 13-acetate
Red. GSH	Reduced glutathione
ROS	Reactive oxygen species
rpm	Revolutions per minute
S.	Substance
SDS	Sodium dodecyl sulfate
sec. Ab.	secondary Antibody
SEM	*Standard Error of the Mean*
SRB	Sulforhodamine B
SSA	5-Sulfosalicylic Acid
TAM	Tumor-associated Macrophage
TCA	Trichloracetic acid
TE	Trypsin-EDTA
Tris	tris(hyrdoxymethyl)-aminoethane
Via.	Viability

List of figures

List of tables

1. Introduction

Cancer is an uneven swelling, rough, unseemly, darkish, painful, and sometimes without ulceration…and if operated upon, it becomes worse…and spreads by erosion; forming in most parts of the body, but more especially in the female uterus and breasts. It has the veins stretched on all sides as the animal the crab (cancer) has its feet, whence it derives its name.

Paul of Aegina, o.D. (c. 625 – c. 690)

The Seven Books of Paulus Aegineta

1.1. Cancer statistics

Since the description of cancer by Paulus Aegineta 1300 years have passed. Throughout the centuries cancer has been of interest for many scientists (Ritu Lakhtakia, 2014). Due to the enormous expansion of knowledge over the time periods we now know much more about this type of disease. However, despite the huge medical and technical development, cancer is the second leading cause of death worldwide. For 2018 the International Agency for Research in Cancer (IARC) estimated a rise of the global cancer burden to 18.1 million cases and 9.6 million cancer deaths (Fig. 1).

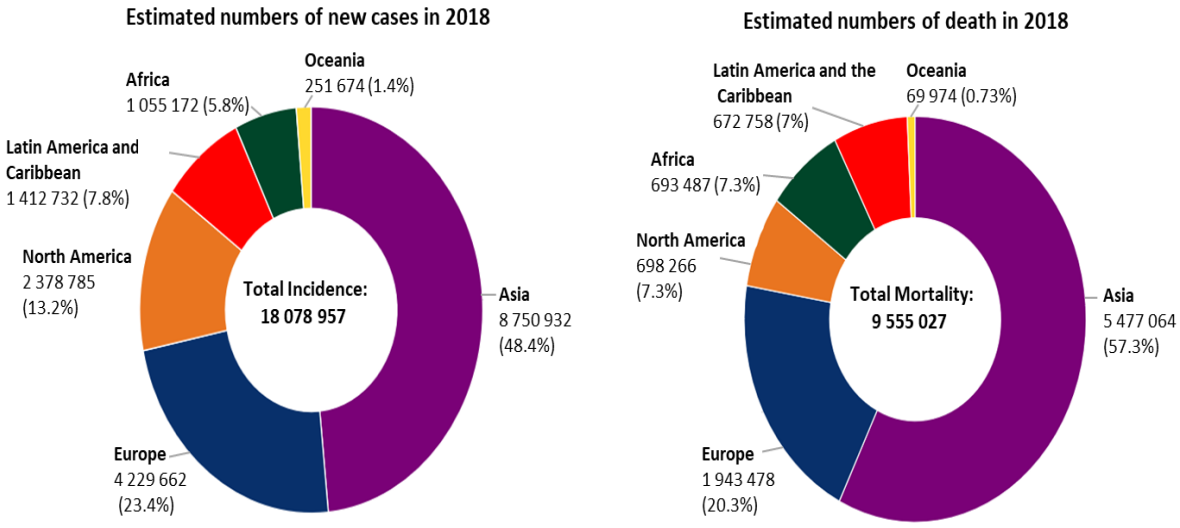

Figure 1: Estimated number of new cases and cancer deaths worldwide in 2018.
Statistics include all cancers, both sexes, all ages.
Data source: GLOBOCAN 2018; Graph production: Global Cancer Observatory (http://gco.iarc.fr/)

Both, cancer incidence and mortality rapidly forced up over the last decades. Today about 1 in 6 deaths is attributed to cancer (WHO, 2018). The reasons for this increase are diverse: the aging and growth of the population as well as the distribution of the main risk factors certainly contribute to this progression (Bray et al., 2018). In 2018, nearly 50 % of all cancer cases and over 50 % of the cancer deaths occurred in Asia (Fig.1). The fact that close to 60 % of the global population resides there, explains this phenomenon in part.

However, Europe only harbors 9 % of the global population and in return accounts for 23.4 % of the total cancer cases and 20.3 % of the total cancer deaths (Bray et al., 2018). Due to this numbers it is obvious that suffering of cancer is not only a statistical probability. The risk factors for developing cancer are versatile. 25 % of cancer cases in low- and middle-income countries are caused by infections, such as hepatitis and human papilloma virus (HPV). Tobacco or alcohol use as well as an unhealthy diet and physical inactivity are not only flashpoints for noncommunicable diseases, but also major cancer risk factors. Around 33 % of cancer deaths are due to the five leading behavioral and dietary risks: high body mass index, low fruit and vegetable intake, lack of physical activity, tobacco and/or alcohol abuse (WHO, 2018).

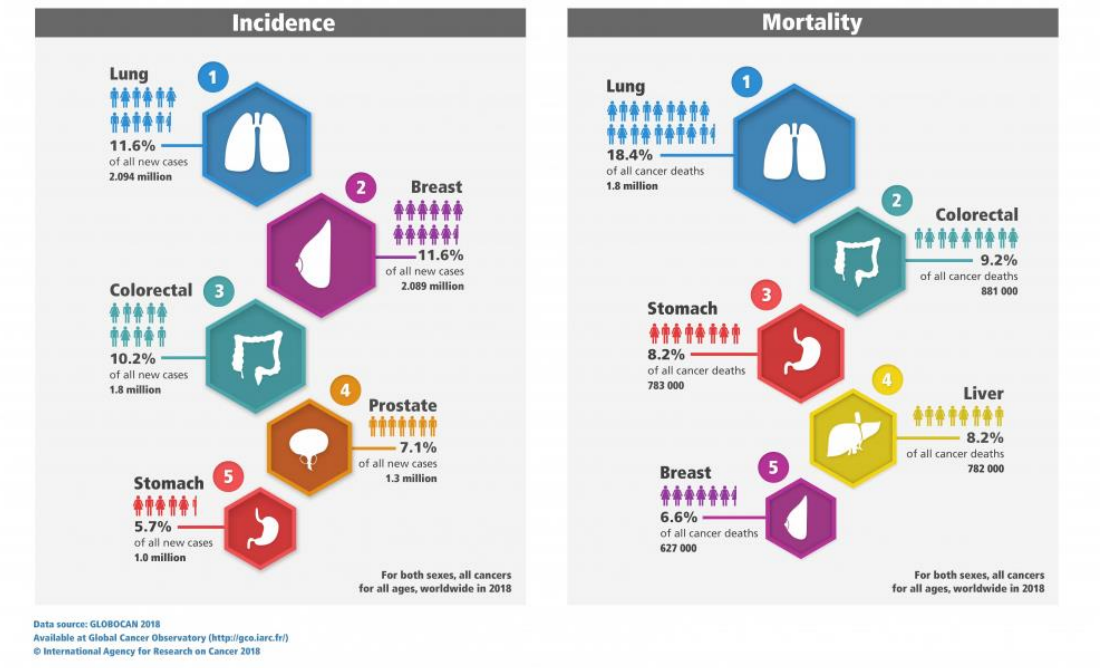

Figure 2: The five most commonly diagnosed cancer types worldwide in 2018.
Statistics include all cancers, both sexes all ages.
Data source: GLOBOCAN 2018; Available at Global Cancer Observatory (http://gco.iarc.fr/)
© International Agency for Research on Cancer 2018.

Tobacco abuse is responsible for approximately 22 % of cancer deaths and thus the most important risk factor for cancer. So it is not astonishing, that lung cancer is the most prominent cancer type among adults (Fig. 2). In 2018 the five most commonly diagnosed cancer types were lung cancer (11.6 %) closely followed by breast cancer (11.6 %), colorectal (10.2 %), prostate (7.1 %) and gastric cancer (5.7 %) (Fig.2). The most lethal cancer types among adults were lung (18.4 %), colorectal (9.2 %), gastric (8.2 %), hepatic (8.2 %) and breast cancer (6.2 %) (Fig.2).

Although tumors of the brain and the nervous system are rather unusual among adults (2 %) (GLOBOCAN 2018), they are the second most common diagnosed types of cancer in childhood. After leukemia (28.6 %), tumors of the brain and nervous system are on second place (11 %), followed by non-Hodgkin lymphoma (8.4 %), Hodgkin lymphoma (5.1 %) and renal disease (4.7 %) (Fig.3).

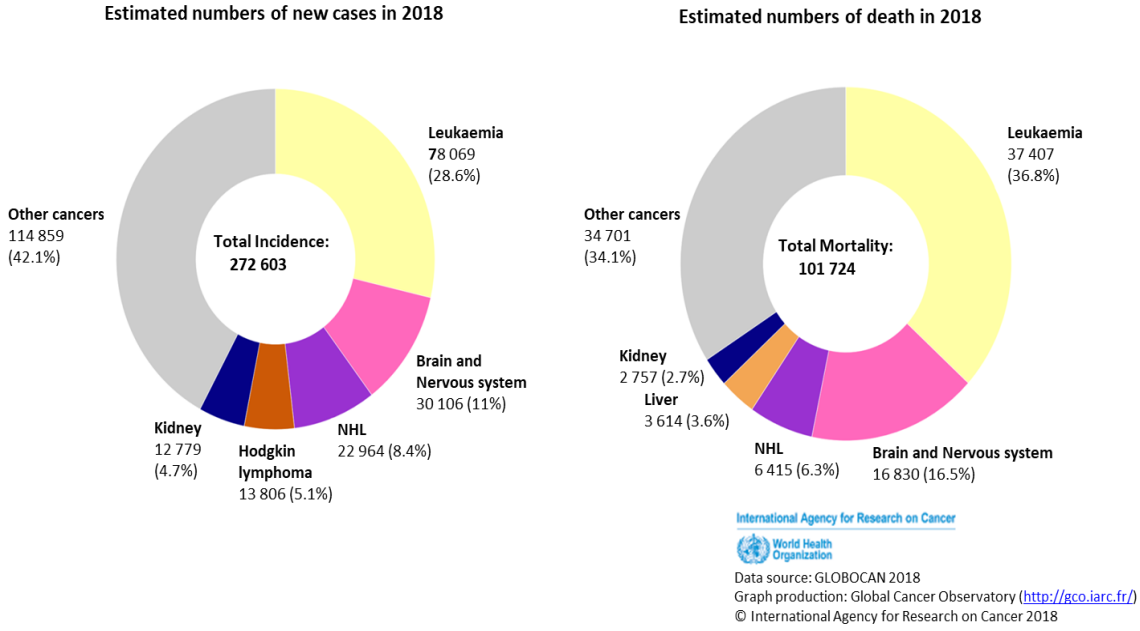

Figure 3: Estimated number of new cases and cancer deaths worldwide in 2018.
Statistics include all cancers, both sexes, ages <19 years.
Data source: GLOBOCAN 2018; Graph production: Global Cancer Observatory (http://gco.iarc.fr/)
© International Agency for Research on Cancer 2018.

In the central nervous system (CNS) meningioma and gliomas are the most frequent types of brain tumors and account for 30 % of all brain and central nervous tumors and 80 % of all malignant intracranial tumors (Goodenberger & Jenkins RB, 2012). Gliomas are further categorized by their cell origin like astrocytes or oligodendrocytes. Additionally, the World Health Organization defines four grades of classified tumors by

their proliferation, migration and invasion behavior (Vigneswaran et al., 2015). They differentiate among:

- Grade I, bordered tumors
- Grade II, tumors which diffusely infiltrate surrounding tissue, but with no or just low mitosis and necrosis such as astrocytomas or oligodendrogliomas
- Grade III, highly infiltrating tumors with increased mitotic activity but no necrosis or vascular proliferation like anaplastic-astrocytomas/oligodendrogliomas
- and Grade IV, infiltrating tumors with necrosis and micro-vascular proliferation as well as a high rate of mitosis, called glioblastomas (Taal, Bromberg & Van den Bent, 2015, Fig. 4)

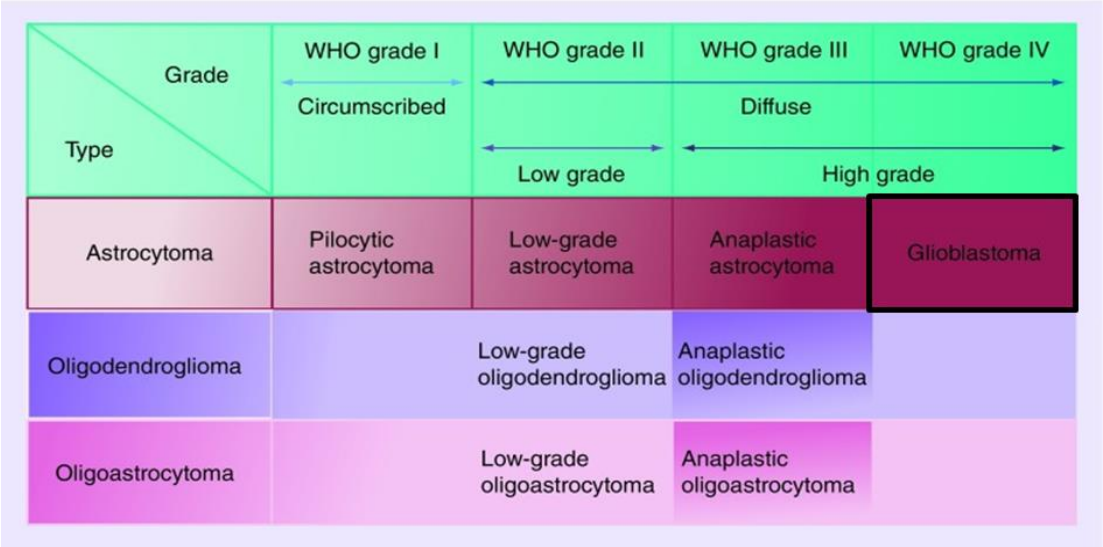

Figure 4: Categorization of gliomas.
(Taal, Bromberg & Van den Bent, 2015 [modified])

1.2. Cancer treatment

By now a lot of new therapy approaches, so-called targeted therapies (Krebsgesellschaft, 2019), have been developed but the surgical intervention, radio- and chemotherapy are still standard methods. For superficial or well-delimited cancer types like skin- or breast cancer, the surgical excision is the first method of choice. Though, in a lot of cases the tumorous tissue is not very well differentiated and a complete elimination rarely successful. Especially for gliomas, a surgical excision is, through the mainly intracranial location, extremely risky. However, there are often remaining cancer cells,

which can lead, due to their fast and invasive growing behavior (grade IV, Fig.4), to a rapid recrudescence. Therefore, radio-, chemotherapy or a combination of both following upon excision are frequently used (Krebsgesellschaft, 2019).

1.2.1. 5-Fluorouracil

Antimetabolites represent a large group of anticancer agents that structurally are similar as natural molecules, but differ enough to interfere with their metabolism.
1954 Rutman et al. described that rat hepatoma cells incorporated uracil more actively than the normal liver cells for nucleic acid pyrimidine biosynthesis (Rutman et al., 1954). These observations led to an idea, how tumor cells can be influenced by their nuleic acid biosynthesis. In the 1950's Heidelberger et al. developed a pyrimidine analog based on uracil. The name of the antimetabolite 5-Fluorouracil (5-FU) indicates that instead of the usual hydrogen atom at C5-position a fluorine atom is bound (Heidelberger et al., 1957) (Fig.4).

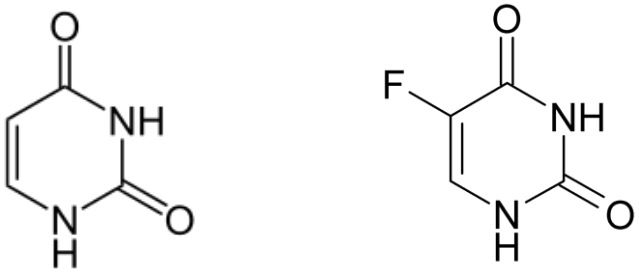

Uracil 5-Fluorouracil

Figure 5: Constitutional formula of uracil and 5-Fluorouracil (5-FU).

The following years different scientific groups (Bosch et al., 1958; Chaudhuri et al., 1958; Dannberg et al. 1958) tried to figure out, what the cellular mechanism behind the effect of 5-FU is. Today it is known that the cells take up 5-FU to synthesize several active metabolites (Weiss et al., 2014; Fig. 5), e.g. fluorodesoxyuridine monophosphate (FdUMP), fluorodesoxyuridine triphosphat (FdUTP) as well as fluorouridine triphosphat (FUTP) (Longley et al. 2003).

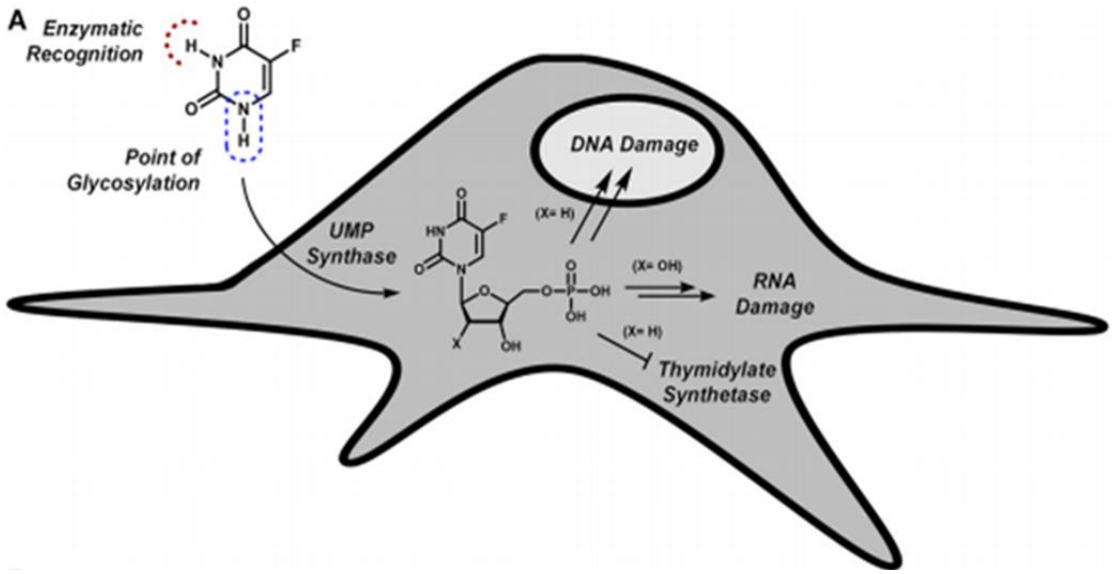

Figure 6: Intracellular bio-functionalization of 5-FU to generate cytotoxic metabolites
(Weiss et al. 2014[modified]).

FdUMP and FUMP are then used as basic components and integrated into the DNA or RNA (Marin-Vicente et al., 2013). In addition, the synthesized FdUMP together with 10-methylentetrahydrofolate (CH_2THF) bind the thymidylate synthase, causing an irreversible inhibition. This leads to an interruption of the synthesis of deoxythymidine monophosphate (dTMP) out of deoxyuridine monophosphate (dUMP) (Grogan et al. 2011). Due to this blocked synthesis of dTMPs, the sensible balance of deoxynucleotides is disturbed.

Auxiliary, due to the inhibition of the thymidylate synthase an accumulation of dUTP within the cells occurs (Aherne et al., 1996). The hoarded dUTPs and the affiliated FdUTPs are then spuriously used as component for the assembly of the double-strand DNA, causing severe damage to the DNA. The emerging strand breaks and the incorrect DNA synthesis lead to an activation of the uracil-DNA-glycosylase (Lindahl, 1974). This enzyme in turn tries to rescue the wrong assembled DNA strand by removing the dUTPs or FdUTPs. But, due to the imbalance of desoxynucleotides, DNA repair mechanisms are also faulty (Longley et al., 2003).

Another effect following upon 5-FU application is the integration of the 5-FU metabolite FUTP into the RNA (Pettersen et al., 2011). Thereby the functions of the transfer RNA (tRNA) and the small nuclear ribonucleic acid (snRNA), as well as the splicing of

the pre-messenger (m)RNA are remolded, resulting in an impairment of the normal RNA-function (Santi & Hardy, 1987; Patton, 1993; Doong & Dolnick, 1988).

At the end, all these effects appear to diminish cell proliferation and seem to trigger cell death (Beck et al., 1986; Kufe et al., 1981).

Although until today it is not completely clarified or precisely understood how 5-FU works, it is used for the therapy of stable tumors, like gastric adenocarcinomas, colon and breast cancer (Bodner-Adler et al., 2007; Carrato, 2006; Khosravi Shahi et al., 2007). Due to the fast degradation within the liver, the half-life of 5-FU within the blood is only a few minutes. More than 80 % of 5-FU are eliminated by the enzyme dihydropyrimidine dehydrogenase (Diasio & Harris, 1989; Cheng et al., 2012).

Unfortunately, 5-FU does not only specifically target fast proliferating cancer cells. Therefore, it carries along aggravating side effects (Lévi et al., 1998; Wettergren et al., 2012). Looking at these unpleasant side effects, there must be a consideration of the helpful effects against tumors and the consequences for the rest of the healthy cells. Thus, chemotherapeutic drugs are usually given in low dosages to keep the balance between the positive and negative outcome.

To escape this dilemma, there is always the effort to develop novel drugs with an improved effectivity. However, one crucial limiting factor of the effectiveness of such molecules, used in cases of neuroectodermal cancer, is the blood-brain barrier. This barrier is formed by astrocytes and endothelial cells, which are connected by tight junctions with an extremely high electrical resistivity of at least 0.1 Ω·m. The blood–brain barrier restricts the passage of pathogens, the diffusion of large or hydrophilic molecules into the cerebrospinal fluid, while allowing the diffusion of hydrophobic molecules (O_2, CO_2, hormones) and small polar molecules (Johansen et al., 2017). Moreover the selective transport of molecules such as glucose and amino acids, which are crucial to neural function, is regulated. Beyond that, the blood-brain barrier prevents the entry of lipophilic, potential neurotoxins by way of an active transport mechanism mediated by P-glycoprotein (Butt et al., 1990)

Beside this, other limiting factors are the resorption properties of the cells and the blood supply of the tissue. The possibilities to manipulate the last two parameters are

rather restricted. In contrast the characteristics like lipo- and water solubility or the size of chemotherapeutic drugs can be modified in different ways. Rosemeyer et al. focus on the generation of new 5-FU derivatives, which expose a better effectivity (Malecki & Rosemeyer, 2010; Rosemeyer et al., 2012; Rosemeyer & Malecki, 2012; Köstler et al., 2013; Malecki E. 2013; Malecki et al., 2013; Malecki, Viere & Rosemeyer, 2013; Malecki et al., 2014; Werz et al. 2013; Farhat et al., 2014; Knies et al., 2015a; Knies et al., 2015b; Farhat, 2016; Knies et al., 2016; Hammerbacher et al., 2018; Knies et al., 2018; Rosemeyer et al., 2019; Reuter et al., 2019). Taking a look at a model of such a uridine derivative (Fig. 7) several structural groups appear to be changeable. The basic module in the center (green) can be formed by a purine or pyrimidine structure. Beside this, there are three side groups (yellow, blue, pink) which influence the solubility of the molecule and thus contribute to an improvement of the uptake into the cell or passage through the blood brain barrier. These groups can vary in size (C-chain length), hydrophobic parts (O, OH–groups) and saturation of the C-chain (C=C).

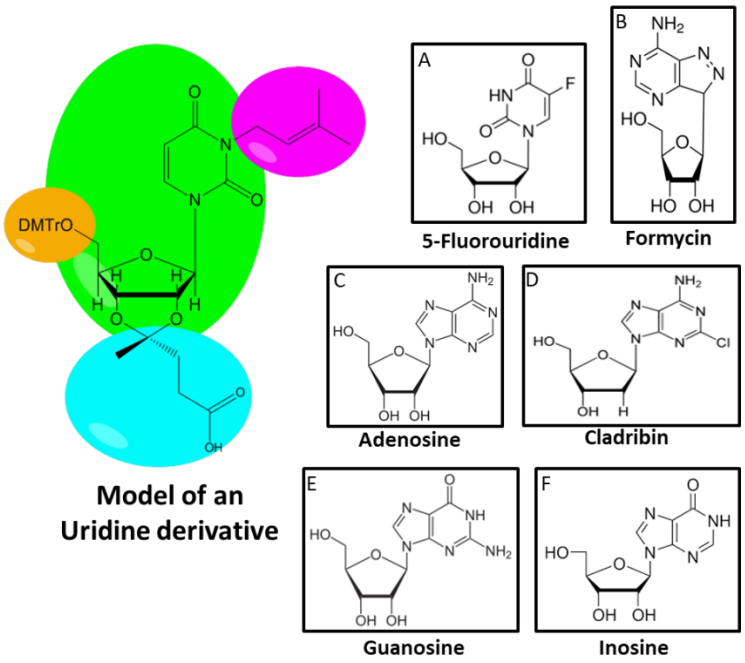

Figure 7: Basic structure of a uridine derivative.
The basic module is colored in green and the different changeable side groups are shown in blue, yellow and pink (Knies & Rosemeyer, 2015 [modified]). Beside the chemical structure of 5-FUrd (A), formycin (B), adenosine (C), cladribin (D), guanosine (E) and inosine (F) are illustrated.

For the generation of new nucleolipids the research group of Prof. Rosemeyer used 5-Fluorouridine as well as other substances like adenosine, cladribin, formycin, guanosine and inosine (Fig. 7) to synthesize more than 120 novel nucleolipids.

1.3. Aim of the thesis

In this study the cytotoxic effects of these novelly synthesized nucleolipids are analyzed, to find out whether these derivatives are more efficient for the treatment of neuronal cancer cells than 5-FUrd, a metabolite of 5-FU. 5-FU, which is one of the usually utilized chemotherapeutics, is effective on fast proliferating cancer cells. But it causes a broad range of adverse side effects in multiple organ systems. Beside this, 5-FU seems to induce neuron damage in the CNS (Han et al., 2008). To eliminate these unwanted side effects and to gain a better effectivity, Rosemeyer et al., synthesized in a cooperative project a series of modified 5-FUrd, adenosine, cladribin, formycin, guanosine and inosine derivatives (Malecki & Rosemeyer, 2010; Rosemeyer et al., 2012; Rosemeyer & Malecki, 2012; Köstler et al., 2013; Malecki E. 2013; Malecki et al., 2013; Malecki, Viere & Rosemeyer, 2013; Malecki et al., 2014; Werz et al. 2013; Farhat et al., 2014; Knies et al., 2015a; Knies et al., 2015b; Farhat, 2016; Knies et al., 2016; Hammerbacher et al., 2018; Knies et al., 2018; Rosemeyer et al., 2019; Reuter et al., 2019). These derivatives have different additional chemical side groups, which influence mainly their water and lipid solubility. By that, the permeability across the blood-brain-barrier as well as the uptake by the cells is intended to be improved.

The first part of this thesis screens the impact of the 120 novelly synthesized nucleolipids, in comparison to 5-FUrd, on the viability of rat BT4Ca and human GOS3 glioma cells used as a model for neuronal cancer cells (Graphic 1). Additionally, the occurrence of possible side effects are analyzed by using the human THP-1 derived macrophages representing tumor associated immune cells. The novelly synthesized derivatives which are not too harmful for the macrophages and reveal an increased or a similar cytostatic/cytotoxic effect compared to 5-FUrd towards both tested glioma cell lines (BT4Ca and GOS3), are examined on several other tumor entities, too (Graphic 1). The second part of the study focuses on the investigation of effects of the five most interesting derivatives and 5-FUrd. In this context, our goal is to find out, which way of cell death is related to the potentially observed cytotoxic effects and if the active derivatives have an impact on the induction of apoptosis, necrosis, oxidative stress, NFκB, proliferation and migration in the rat BT4Ca glioma cells used as a model cell line (Graphic 1). Thus, the signaling of the novelly synthesized nucleolipids (and 5-FU) is even more precisely specified. Finally, we intend to identify derivatives with the potential to combat cancer, at best more efficient than conventional chemotherapeutics like 5-FU.

1.4. Schematic layout of the thesis

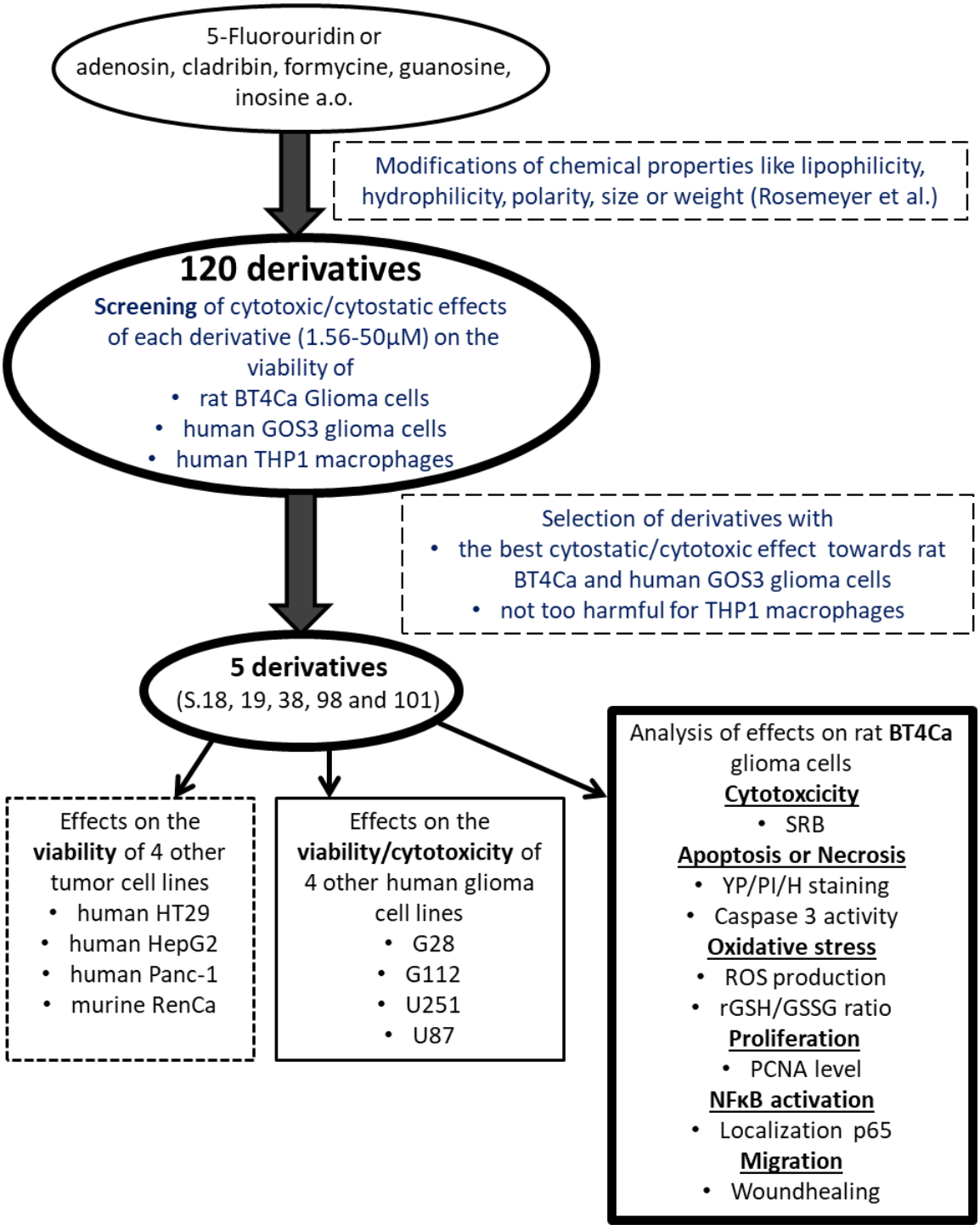

Graphic 1: Schematic layout of the thesis. The flowchart illustrates the work process of the thesis.

2. Material

2.1. Instruments/Equipment

Instruments	Producer
Autoklav Heratherm Oven OMS 100	Fisher Scientific GmbH, Schwerte
AxioCam MRm Camera	Carl Zeiss AG, Oberkochen Germany
Centrifuge Perfect Spin P	PEQLAB Biotechnologie GmbH, Erlangen, Germany
Centrifuge Pico 17	Heraeus Holding GmbH, Hanau, Germany
Camera AxioCam MRc	Carl Zeiss AG, Oberkochen Germany
Confocal laser scanning microscope Nikon Eclipse Ti	Nikon GmbH, Geschäftsbereich Mikroskope Düsseldorf Germany
Cytation™ 3 microplate reader	BioTek Instruments, Inc., headquartered in Winooski, VT, USA.
Fusion-SL 3500.WL Imaging System	PEQLAB Biotechnologie GmBH, Erlangen, Germany
Ice-Crasher Scotsman AF103	Kaelte-kameath GmbH & Co.KG, Linden, Germany.
Incubator B 5042	Heraeus Holding GmbH, Hanau, Germany
Kern KB 3600-2N Precision balance 0,01 g : 3600 g	Kern & Sohn GmbH, Balingen, Germany
Multipette® plus	Eppendorf AG, Hamburg, Germany
Nikon Eclipse TS100 Inverted Microscope	Nikon GmbH, Düsseldorf, Germany
Pipetman Classic™ P10, P20, P100, P200, P1000	Gilson Inc., Middleton, USA
PowerEase® 500 Power Supply	Invitrogen, Eugene, USA
Promax 1020 Shaker	Heidolph Instruments GmbH & Co. KG, Schwabach, Germany
Sunrise microplate reader	Tecan Group Ltd; Männedorf, Switzerland
Thermoshaker PHMT-PSC-18	Grant Instruments Ltd., Cambridge, UK
Ultrasonic bath Sonorex	BANDELIN electronic GmbH & Co. KG, Berlin, Germany
Ultrospec III, UV Visible Spectrophotometer	Pharmacia Biotech Inc. Massachusetts, USA
Vortexer MS 3	IKA®-Werke GmbH & CO. KG, Staufen, Germany
Zeiss Axiovert 135 (inverted epiflourescence microscope)	Carl Zeiss AG, Oberkochen, Germany

Table 1: List of instruments

2.2. Consumption items

Material	Company
6-well tissue culture plate	Bectin Dickinson Labware, Franklin Lakes, USA
96- well- plate (cell culture)	BD Falcon™, Becton Dickinson GmbH, Heidelberg, Germany
C-Chip DHC-N01	Digital Bio; Hopkinton, USA
Cell Scraper 300 mm	TPP Techno Plastic Products AG, Trasadingen, Switzerland
Disposable Cuvettes 1.5 ml	BRAND GMBH + CO KG, Wertheim, Germany
Filtertips, 1-1000 µl, steril	SARSTEDT AG & Co., Nümbrecht, Germany
Filtertips, 5-10 ml	SARSTEDT AG & Co., Nümbrecht, Germany
Lumox® multiwell, 96- well plate	SARSTEDT AG & Co., Nümbrecht, Germany
Microcentrifuge Tube w/lid, 0.5 ml	BrandTech Scientific Inc., Essex, UK
Nobaglove-Nitril	NOBA Verbandmittel Danz GmbH u. Co KG, Wetter, Germany
PARAFILM® "M"	Pechiney Plastic Packing, Chicago Il., USA
Safe Seal Micro Tube, 1.5 ml und 2 ml	SARSTEDT AG & Co., Nümbrecht, Germany
TC-Flask T175 Stand.,Vent. Cap.	SARSTEDT AG & Co., Nümbrecht, Germany
TC-Flask T75 Stand.,Vent. Cap.	SARSTEDT AG & Co., Nümbrecht, Germany
Tube, 15 ml und 50 ml	SARSTEDT AG & Co., Nümbrecht, Germany

Table 2: List of consumption items

2.3. Reagents and substances

Reagents/ substances	Company
2-Amino-2-(hydroxymethyl)propane-1,3-diol (Tris) 99.9% PA	Carl Roth GmBH & Co. KG, Karlsruhe, Germany
5-Fluorouracil (F6627) 20mM	Sigma-Aldrich Co. LLC, ST. Louis, USA
5-Fluorouridine (F0636) 20mM	TCI Europe, Zwijndrecht, Belgien
5-Sulfosalicyl acide dihydrate (SSA)	Sigma-Aldrich Co. LLC, ST. Louis, USA
Camptothecin	Cayman Chemicals, Biomol GmbH

	Hamburg, Germany
CellEvent™ Caspase-3/7 Green Detection Reagent, 2mM	Invitrogen, Eugene,USA
Dimethyl sulfoxide (DMSO)	MERCK-Schuchardt, Hohenbrunn, Germany
DMEM low Glucose (1g/l)	PAA Laboratories GmBH; Pasching, Germany
Dulbecco's Modified Eagle Medium (DMEM) High Glucose (4.5g/l)	Capricorn Scientific GmbH; Ebsdorfergrund, Germany
Dulbecco's Phosphate-Buffered Saline PBS (1x) (without Ca & Mg)	Capricorn Scientific GmbH; Ebsdorfergrund, Germany
EDTA (ethylene diamine tetraacetic acid)	Thermo Scientific, Schwerte, Germany
Ethanol 70 %	AppliChem GmbH, Darmstadt Germany
Ethanol 96 %	Sigma-Aldrich Co. LLC, ST. Louis, USA
Fetal bovine serum (FBS)	Capricorn Scientific GmbH; Ebsdorfergrund, Germany
High-purity sodium chloride (NaCL > 99.8%)	Carl Roth GmBH & Co. KG, Karlsruhe, Germany
Hoechst 33342 16.2mM	Invitrogen, Eugene, USA
Hydrogen peroxide 30%	Carl Roth GmBH & Co. KG, Karlsruhe, Germany
Natriumhydroxide (NaOH)	MERCK-Schuchardt, Hohenbrunn, Germany
Penicillin/Streptomycin 100x	Capricorn Scientific GmbH; Ebsdorfergrund, Germany
Phorbol 12-myristate 13-acetate (PMA)	Sigma-Aldrich Co. LLC, ST. Louis, USA
PrestoBlue® cell viability reagent	Invitrogen, Eugene, USA
Propidium iodine 1.5mM	Invitrogen, Eugene, USA
Protease Inhibitor Cocktail (100X)	Cell Signaling Technology, Inc., Danvers, USA
Radioimmunoprecipitation assay (RIPA) Lysis Buffer, 10x	Cell Signaling Technology, Inc., Danvers, USA
RPMI 1640 medium (low glucose)	Capricorn Scientific GmbH; Ebsdorfergrund, Germany
Sulforhoadmine B sodium salt	Sigma-Aldrich Co. LLC, ST. Louis, USA
Trichloroacetic acid (TCA)>99%	Carl Roth GmBH & Co. KG, Karlsruhe Germany
tri-ethanolamine (TEA) ≥99.5%	Carl Roth GmBH & Co. KG, Karlsruhe, Germany
Triton™ X-100	Thermo Scientific, Schwerte, Germany
Trypan blue 0.4%	Sigma-Aldrich Co. LLC, ST. Louis, USA
Trypsin-EDTA (0.05 % Trypsin; 0.02 %	PAA Laboratories GmBH; Pasching, Ger-

EDTA)	many
Tween® 20	Carl Roth GmBH & Co. KG, Karlsruhe, Germany
UltraPure™ Destilled water, DNase/ RNase free	Life Technologies GmbH, Darmstadt, Germany
YO-PRO®-1 Iodide 1mM	Thermo Scientific, Schwerte, Germany

Table 3: List of reagents and substances

2.4. Buffers and solutions

Buffers/solutions	Recipe/Company
2.5 % Sulfosalicylic acid (SSA)	2.5g SSA solved in sterile a.dest. Sigma-Aldrich Co. LLC, ST. Louis, USA
Freezing Medium	Appropriate cell culture medium containing 20% DMSO
Glutathione buffer	0.1M Na_2HPO_4 * $2H_2O$; 5mM EDTA; pH 7.5
Glutathione-reductase 120units/mg protein	Sigma-Aldrich Co. LLC, ST. Louis, USA
GSH revealing solution	4.5ml SSA solved in 300ml triethanolamine (TEA)
GSH standard	0.025, 0.05, 0.1 and 0.25 nmol/ml Carl Roth GmBH & Co. KG, Karlsruhe, Germany
GSSG standard	0.025, 0.05, 0.1 and 0.25 nmol/ml Carl Roth GmBH & Co. KG, Karlsruhe, Germany
NADPH-Tetra-Natriumsalt 0.83mM	Carl Roth GmBH & Co. KG, Karlsruhe, Germany
Phosphate-buffered saline (PBS) 10 x	82g NaCl 2g KCl 15.1g Na_2HPO_4 2g KH_2PO_4 In 1l a.dest. pH 7.4
Vinyl pyridine	Sigma-Aldrich Co. LLC, ST. Louis, USA
5,5-dithio-bis-2-nitrobenzoic acid (DTNB) 3mM	Carl Roth GmBH & Co. KG, Karlsruhe, Germany

Table 4: List of buffers and solutions

2.5. Kits

Name	Components	Company
CytoSelect™ Proliferating Cell Nuclear Antigen (PCNA) ELISA Kit	Anti-PCNA Antibody Coated Plate Anti-PCNA Antibody (1000X) Secondary Antibody HRP Conjugate Assay Diluent 10 X Wash Buffer Substrate Solution	Cell Biolabs, Inc., San Diego, USA
Pierce™ BCA Protein Assay Kit	Reagent A Reagent B	Thermo Fisher Scientific Germany BV & Co KG, Braunschweig, Germany

Table 5: List of Kits

2.6. Antibodies

Antibody	Description	Catalog-number	Company	Dilution
Primary antibody				
Anti- NFκB p65	Goat polyclonal to NFκB p65	Sc-372-G	Santa Cruz Biotechnology, Inc. Bergheimer Str. 89-2, 69115 Heidelberg, Germany	1:50
Anti- PCNA				
Cy™3-conjugated Anti-Goat	Cy™3-conjugated Affin Pure Rabbit Anti-Goat polyclonal IgG	305165003	Jackson ImmunoResearch Europe Ltd. Cambridgeshire CB7 4EX | UK	1:100

Table 6: List of primary- and secondary antibodies

2.7. Software

Software / Equipment	Software	Company
Confocal laser scanning microscope Nikon Eclipse Ti	NIS-Elements AR 4.30.01 64-bit 2014	Nikon GmbH Düsseldorf, Germany
Graphical Illustration	Microsoft Excel 2013	Microsoft Corporation, Redmond, USA
Java-based image processing	Image J 1.52a	National Institutes of Health, Bethesda, USA
Light- and Fluorescence microscopic images	AxioVision Release 4.8.2	Carl Zeiss, AG, Oberkochen, Germany
Statistical Analyses	Sigma Plot 12.0	Systat Software, Inc, Chicago, USA
	Microsoft Excel 2013	Microsoft Corporation, Redmond, USA

Table 7: List of software

Characteristics and the chemical structure of the five derivatives of interest are listed. The properties of these and all other tested derivatives, shown in the supplements (see supplements page 174-195 Figs 52-96 and following table). , can be found in the dissertations of Dr. Christine Knies “Nucleolipide: Synthese und Biomedizinische Aspekte“(2017) and in Knies & Rosemeyer, 2015.

Unmodified molecule	Derivative	Code	Mw [g/mol]	log Pow	Chemical structure
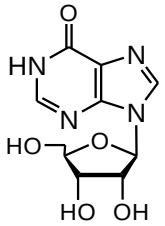 NL_6.0.0.0 Inosine	S.18	NL_6.1.[1]3.0	598.73	3.50 ± 0.74	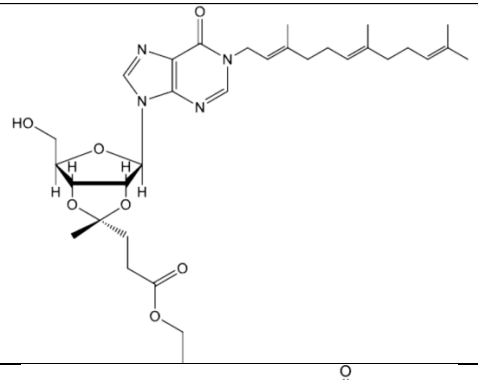
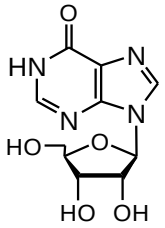 NL_6.0.0.0 Inosine	S.19	NL_6.3.0.0	532.72	5.30 ± 0.74	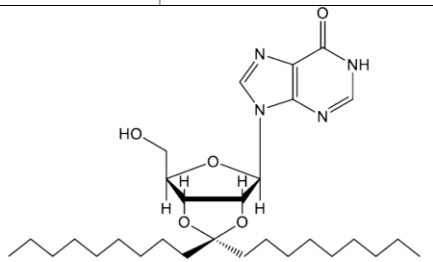

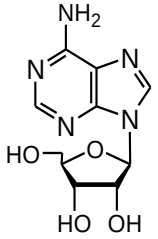 NL_5.0.0.0 Adenosine	S.38	NL_5.1.[1]3.0	598.75	-0.79 unit ± 0.74	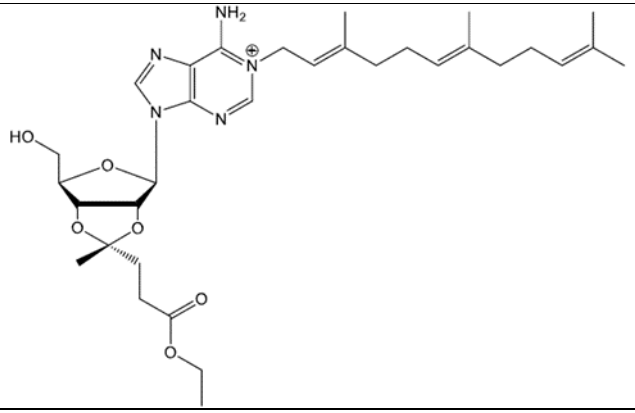
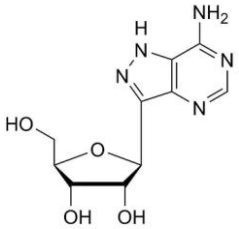 Formycin A NS_8.0.0.0	S.98	NL_8.1.[1]3.0	597.75	3.61 ± 0.74	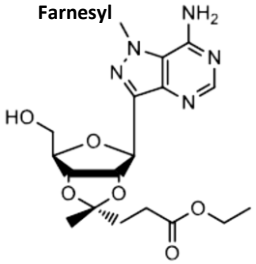
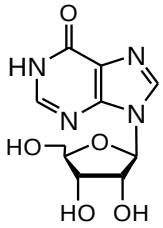 NL_6.0.0.0 Inosine	S.101	NL_6.0.3.0	472.58	2.29 ± 0.74	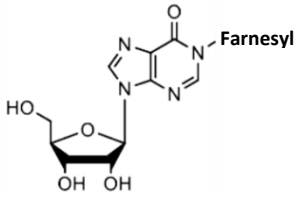

Table 8: List of derivatives/nucleolipids under test

2.8. Cell lines

2.8.1. Rat BT4Ca glioma cells

Cell line:	**BT4Ca**
Species:	Rat
Cell type:	multipolar glia-like cells
Origin:	A kind gift from Dr. N. John, Hannover Medical School. First published by Laerum et al., 1977: “fetal BD IX-rat brain cells (FBC), transferred to long-term culture after a transplacental pulse of EtNU on the 18th day of gestation, undergo neoplastic transformation in vitro ("BT-cell lines"). Tumors developed upon s.c. reimplantation of BT-cells into baby BD IX-rats”.
Histology:	neurinoma-, glioma- or glioblastoma-like, and frequently as pleiomorphic neoplasms
Biosafety level:	1
Morphology:	gliomacells, adherent cells growing as monolayer
Medium:	90% Dulbecco's MEM + 10% h.i. FBS + P/S
Incubation:	at 37 °C with 5% CO_2
Doubling time:	ca. 12 hours
Harvest:	at saturation density
Storage:	frozen with 70% medium, 20% FBS, 10% DMSO

Source: (Laerum et al., 1977)

2.8.2. Human GOS-3 glioma cells

Cell Line:	**GOS-3**
DSMZ no.:	ACC 408
Species:	human (*Homo sapiens*)
Cell type:	glioma (derivative of U-343-MG)
Origin:	originally described as a glioma cell line established from the tumor material of brain from a 55-year-old man with a mixed astro-oligodendroglioma (grade II/III); however, DNA fingerprinting at DSMZ showed clearly that this cell line is in reality a derivative of the human glioma cell line U-343-MG; described to express neuroepithelial markers GFAP, vimentin and S-100 protein as well as $pp60^{C\text{-}SRC}$, but not the neuro-specific variant $pp60^{C\text{-}SRCN}$ and to express neuropoietic factors CNTF, LIF and their receptors; LIF and oncostatin M induce growth inhibition and differentiation
Reference(s):	14590, 14591, 19087
Biosafety level:	1
Permissions and restrictions:	A

DSMZ Cell Culture Data:	
Morphology:	fibroblastoid, adherent cells growing as monolayer
Medium:	90% Dulbecco's MEM + 10% h.i. FBS + 4 mM L-glutamine +P/S
Subculture:	split confluent culture 1:2 to 1:3 every third day using trypsin/EDTA; maintain at 7-10 x 10^6 cells/175 cm^2; seed out at ca. 1 x 10^6 cells/25 cm^2 in 10 ml medium
Incubation:	at 37 °C with 5% CO_2
Doubling time:	ca. 50 hours
Harvest:	cell harvest of ca. 10-15 x 10^6 cells/175 cm^2; maximal density of 17 x 10^6 cells/175 cm^2
Storage:	frozen with 70% medium, 20% FBS, 10% DMSO

Source: (DSMZ, 2019)

2.8.3. Human G28 glioma cells

Cell line:	**G 28**
Synonyms:	NCE G-28; NCE-G28; G-28; G28; NeuroChirurgie Eppendorf-Glioma 28
Accession:	CVCL_N724
Resource Identification Initiative:	To cite this cell line use: NCE-G 28 (RRID:CVCL_N724)
Disease:	Gliosarcoma (NCIt: C3796)
Species of origin:	Homo sapiens (Human) (NCBI Taxonomy: 9606)
Hierarchy:	Children: CVCL_0V15 (NCE G-28T)
Sex of cell:	Male
Category:	

Source: (ExPASy, 2019b)

2.8.4. Human G112 glioma cells

Cell line:	**G112**
Synonym:	NCE G-112; NCE G 112; NCE-G112; G-112; G112; NeuroChirurgie Eppendorf-Glioma 112
Accession:	CVCL_N740
Resource Identification Initiative:	To cite this cell line use: NCE-G 112 (RRID:CVCL_N740)
Comments:	Omics: Deep RNAseq analysis. Omics: SNP array analysis.
Disease:	Glioma (NCIt: C3058)
Species of origin:	Homo sapiens (Human) (NCBI Taxonomy: 9606)
Sex of cell:	Male
Category:	Cancer cell line

Source: (ExPasy, 2019)

2.8.5. Human U87 glioma cells

Cell line:	**U87**
Synonym:	ATCC® HTB14™
Organism:	*Homo sapiens*, human
Tissue:	brain
Disease:	Likely glioma
Biosafety:	1
Age:	unknown
Gender:	male
Morphology:	epithelial
Growth Properties:	adherent
Medium:	The base medium for this cell line is ATCC-formulated Eagle's Minimum Essential Medium, Catalog No. 302003. To make the complete growth medium, add the following components to the base medium: fetal bovine serum to a final concentration of 10 %
Storage:	liquid nitrogen, vapor phase

Source: (ATCC, 2019c)

2.8.6. Human U251 glioma cells

Cell line:	**U251**
CLS order number:	Cryovial: 300385 Vital: 330385
Origin and General Characteristics	
Organism:	Homo sapiens (human)
Ethnicity:	Caucasian
Gender:	Male
Tissue:	Brain
Morphology:	Epithelial
Celltype:	Glioma
Growth Properties:	Monolayer, adherent
Description:	Authentication studies performed at ATCC and others, the identity of the U-373 MG cell line has been questioned. Authentication via STR analysis, conducted by CLS GmbH, as well as morphological and immunological analysis has revealed that U-373 MG is identical to U-251 MG.

Source: (CLS, 2019)

2.8.7. Human HT29 (adenocarcinoma) cells

Cell line:	**HT29**
Biological source:	Colon from human
Growth mode:	Adherent
Karyotype:	2n = 46, hypertriploid
Morphology:	Epithelial
Products:	Secretory component of Immunoglobulin A (IgA), Carcinoembryonic antigen (CEA)
Receptors:	Not specified
Application(s):	cell culture | mammalian: suitable Tumourigenicity studies
Cell Line Origin:	Human Caucasian colon adenocarcinoma
Cell Line Description:	Isolated from a primary tumour in a 44 year old Caucasian female. Forms a well-differentiated adenocarcinoma consistent with colony primary, grade I. Tumours also form in steroid treated hamsters. Has the following HLA profile A1,3; B12,17; Cw5.

Source: (ATCC, 2019d)

2.8.8. Human HepG2 (hepatocellular carcinoma) cells

Cell line:	**HepG2**
Biological source:	Liver from human
Growth mode:	Adherent
Karyotype:	Modal no. 55
Morphology:	Epithelial
Products:	Prothrombin, antithromin III, alpha-foetoprotein complement, C3 and C4 activator, fibrinogen
Receptors:	Not specified
Application(s):	cell culture | mammalian: suitable Study of hepatocyte function and specific protein expression
Cell Line Origin:	Human Caucasian hepatocyte carcinoma
Cell Line Description:	The Hep G2 cell line has been isolated from a liver biopsy of a male Caucasian aged 15 years, with a well differentiated hepatocellular carcinoma. The cells secrete a variety of major plasma proteins e.g. albumin, α2-macroglobulin, α 1-antitrypsin, transferrin and plasminogen. They have been grown successfully in large scale cultivation systems. Hepatitis B virus surface antigens have not been detected. The cells will respond to stimulation with human growth hormone.

Source: (ATCC, 2019e)

2.8.9. Human Panc-1 (pancreatic carcinoma) cells

Cell line:	**Panc-1**
DSMZ no.:	ACC 783
Species:	human (Homo sapiens)
Cell type:	pancreas carcinoma
Origin:	established in 1972 from the ductal cells of a tumor located in the head of the pancreas of a 56-year-old man; the cells are described in the literature to be tumorigenic in nude-athymic mouse, to carry three marker chromosomes and a small ring chromosome
Biosafety level:	24155, 24156, 24157 1
DSMZ Cell Culture Data:	
Morphology:	epithelioid cells growing adherently as monolayer
Medium:	90% Dulbecco´s MEM + 10% h.i. FBS
Subculture:	seed out at ca. 1-2 x 106 cells/80 cm2 flask; split confluent culture 1:4 twice a week using trypsin/EDTA
Incubation:	at 37 °C with 5% CO2
Doubling time:	ca. 40-45 hours
Harvest:	cell harvest of ca. 18-20 x 106 cells/175 cm2
Storage:	frozen with 70% medium, 20% FBS, 10% DMSO

Source: (DSMZ, 2019b)

2.8.10. Murine RenCa (renal carcinoma) cells

Cell line:	**RenCa**
Description:	Murine Renal carcinoma cell line.
Origin:	The RenCa cell line has been established from the murine transplantable renal adenocarcinoma of spontaneous origin. The species was confirmed by Real-Time PCR.
Organism:	Mus musculus, mouse
Strain:	Balb/c
Tissue Source:	Kidney
Cell type:	Carcinoma
Morphology:	Epithelial
Growth Properties:	Monolayer, adherent
Medium:	RPMI-1640 medium supplemented with 2 mM L-glutamine and 10% fetal bovine serum.
Culture Conditions:	Temperature: 37°C Atmosphere: air, 95%; carbon dioxide (CO2), 5%Quality Sub cultivation ratio: A sub cultivation ratio of 1:4 to 1:10 is recommended. Medium renewal: Every 2 to 3 days.
Population:	Doubling Time: approximately 24 hours.

Source: (ATCC, 2019b)

2.8.11. Human THP-1 (monocytic leukemia) cells / macrophages

Cell line:	**THP-1**
DSMZ no.:	ACC 16
Species:	human (Homo sapiens)
Cell type:	acute monocytic leukemia
Origin:	established from the peripheral blood of a 1-year-old boy with acute monocytic leukemia (AML) at relapse in 1978; the cells can be used for induction of differentiation studies; the cells were described to produce lysozyme and to be phagocytic; carries t(9;11)(p21;q23) leading to MLL-MLLT3 (MLL-AF9) fusion gene
Reference(s):	14493, 15021, 15022
Biosafety level:	1
Permissions and restrictions:	A
DSMZ Cell Culture Data:	
Morphology:	round, single cells in suspension, partly in clusters; image
Medium:	90% RPMI 1640 + 10% h.i. FBS
Incubation:	at 37 °C with 5% CO2
Doubling time:	ca. 35-50 hours
Harvest:	saturation density at about 1.0 x 106 cells/ml
Storage:	frozen with 70% medium, 20% FBS, 10% DMSO

Source: (DSMZ, 2019c)

3. Methods

3.1. Cell culture

All experiments were performed under a sterile working bench.

3.1.1. Cell culture conditions

For culturing the glioma cell lines BT4Ca, GOS-3, G28, G112, U87 and U251 DMEM high glucose (4.5 g/l) medium, supplemented with 10 % heat-inactivated (30 minutes at 56°C), fetal bovine serum (FBS), 100 U/ml Penicillin as well as 0.1mg/ml Streptomycin, was used.

The other cell lines, THP-1, HT29, HepG2, RenCa and Panc-1, were cultured in RPMI 1640 low glucose (1g/l) medium, supplemented with 10% heat-inactivated FBS 100 U/ml Penicillin and 0.1 mg/ml Streptomycin (P/S). The cell cultures were maintained at 37°C in a humidified incubator in an atmosphere of 5 % CO2 – 95 % air and passaged after reaching the 80-90 % confluency every 48-72 h in a 75 cm^2 flask with fresh medium.

3.1.2. Defrosting and freezing of cells

The cells, which were stored in liquid nitrogen were quickly defrosted and mixed with 10 ml fresh DMEM high glucose or RPMI 1640 low glucose medium, depending on the cell line. After centrifugation (10 min, 250 x g) the supernatant was removed and the cell pellet was resuspended in 1 ml fresh medium and added to 45 ml medium. Afterwards the cells were cultured as described above.

For freezing the cells, pellet was resuspended with 400 µl fresh medium transferred into a freezing tube and cooled down on ice for 1-2 h. Afterwards 400 µl freezing medium was added and the cells were stored at -80°C for at least 3 days. For longer storage times the tubes were transferred into liquid nitrogen.

3.1.3. Cell Splitting

After the cells reached confluence, normally three to four days, the cells were cultured at a split ratio of 1:20 (BT4Ca), 1:5 (GOS3), 1:5 (G28), 1:3 (G112), 1:20 (U87), 1:5 (U251), 1:3 (HT29), 1:5 (HepG2 and RenCa), 1:10 (Panc-1) and 1:10 (THP1) and transferred into another culture flask with warm (37°C) fresh medium (RPMI or DEMEM + 10%FBS + P/S).

3.1.3.1. Culturing of human THP1 cells

The non-adherent THP1 cells were transferred to a 50 ml tube and centrifuged 5 min at 100 x g. Subsequently the supernatant was removed and the cell pellet was resuspended in 10 ml warm (37°C) fresh RPMI 1640 (low glucose) medium. 1 ml of the cell-suspension was then added to 45 ml medium in a culture flask and maintained at 37°C in a humidified incubator in an atmosphere of 5 % CO2 – 95 % air.

3.1.3.2. Culturing of cancer cells

The adherent cancer cells were at first detached by Trypsin treatment. Therefore, the old medium was drained off and the cells were shortly washed with 10ml DPBS. After removing the DBPS, 1 ml Trypsin-EDTA (0.05 % Trypsin; 0.02 % EDTA) was added into 75 cm² culture flask to completely cover the monolayer of the cells and incubated for 1-5 min at 37°C. The detached cells were then rinsed twice with 5 ml high glucose medium and collected in a 50 ml tube. Next the cell suspension was centrifuged for 7 min at 200 x g and the cell pellet was resuspended in 10 ml fresh medium. Afterwards the cells were splitted, depending on their proliferation rate (see 3.1.1.) and maintained at 37°C in a humidified incubator in an atmosphere of 5 % CO2 – 95 % air.

3.1.4. Cell counting

For further experiments a defined amount of cells, according to the area of the well, had to be seeded. Therefore, the cells were counted using a C-Chip, which is based on the improved Neubauer counting chamber principle. 10 µl of a cell suspension (see 3.1.1.1/3.1.1.2) were mixed with 90 µl 0.4 % Trypan blue dye exclusion test (1 min) to determine the number of viable cells. Then, 10 µl of this cell suspension were placed on the C-Chips and, with the use of a light microscope (magnification 100 x), the living cells (Trypan blue negative) in all 4 squares were counted. Calculation of the cell concentration was performed by using the formula:

$$\frac{\frac{\boldsymbol{living\ cells}}{(\boldsymbol{in\ 4squares})}}{\mathbf{4}\ [\boldsymbol{squares}]} \times \mathbf{10}\ [\boldsymbol{dilution\ factor}] \times \mathbf{10.000}\ [\boldsymbol{chamber\ factor}] = \frac{\boldsymbol{cells}}{\boldsymbol{ml}}$$

3.2. Viability assay

Cell viability was analyzed after 48h of treatment with different concentrations of the novelly synthesized derivatives. Distinct cell numbers were used as follows: BT4Ca 5 x 10^3 cells/well, GOS3 1.5 x 10^4 cells/well, G28 1.5 x 10^4 cells/well, G112 1.5 x 10^4 cells/well, U87 5 x 10^3 cells/well, U251 7.5 x 10^3 cells/well, HT29/HepG2/RenCa 10 x 10^4 cells/well, or Panc-1 1.5 x 10^4 cells/well were seeded on a 96 well plate. Moreover, THP1 3.0 x 10^4 cells/well were seeded on a 96-well plate and differentiated into macrophages for 72h with 100 nM PMA. All cell lines were cultured at 37°C in a humidified incubator in an atmosphere of 5 % CO_2 and 95 % air.

After 24 h the medium was changed and the derivatives were added at different concentrations. As negative control, the cells were cultured in medium alone. For the DMSO control, the cells were cultured with medium containing 0.05% DMSO (= same DMSO concentration as in the highest concentration (50 µM) of the derivatives).

After 48 h treatment the medium was carefully changed and the cell viability was measured by using PrestoBlue® assay (see below 3.2.1).

3.2.1. PrestoBlue® assay

PrestoBlue® is a cell permeable, resazurin-based, blue solution, functioning as a cell viability indicator. Based on the reducing power of living cells a quantitative measurement of the viability/cytotoxicity can be determined. After addition to the cells, the reagent is modified by the reducing environment of the viable cells and turns from blue to red color (absorbance at 570 nm and 600 nm as a reference wavelength) and becoming highly fluorescent at 560 nm (excitation) measured at 590 nm (emission) (Xu et al., 2015).

After the incubation (48h) with the derivatives under test, the medium was removed and 100 µl fresh medium was added. Afterwards PrestoBlue® reagent was directly added to the fresh medium at a final concentration of 10 %. At least 15 min after addition of PrestoBlue®, the optical density (OD) was measured with a SUNRISE ELISA-reader (Tecan, Salzburg, Austria) or fluorescence with a Cytation™ 3 microplate reader (BioTek Instruments, USA), respectively. The effects of different concentrations of each derivative on the cell viability were measured in four replicates, whereas the mean of the blank (medium with PB alone) was subtracted. The assay was repeated at least five

times. The cells in the negative control wells were incubated with culture media alone. Then the viability compared to the negative control was calculated and the mean values were determined according to the formula:

Results are expressed in % of viability:

$$viability\ in\ \% = [\frac{\text{OD570/600nm of samples} \times 100}{\text{OD570/600nm of control without substances}}]\ .$$

3.2.2. Sulforhodamine B assay

The sulforhodamine B (SRB) assay is used for cell density determination, based on the measurement of cellular total protein content. The method relies on the property of SRB, which binds stoichiometrically to proteins under mild acidic conditions. It can be extracted using basic conditions; thus, the amount of bound dye can be used as a proxy for the protein concentration or cell mass of a sample. Thereby the cytotoxicity of the different test derivatives and the used controls can be examined (Orellana & Kasinski, 2016).

Following the PrestoBlue® assay the cells were shortly washed with PBS and fixed with 10 % (wt/vol) trichloroacetic acid (TCA) for 30 min at 4°C. Hence the TCA was removed and the fixated cell monolayers were washed 3 times with water. Upon drying the samples were stained with 0.4 % SRB solved in 1 % (vol/vol) acetic acid for 30 min in the dark. The excess dye was removed by shortly washing 3 times with 1% (vol/vol) acetic acid. After a second drying step, the protein-bound dye was dissolved in 10 mM Tris base solution. At the end the OD was measured at 560 nm and 690 nm as reference using the SUNRISE ELISA-reader (Tecan, Salzburg, Austria). The protein content of each well after treatment with the derivatives of interest was measured in four replicates and the mean of the blank (SRB reagents alone) was subtracted. The assay was repeated at least five times. The cells in the negative control were incubated with culture media alone. Then the percentage of the protein content compared to the negative control was calculated and the mean values were determined according to the formula:

Results are expressed in % of protein content:

$$protein\ content\ x\ well\ \ in\ \% = [\frac{\text{OD560/690nm of samples} \times 100}{\text{OD560/690nm of control without substances}}]\ .$$

$$cytotoxicity\ in\ \% = 100 - [\frac{\text{OD560/690nm of samples} \times 100}{\text{OD560/690nm of control without substances}}]$$

The loss of proteins represents the cytotoxicity of the derivatives, assuming the higher the loss of protein the higher the cytotoxicity.

3.3. Apoptosis and necrosis assay

3.3.1. Apoptosis and necrosis staining

A more detailed view on the possible mechanism of cell death was achieved by performing an apoptosis and necrosis assay. Due to apoptosis the integrity of the cell membrane becomes permeable allowing YO-PRO®-1, a green-fluorescent stain, to enter the cells. Hence YO-PRO®-1 can bind to the nuclear DNA, enabling the identification of apoptotic cells (Gawlitta et al., 2005; Fujisawa et al., 2014).

In contrast to apoptosis, necrosis is associated with the ultimate breakdown of the plasma membrane. The rupture permits propidium iodide, a membrane impermeable and red-fluorescent intercalating agent, to bind to the DNA, identifying necrotic cells by red colour (Gawlitta et al., 2005; BioLegend Inc., 2019).

Living cells are neither stained with YO-PRO®-1 nor with propidium iodide. Thus, to calculate the rate of apoptotic and necrotic cells after treatment the nuclei of all cells were counterstained with Hoechst 33342 dye, representing the total amount of cells in a sample (Merck, Sigma-Aldrich, 2019).

The BT4Ca cells were seeded as described above (see. 3.2) and incubated for 48 h with 5-FUrd and the five derivatives, which have shown the most effective cytotoxic/cytostatic results in the viability assay (5-FUrd, S.18, S.19, S.38, S.98 and S.101; 1 µM Camptothecin served as a positive control). To differentiate between apoptotic and necrotic processes the cells were stained with YO-PRO®-1 (1 µM), Propidium iodine (3 µM) and Hoechst 33342 (5.4 µM) for 10 min. Photos were taken (magnification 100x) using an inverted epiflourescence microscope Zeiss Axiovert 135 equipped with a X–Y motorized stage and AxioVision 4 Modul Mark & Find 2 software (Carl Zeiss GmbH) and a digital AxioCam MRc camera with the AxioVision Rel. 4.8 software (Carl Zeiss GmbH). The total number of apoptotic and necrotic cells were determined by manual and automatic counting using Image J 1.46r software (National Institute of Health).

Moreover, an additional second evaluation method was used to measure the percentage of apoptotic and necrotic cells. For this purpose the total fluorescence of all three dyes were recorded via the Cytation3 image reader at 490 nm excitation/530 nm emis-

sion for YO-PRO®-1, 535 nm excitation/617 nm emission for propidium iodide and 350nm excitation /462 nm emission for Hoechst 33342. Hence the background (blank) was measured at the three wavelength conditions as described previously. The background was subtracted and the cell amount compared to the negative control as well as the fluorescence ratios of YO-PRO®-1 /Hoechst and propidium iodide /Hoechst were calculated. DMSO was used as control for the dissolver and camptothecin was used as positive control for apoptosis. The assay was repeated four times.

Both data, the fluorescence measurement (Fig.24-47) and the fluorescent images (see supplements page 150-163, Fig. 27-39), were analyzed independently.

The Hoechst fluorescence was calculated in % of the negative control (= 100 %) and the significances are given compared to the DMSO control as well as to 5-FUrd and camptothecin. The fluorescence intensity of YO-PRO®-1 or PI is divided by the cell amount (Hoechst 33342 nuclei) and the mean rate of fluorescence ratio ± SEM are illustrated in the graphics; the significances are given compared to the DMSO control as well as to 5-FUrd and camptothecin.

3.3.2. Active caspase 3 activity assay

For the determination of activated caspases 3 and 7 the CellEvent™ Caspase-3/7 Green Detection Reagent was used. The reagent is a novel fluorogenic substrate consisting of four amino acid peptide (DEVD) conjugated to a nucleic acid binding dye. DEVD peptide inhibits the ability of the dye to bind to DNA so the cell-permeant substrate is intrinsically non-fluorescent. After activation of caspase-3 or caspase-7 in apoptotic cells, the DEVD peptide is cleaved, enabling the dye to bind to DNA and produce a bright, fluorogenic response with absorption/emission maxima of ~502 nm/530 nm respectively (ThermoFisherScientific, 2019).

The BT4Ca cells were seeded as described above (see. 3.2) on a black Lumox® 96-multiwell plate. After attachment (24 h), the cells were treated with 5-FUrd and the five most effective derivatives (S.18, 19, 38, 98 and 101; at the concentration of 12.5, 25 and 50 µM. The proapoptotic camptothecin (1 µM) was used as positive control. Directly after the treatment the CellEvent™ caspase-3/7 green detection reagent was added at a concentration of 2.5 µM. Caspase 3/7 activity was measured after 0 h, 24 h and 48 h of treatment. The fluorescence intensity was measured at 502 nm excita-

tion/530 nm emission with the Cytation™ 3 image microplate reader. At the end of the treatment (48 h) the cells were additionally counterstained with Hoechst 33342 (5.4 µM) without exchanging the medium. The fluorescence was detected at 350 nm excitation/462 nm emission. The fluorescence of DEVD was measured in four replicates and the mean of the blank was subtracted. Then the percentage of the active caspase 3 compared to the negative control (= 100%) was calculated and the mean values were determined. The assay was at least repeated five times.

Therefor the CellEvent™ Caspase-3/7 Green Detection assay was used. This method is based on the cleavage of DEVD by the active caspase 3, causing a fluorescent signal, which can be detected with an emission maximum of 530nm after excitation by 502 nm.

3.4. Oxidative stress

3.4.1. Reactive oxygen species (ROS) Detection

Reactive oxygen species (ROS) may lead to oxidative stress, when an intracellular imbalance between oxidative and anti- oxidative systems occurs (Newsholme et al., 2016).

To analyze the production of ROS the cells were loaded with the cell-permeant reagent 2',7' –dichlorofluorescin diacetate (DCFDA). After the diffusion of DCFDA into the cells, it gets oxidized by ROS into 2', 7' –dichlorofluorescein (DCF), which is a highly fluorescent compound. Hence DCF can be detected by fluorescence spectroscopy with maximum excitation and emission spectra of 495 nm / 529 nm (Figueroa et al., 2018).

The BT4Ca cells were seeded as described above (see. 3.2) and cultured for 24 h. The following steps were performed using only medium (DMEM high Glucose) without phenol red. After washing with medium alone the cells were incubated (45 min) with 25 µM DCFDA reagent. Next the cells were treated (48 h) with 5-FUrd or the five derivatives, S.18, S.19, S.38, S.98 and S.101, as well as H_2O_2 served as a positive control). During the treatment the fluorescence was measured at 485/ 535 nm with Cytation3 multi-mode reader at several time points (30 min, 1, 2, 3, 4, 5, 24 and 48 h). At the end the viability of the cells was measured by PrestoBlue® assay. The amount of ROS was measured in four replicates and the mean of the blank was subtracted. The assay was repeated at least five times.

3.5. Activation of the transcription factor nuclear factor κappa B

The nuclear factor kappa light chain enhancer of activated B cells (NFκB) is expressed in nearly all mammalian cells and is of prime importance for the regulation of the immune response, cell proliferation as well as cell death. p65, also known as RelA, is one of the five components that form this transcription factor complex. Under physiological/normal conditions, the p50/p65 heterodimer is selectively bound to IκBα or IκBβ. Hence the NFκB subunits are localized in the cytoplasm due to the binding of the inhibitors of the IκB family, preventing the nuclear translocation of p50/p65. After stressful stimuli the IκB kinase complex gets activated inducing the disassociation of IκBα. The p50/p65 heterodimer is able to translocate to the nucleus and bind to specific gene promoters to modulate the expression amongst others, of pro- and anti-inflammatory proteins (Fig. 8). Furthermore, the expression of IκBα and IκBβ are also up-regulated by the NFκB heterodimers in order to terminate the signaling pathway, functioning as a negative feedback loop (Moynagh, 2015).

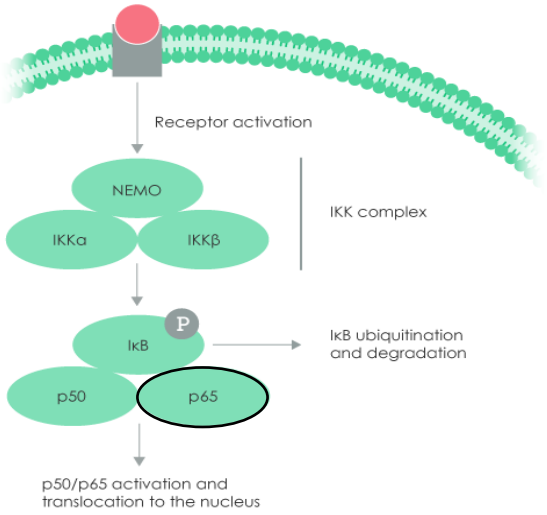

Figure 8: The canonical pathway.
Ligand binding to a receptor leads to the recruitment and activation of an IKK complex comprising IKK alpha and/or IKK beta catalytic subunits and two molecules of NEMO. The IKK complex then phosphorylates IκB leading to degradation by the proteasome. NFκB then translocate to the nucleus to activate target genes (Abcam, 2019b [modified]).

3.5.1. NFκB p65 staining

The BT4Ca cells were seeded as described before (see. 3.2) on a 96-lumox multiwell plate and incubated for 48h with 5-FUrd and the 5 most effective derivatives (5-FUrd, S.18, S.19, S.38, S.98 and S.101). After the treatment the cells were washed with PBS and fixed with ice-cold methanol for 10min at 4°C. After removing the methanol and washing with PBS the cells were incubated with PBS containing 0.1 % Triton x100 for 15 min. The cells were then washed again with PBS and blocked for 30 min. with 2 % goat serum in PBS. Afterwards, the cells were incubated with the polyclonal goat anti-NFκB antibody (1:50 in PBS) at 4 °C overnight. The next day, the cells were washed

with in PBS containing 0.1 % Triton x100. Subsequently the secondary antibody (anti goat -Cy3 -conjugated, 1: 100 in PBS) and DAPI (1:1000 in PBS) were added for 1 h at room temperature. Thereafter, the cells were washed again with PBS containing 0.1 % Triton x100 and covered with PBS. 24 h later microscopic pictures were taken with the confocal laser scanning microscope Nikon Eclipse Ti. The pictures were taken at a magnification of 200x and 400x and qualitative analysis was done.

3.6. Migration

3.6.1. Scratch assay

Because migration and invasion play a significant role in GBM progression/metastasis, too, we tried to verify if the migration behavior of the cells is influenced by the treatment with the most effective derivatives (5-FUrd, S.18, S.19, S.38, S.98 and S.101). Therefore, a wound healing assay ("Scratch assay") was performed.

The BT4Ca cells were seeded in a density of $3x10^5$ cells/well as described before (see. 3.2) on a 12 multiwell plate. The cells were cultured for 24 h, obtaining a 90 % – 100 % confluent monolayer, afterwards "wounds" were made with a 10 µl pipette tip in the middle of each well. Thereafter the cells were washed five times with PBS to remove detached cells. Afterwards the cells were treated with the derivatives and incubated for 24 h. The "wound" was photographed at the identical X-, Y-coordinate in each well (magnification 100x) at time 0 and every 3 hours (0, 3, 6 or 9 h), using an epiflourescence microscope Zeiss Axiovert 135 equipped with a X–Y motorized stage and AxioVision 4 Modul Mark & Find 2 software (Carl Zeiss GmbH) and a digital AxioCam MRc camera with the AxioVision Rel. 4.8 software (Carl Zeiss GmbH). Effects on migration were plotted as a percentage of wound closure (% of wound closure = [(Δt) × 100 %]/At 0 h; where "At 0 h" is the area of wound measured immediately after scratching, "At 3, 6 or 9 h" indicates the area of wound measured 3, 6 or 9 h after scratching and Δt= At 0 h – At 3, 6 or 9 h (Yue et al., 2010).

The assay was repeated three times and the size of the wound area was measured and calculated in % of the area at time point 0h.

3.6.2. Light microscopy

At the end of the incubation (48 h) with 5-FUrd or the derivatives, the morphological integrity of the cells was controlled by microscopy. Light microscopy photos of the cells treated with 12.5, 25 and 50 µM of 5-FUrd or the derivatives, as well as the negative and the DMSO control were taken by AxioCam MRm Camera using phase contrast approach.

3.7. Biochemistry

3.7.1. Protein extraction

After culture the medium was collected and the adherent cells were washed with 1 ml ice-cold DPBS. DPBS together with the supernatant was centrifuged for 10 min at 250 x g to collect the non-adherent cells, whereas the supernatant was discarded.

Meanwhile the adherent cells were scratched off, diluted with pure medium (without FBS) and transferred to a low-binding tube. The cell pellet, which was gained from the culture medium before, was added to the harvested cells. After centrifugation (10 min 250x G) the complete cell pellet (non-adherent and adherent cells) was washed with pure medium (without FBS) to remove the remaining FBS. For the GSH-GSSG assay 400 µl 2.5% sulfosalicylic acid (SSA) were added to the cell pellet, for the PCNA ELISA the pellet was resuspended in 400 µl $RIPA^{+}$ (Radio-Immunoprecipitation Assay mixed with protease inhibitor cocktail) lysis buffer pH 7.5. After centrifugation (10 min at 13,000 x G at 4°C) to remove the cellular debris, the protein concentration in the supernatant was determined by BCA assay.

3.7.2. Protein quantification, BCA assay

The bicinchoninic acid assay (BCA) is a spectrophotometric analytical method to measure the concentration of proteins in a solution. Cu^{2+} is reduced by protein in an alkaline medium to Cu^{1+}. Following, the so arisen cuprous cation (Cu^{1+}) can be detected by bicinchoninic acid, which induces a colorimetric switch. Therefore, the proteins are transferred into an alkaline environment, where the peptide bonds react with copper to a light blue complex (~biuret reaction). Then the bicinchoninic acid binds to the emerging, reduced Cu^{1+} cations, which can be observed as an intense purple-colored reaction. The complex of BCA and Cu^{1+} cations exhibit a strong linear absorbance with

increasing protein concentration, which can be measured at 562 nm (Thermo Fisher Scientific, 2019).

For protein quantification the absorbance of bovine serum albumin (BSA) standard, as well as the samples were measured in duplicates on a 96-well plate. After adding the BCA reagent, the plate was incubated for 30 min in the dark. The absorbance at 562 nm was measured with a Microplate reader and a standard curve (0, 25, 125, 250, 500, 750, 1000, 1500 and 2000 mg/ml) was generated. Thereafter, the protein concentration of the samples was calculated by linear interpolation using the standard curve (Fig.9).

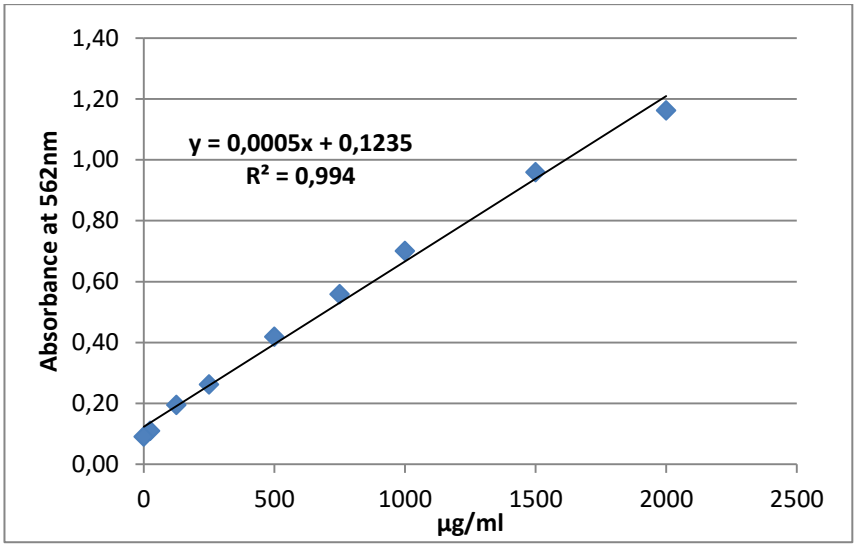

Figure 9: BCA standard curve.
Representative example of a standard curve, generated by the measurement and use of the protein standards (0, 25, 125, 250, 500, 750, 1000, 1500 and 2000 µg/ml). The formula of the curve can be used to calculate the protein concentration of (unknown) samples.

The measurements were performed in four replicates and the mean of the blank was subtracted. The assay was repeated three times and calculated in µg/ml.

3.7.3. GSH/GSSG Assay

BT4Ca cells were seeded, cultured, treated and collected as described above (see 3.8.1). To measure the amount of total glutathione (tGSH) and oxidized (GSSG) form, a glutathione assay was performed according to Tietze (Tietze, 1969) based on the determination of total GSH (GSH + GSSG) in the absence of 2-vinylpyridine (thiol scavenger) and GSSG, determined with use of 2-vinylpyridine, in presence of the enzyme glutathione reductase (GR).

For the determination of the total glutathione (tGSH) 30 µl of the sample or tGSH standards (0, 0.025, 0.05, 0.1 and 0.25 nmol/ml) were mixed with 288 µl tri-ethanolamine (TEA/SSA) (solution 1). Following, 100 µl of solution 1, were added to 500 µl glutathione buffer and 200 µl 5,5-dithio-bis-2-nitrobenzoic acid (DTNB, containing 2.5units GR), mixed in a plastic cuvette (semi-micro) and first measured after 6 min at 412 nm with a photometer, this value is taken as tGSH time 0 (T0).

For the measurement of the oxidized glutathione (GSSG), 200 µl of sample or GSSG standards (0, 0.025, 0.05, 0.1 and 0.25 nmol/ml) were incubated at room temperature for 30 min with 4 µl 2-vinylpyridine. By adding 12 µl TEA the reaction was stopped (solution 2) and 100µl of solution 2 were mixed with 500 µl glutathione buffer and 200 µl DTNB (containing 2.5units GR) in a plastic cuvette. Then after 6 min the samples were measured at 412 nm with a photometer (T0).

The reaction (tGSH or GSSG) was started after the first measurement (T_0) by addition of 200µl NADPH and 6 min later the samples were measured again at 412 nm (T6). After the subtraction of the mean of the blank (Blank = 0 nmol/ml) the difference of the absorbance between T0 and T6 was calculated. All measurements were performed in duplicates. The assay was repeated three times and calculated in % of the negative control. The concentration of tGSH or GSSG of the samples were calculated by linear interpolation using the respective standard curve (Fig.10).

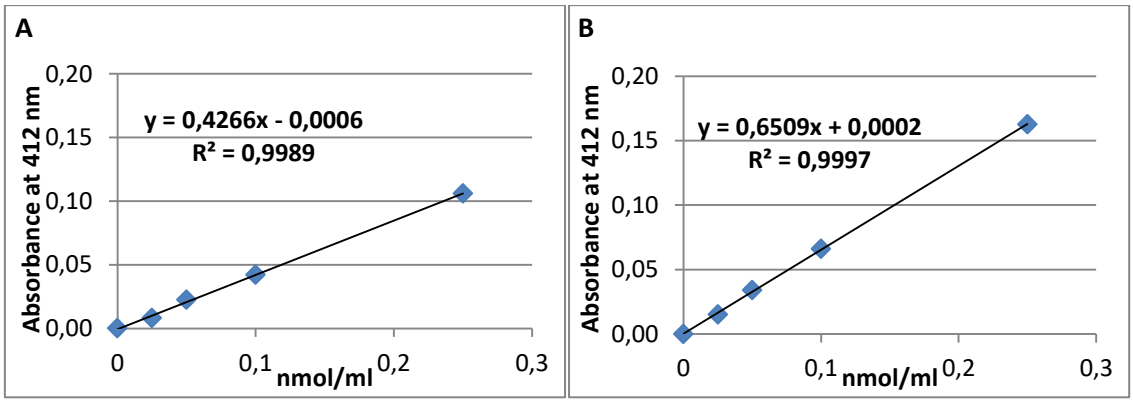

Figure 10: GSH and GSSG standard curves.
Representative example of a GSH (A) and GSSG (B) standard curves generated by the measurement and use of the standards (0, 0.025, 0.05, 0.1 and 0.25 nmol/ml). The formula of the curves can be used to calculate the GSH or GSSG concentration of (unknown) samples.

The amount of tGSH and GSSH in the samples was normalized with the respective protein amount determined by BCA. Reduced (r)GSH was computed by subtraction (rGSH=tGSH-GSSG).

3.7.4. PCNA ELISA

The assay was performed according to manufacturer's instructions of the CytoSelect Proliferating Cell Nuclear Antigen (PCNA) ELISA Kit from Bio Celllabs (Cell Biolabs, Inc., 2019).

The BT4Ca cells were seeded, cultured, treated and collected as described above (see 3.8.1). For the quantification of the PCNA fraction, duplicates of the standard as well as 60 ng protein of the samples were loaded on the pre-coated 96 plates with capture antibody and incubated for 24 h at 4°C on an orbital shaker (100 rpm/min). After three times washing with washing buffer the primary PCNA antibody, diluted 1:1000 with diluent reagent, was added and incubated for 1h at RT on an orbital shaker (100 rpm/min). After another three washing steps, the HRP-conjugated secondary antibody (1:1000) was added. Afterwards the unbound antibody was removed by washing with washing buffer and 100 µl HRP-substrate TMB (3,3´,5,5´-tetramethylbenzidine) were added. After 30 min 100 µL of the stop solution (2N H_2SO_4) were added and the absorbance was measured at 450 nm. By generating a standard curve (0, 6.25, 12.5, 25, 50, 100, 200 and 400 ng/ml), the amount of PCNA was calculated by linear interpolation (Fig. 11).

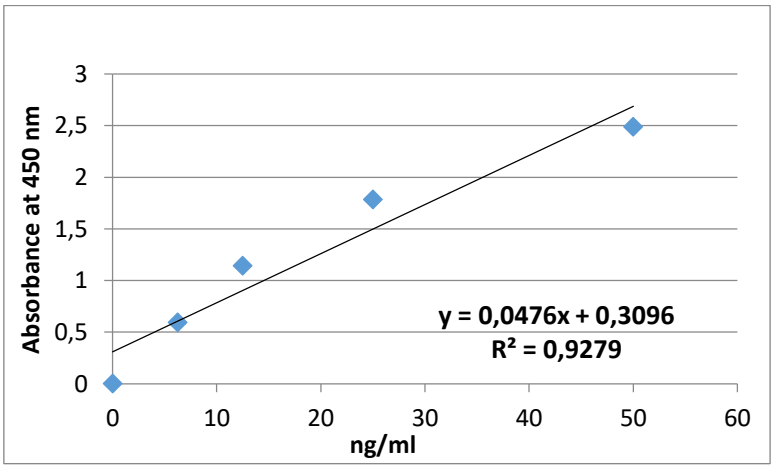

Figure 11: CytoSelect™ Proliferating Cell Nuclear Antigen (PCNA) Standard Curve.
Representative example of a standard curve generated by the measurement and use of the PCNA-standard (0, 6.25, 12.5, 25, 50, 100, 200 and 400 ng/ml). The formula of the curve can be used to calculate the PNCA concentration of (unknown) samples.

The amount of PCNA was measured in four replicates and the mean of the blank was subtracted. The assay was repeated three times and calculated in % of the negative control.

3.8. Evaluation and statistics

At the end of every assay the mean values of all experiments were calculated with Excel2010. Additionally, the standard deviation (SEM) and the significance versus DMSO, camptothecin and 5-FUrd were calculated. For all experiments SigmaPlot®12 software was used to carry-out statistical analyses. Results are presented as means ± standard error of the mean (SEM). After testing for normality (by Shapiro–Wilk), the unpaired Student's t-test or Mann–Whitney U-test were used, whereby a P value of < 0.05 was chosen as failure criterion. $^{*}p < 0.05$, $^{**}p<0.01$ and $^{***}p<0.001$ considered to be statistically significant vs DMSO; $^{\#}p < 0.05$, $^{\#\#}p<0.01$ and $^{\#\#\#}p<0.001$ statistically significant vs. 5-FUrd; $^{\circ}p < 0.05$, $^{\circ\circ}p<0.01$ and $^{\circ\circ\circ}p<0.001$ statistically significant vs. camptothecin. Results were plotted by the use of Microsoft Excel.

4. Results

4.1. Effects of the novel derivatives on cell morphology

After the treatment of the different cell lines with the novelly synthesized derivatives, morphological alterations and changes of the cell density were controlled by light microscopy and photographically documented (magnification 100x). Thereby a first impression of the impact of the novel derivatives on the cells was gained. The photos of the cells treated with 5-FUrd and the five most effective derivatives (S.18, 19, 38, 98 and 101) at the concentrations of 12.5, 25 and 50 µM can be found in the supplements page 126-146, Fig. 1-21. These pictures illustrate an explicit reduction of the cell density and a destruction of the cell morphology depending on the added derivative and its concentration as well as the specific cell line.

4.2. Effects of the novel derivatives on the cell viability

To identify nucleolipids with any cytotoxic or cytostatic effects, all 120 derivatives were tested by using the PrestoBlue™ cell viability assay. The viability of the rat BT4Ca, human GOS3 glioma cells as well as PMA differentiated macrophages (THP1) was measured after an incubation of 48 h with the derivatives under test at concentrations of 1.56-50 µM. Following, the effects of the five most interesting derivatives (S.18, 19, 38, 98 and 101) on the viability of rat **BT4Ca** and human **GOS3** glioma cells are shown (Fig. 12 and 13).

All derivatives were solubilized in DMSO; hence a DMSO control was performed using medium with 0.25 % DMSO, corresponding to the concentration of DMSO in 50 µM maximal working concentration of the derivatives under test. No significant cytotoxic effect of 0.25 % DMSO control on the viability of any cell type under test was observed, compared to the negative control (incubation with medium alone; = 100 % viability) (Fig. 12-17). The viability is calculated in % of the negative control (= 100% viability) and the significances are given compared to the 0.25 % DMSO control as well as to 5-FUrd.

After the incubation (48 h) of the rat **BT4Ca** glioma cells with **5-FUrd** (1.56-50 µM) a significant ($p<0.001$) cytostatic effect with a reduction of the viability by ca. -75.0 % to -85.0 % was detected compared to the negative control (= 100 % viability) (Fig.12).

The treatment of the rat **BT4Ca** glioma cells with derivative **S.18** at the concentrations of 25 and 50 µM resulted in a significant reduction of the viability by -58.6 % ($p<0.01$) and -81.8 % ($p<0.001$) compared to the negative control (Fig.12).

The incubation with derivative **S.19** showed a significant decrease of the viability of rat **BT4Ca** glioma cells by -20.4 % (6.25 µM, $p<0.01$), -33.3 % (12.5 µM, $p<0.01$), -100.0 % (25 µM, $p<0.001$) and -100 % (50 µM, $p<0.001$) compared to the negative control. In comparison to 5-FUrd, the treatment with **S.19** significantly ($p<0.05$) reduced the viability of rat **BT4Ca** glioma cells by -18.5 % (25 µM) and -15.4 % (50µM) (Fig. 12).

The incubation of the rat **BT4Ca** glioma cells with derivative **S.38** resulted in a significant ($p<0.001$) decrease of the viability by -21.2% (12.5 µM), -70.0 % (25 µM) and -95.9 % (50µM) compared to the negative control (Fig.12).

The treatment with derivative **S.98** led to a significant inhibition of the viability of rat **BT4Ca** glioma cells by -37.9 % (1.56 µM, $p<0.01$), -65.1% (3.12 µM, $p<0.01$), -80.3 % (6.25 µM, $p<0.01$), -87.5 % (12.5 µM, $p<0.001$), -92.4 % (25 µM, $p<0.001$), -95.1 % (50 µM, $p<0.01$) compared to the negative control (Fig.12).

The incubation of the rat **BT4Ca** glioma cells with derivative **S.101** (12.5, 25 or 50 µM) revealed a significant reduction by -43.2 % ($p<0.01$), - 58.6 % ($p<0.001$) and -74.9 % ($p<0.001$) compared to the negative control (Fig.12).

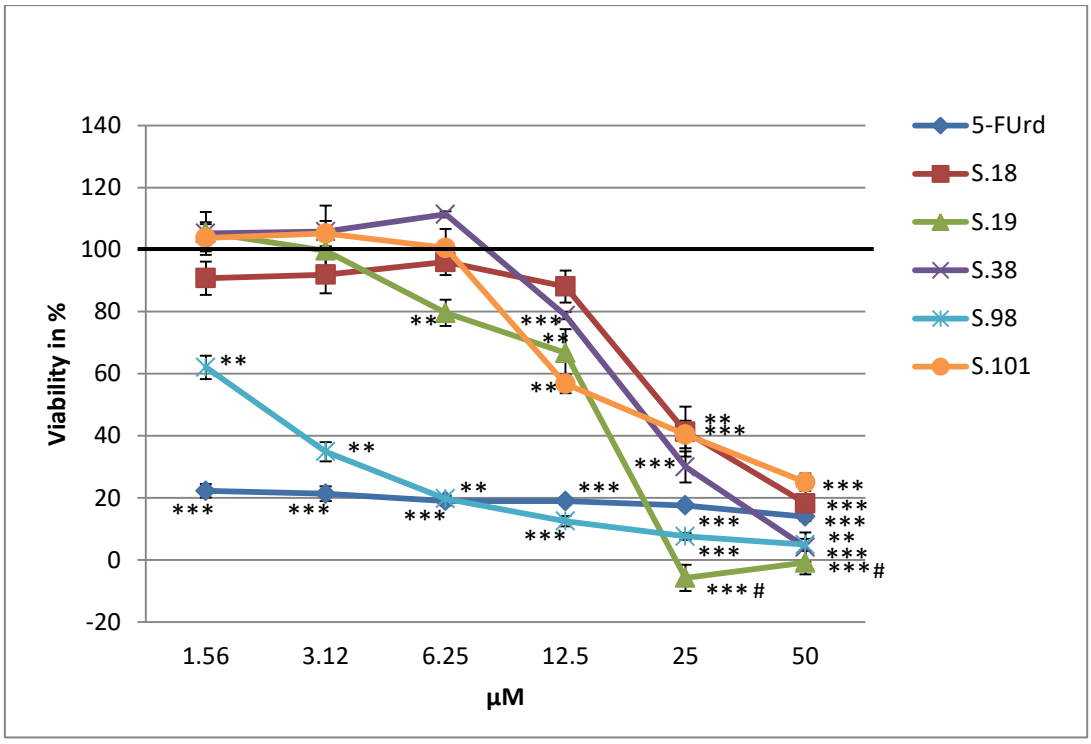

Figure 12: Viability (in %) of rat BT4Ca glioma cells after treatment (48h).
Viability (in % of the negative control) of rat BT4Ca glioma cells after 48 h incubation with 5-FUrd (positive control) or the derivatives S.18, S.19, S.38, S.98 and S.101 measured by PrestoBlue® assay. Values are given (in % viability of control [incubation with medium alone; = 100 % viability]) as mean ± SEM; ***p<0.001, significance vs. 0.25 %DMSO control; #p<0.05 significance vs. 5-FUrd at equal concentration; n=5-50 independent experiments assayed in quadruplicates.

The treatment of the human **GOS3** glioma cells with **5-FUrd** (1.56-50µM) also resulted in a significant ($p<0.001$) cytostatic effect with an inhibition of the viability by ca. -20 to -35 % compared to the negative control (Fig.13)

The incubation of the human **GOS3** glioma cells with derivative **S.18** revealed at the concentrations 25 and 50 µM a significant inhibition of the cell-viability by -28.1 % ($p<0.04$) and -91.2 % ($p<0.001$) compared to the negative control. In comparison to 5-FUrd, the treatment with **S.18** significantly ($p<0.01$) reduced the viability of the human **GOS3** glioma cells by -60.3 % (50µM) (Fig.13).

After the incubation of the human **GOS3** glioma cells with **S.19** (25 and 50 µM) the viability of the cells was abolished, so compared to the negative control not any viable cells could be detected. In comparison to 5-FUrd, the treatment with **S.19** significantly inhibited the viability of the human **GOS3** glioma cells by -66.1 % (25 µM, $p<0.001$) and -69.1 % (50µM, $p<0.01$) (Fig. 13).

The incubation with derivative **S.38** significantly ($p<0.01$) diminished the viability of the human **GOS3** glioma cells by -13.0 % (25µM) and -85.9 % (50µM) compared to the

negative control. In comparison to 5-FUrd, the treatment with **S.38** significantly inhibited the viability of the human **GOS3** glioma cells only at the concentration of 50 µM by -55.0 % ($p<0.01$) (Fig. 13).

After the treatment of the human **GOS3** glioma cells with **S.98** the viability was significantly reduced by -26.0 % (6.25 µM, $p<0.01$), -61.5 % (12.5 µM, $p<0.01$), -97.0% (25 µM, $p<0.001$), -100.0 % (50 µM, $p<0.001$) compared to the negative control. In comparison to 5-FUrd the incubation with **S.98** significantly diminished the viability of the human **GOS3** glioma cells at the concentrations 12.5, 25 and 50 µM by -37.0 % ($p<0.001$), -63.0 % ($p<0.001$) and -70.4 % ($p<0.01$), respectively (Fig. 13).

The treatment with derivative **S.101** significantly inhibited the viability of the human **GOS3** glioma cells by -15.8 % (12.5 µM, $p<0.05$), -42.2 % (25 µM, $p<0.001$) and -79.2 % (50 µM, $p<0.001$) compared to the negative control. In comparison to 5-FUrd, the incubation with **S.101** significantly diminished the viability of the human **GOS3** glioma cells only at the concentration of 50 µM by -48.3 % ($p<0.01$) (Fig. 13).

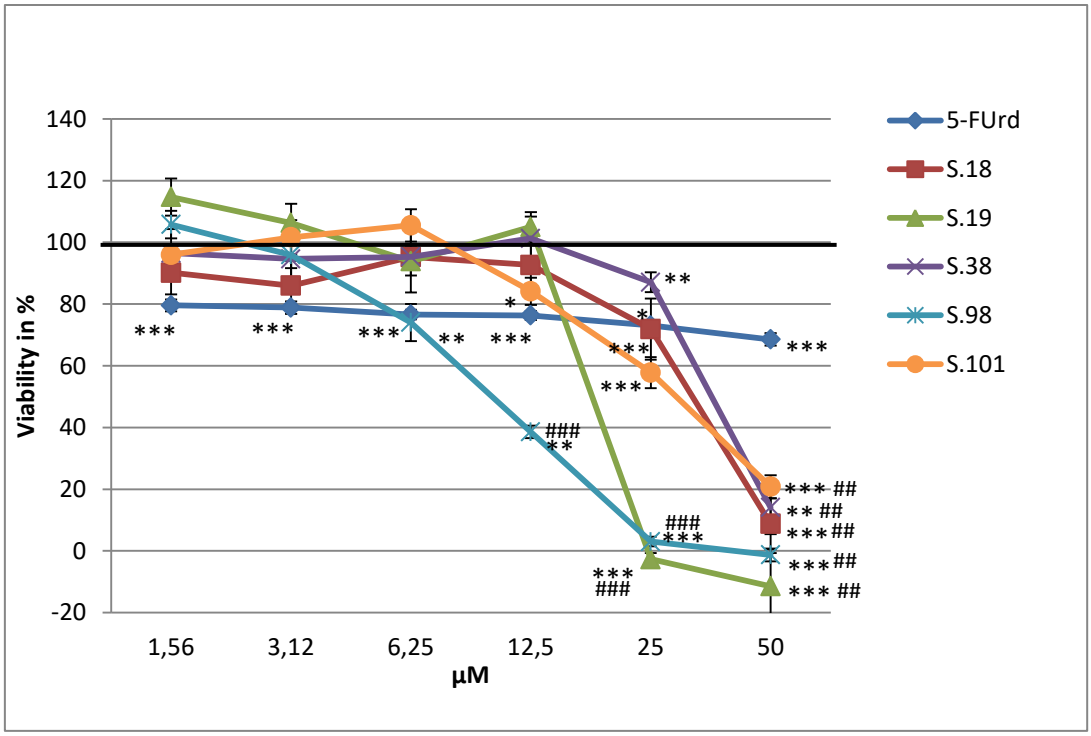

Figure 13: Viability (in %) of human GOS3 glioma cells after treatment (48h).
Viability (in % of the negative control) of human GOS3 glioma cells after 48 h incubation with 5-FUrd (positive control) or the derivatives S.18, S.19, S.38, S.98 and S.101 measured by PrestoBlue® assay. Values are given (in % viability of control [incubation with medium alone; = 100 % viability]) as mean ± SEM; *$p<0.05$, **$p<0.01$, ***$p<0.001$, significance vs. 0.25 % DMSO control; $^{\#\#}p<0.01$, $^{\#\#\#}p<0.001$, significance vs. 5-FUrd at equal concentration; n=5-50 independent experiments assayed in quadruplicates.

Moreover, these five nucleolipids were additionally tested on four further human glioma cell lines (**G28, G112, U251 and U87**) to examine if the derivatives are also effective against other human glioma cell lines with different characteristics and properties (Fig. 14-17).

Incubation of the human **G28** glioma cells with **5-FUrd** revealed a cytotoxic effect and led at the concentrations of 12.5, 25 and 50 µM to a significant ($p<0.001$) decrease by -12.8 %, -23.1 % and -35.2% compared to the negative control (Fig.14).

The treatment with derivative **S.18** significantly decreased the viability of the human **G28** glioma cells at the concentrations of 25 and 50µM by -6.9 % ($p<0.05$) and -100 % ($p<0.001$) compared to the negative control. In comparison to 5-FUrd, the incubation with **S.18** (50µM) significantly ($p<0.001$) reduced the viability of the human **G28** glioma cells by -67.6 % (Fig. 14).

Moreover, the viability of the human **G28** glioma cells was significantly ($p<0.001$) diminished through treatment with derivative **S.19** by -17.1 % (6.25 µM), -84.5 % (12.5 µM), -99.7 % (25 µM) and -98.7 % (50 µM) compared to the negative control. In comparison to 5-FUrd, the incubation with **S.19** significantly decreased the viability of the human **G28** glioma cells at the same concentrations by -18.1 % (6.25 µM, $p<0.01$), -71.7 % (12.5 µM, $p<0.001$), -76.6 % (25 µM, $p<0.001$) and -63.5 % (50 µM, $p<0.001$) (Fig. 14).

After the incubation of the human **G28** glioma cells with **S.38** the viability was significantly reduced by -3.8 % (6.25µM, $p<0.05$), -1.7 % (12.5µM, $p<0.01$), -16.5 % (25µM, $p<0.01$) and -97.5 % (60 µM, $p<0.001$) compared to the negative control. In comparison to 5-FUrd, the treatment with **S.38** significantly decreased the viability of the human **G28** glioma cells only at the concentration of 50 µM by -62.2 % ($p<0.001$) (Fig. 14).

After the incubation with **S.98** (1.56, 3.12, 6.25, 12.5, 25 or 50 µM) the viability of human **G28** glioma cells was significantly decreased by -6.0 % ($p<0.05$), -11.7 % ($p<0.001$), -47.4 % ($p<0.001$), -72.9 % ($p<0.001$), -100 % ($p<0.001$) and -98.2 % ($p<0.001$), respectively, compared to the negative control. In comparison to 5-FUrd, the treatment with **S.98** significantly reduced the viability of the human **G28** glioma cells at the same concentrations by -14.3 % (1.56 µM, $p<0.05$), -22.7 % (3.12 µM, $p<0.01$), -48.4 % (6.25 µM, $p<0.001$), -72.9 % (12.5 µM $p<0.001$), -77.3 % (25 µM, $p<0.001$) and -63.0 % (50 µM, $p<0.001$) (Fig. 14).

The incubation of the human **G28** glioma cells with derivative **S.101** resulted in a significant ($p<0.001$) inhibition of the viability by -5.9 % (6.25 µM), -22.3 % (12.5 µM), -43.4 % (25 µM) and -65.8 % (50 µM) compared to the negative control. In comparison to 5-FUrd, the treatment with **S.101** significantly reduced the viability of the human **G28** glioma cells at the concentrations of 12.5, 25 and 50 µM by -9.5 % ($p<0.01$), -20.3 % ($p<0.001$) and -30.6 % ($p<0.001$) (Fig. 14).

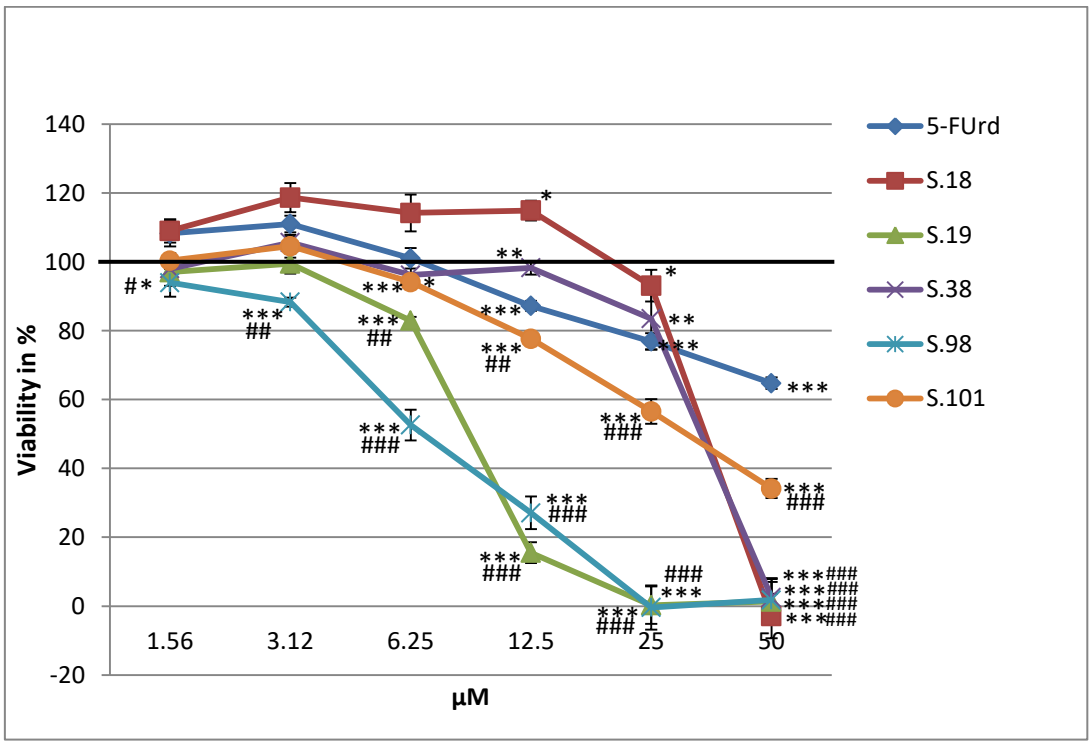

Figure 14: Viability (in %) of human G28 glioma cells after treatment (48h).
Viability (in % of the negative control) of human G28 glioma cells after 48 h incubation with 5-FUrd (positive control) or the derivatives S.18, S.19, S.38, S.98 and S.101 measured by PrestoBlue® assay. Values are given (in % viability of control [incubation with medium alone; = 100 % viability]) as mean ± SEM; *p<0.05, **p<0.01, ***p<0.001, significance vs. 0.25 % DMSO control; #p<0.05, ##p<0.01, ###p<0.001, significance vs. 5-FUrd at equal concentration; n=5 independent experiments assayed in quadruplicates.

After treatment of the human **G112** glioma cells with **5-FUrd** (12.5, 25 and 50µM) the viability was significantly ($p<0.001$) lowered by -17.0 %, -26.8 % and -39.3 % compared to the negative control (Fig. 15).

The incubation with derivative **S.18** significantly reduced the viability of the human **G112** glioma cells by -91.2 % (50 µM) compared to the negative control. In comparison to 5-FUrd, the treatment with **S.18** significantly ($p<0.001$) decreased the viability of the human **G112** glioma cells by -51.9 % (50µM) (Fig. 15).

The incubation of the human **G112** glioma cells with **S.19** (6.25, 12.5, 25 and 50µM) resulted in a significant reduction of the viability by -14.3 % ($p<0.01$), -71.2 % ($p<0.001$), -86.2 % ($p<0.001$) and -86.0 % ($p<0.001$) compared to the negative control. In comparison to 5-FUrd, the treatment with **S.19** significantly ($p<0.001$) inhibited the viability of the human **G112** glioma cells by -54.2 % (12.5 µM,), -59.4 % (25 µM) and -46.6 % (50 µM) (Fig. 15).

After the treatment with derivative **S.38** the viability of the human **G112** glioma cells was significantly diminished by -3.3 % (6.25 µM, $p<0.01$), -8.2 % (12.5 µM, $p<0.001$), -45.2 % (25 µM, $p<0.001$) and -88.2 % (50 µM, $p<0.001$) compared to the negative control. In comparison to 5-FUrd, the incubation with **S.38** significantly decreased the viability of the human **G112** glioma cells only at the concentration of 50 µM by -48.9 % ($p<0.001$) (Fig. 15).

The treatment with derivative **S.98** showed at the concentrations of 3.12, 6.25, 12.5, 25 or 50 µM a significant inhibition of the viability of the human **G112** glioma cells by -37.4 % ($p<0.01$), -49.7 % ($p<0.01$), -60.6 % ($p<0.001$), -87.1 % ($p<0.001$) and -87.5 % ($p<0.001$), respectively, compared to the negative control. In comparison to 5-FUrd, the incubation with **S.98** significantly ($p<0.001$) decreased the viability of the human **G112** glioma cells at the same concentrations by -47.8 % (3.12 µM), -45.5 % (6.25 µM), -43.6 % (12.5 µM), -60.3 % (25 µM) and -48.1 % (50 µM) (Fig. 15).

The incubation of the human **G112** glioma cells with **S.101** (6.25, 12.5, 25 or 50 µM) revealed a significant inhibition of the viability by -10.5 % ($p<0.01$), -36.6. % ($p<0.001$), -43.7 % ($p<0.001$) and -53.3 % ($p<0.001$) compared to the negative control. In comparison to 5-FUrd, the treatment with **S.101** significantly reduced the viability of the human **G112** glioma cells only at the concentrations of 12.5 and 25 µM by -19.6 % ($p<0.05$) and -16.9 % ($p<0.05$) (Fig. 15).

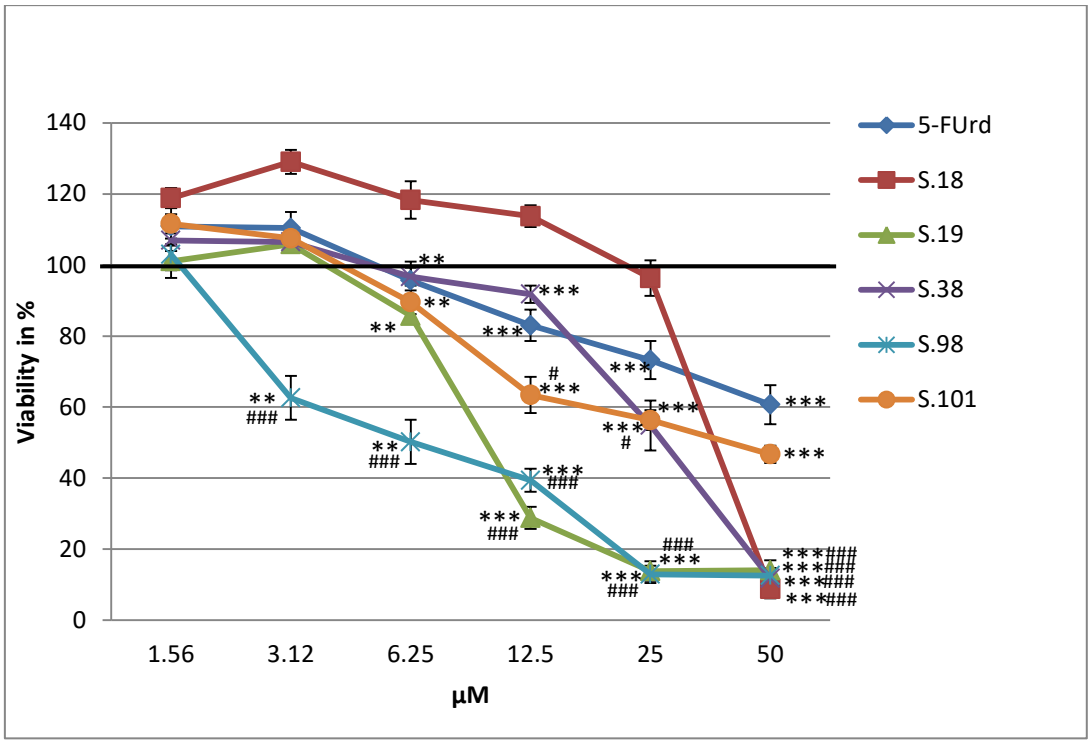

Figure 15: Viability (in %) of human G112 glioma cells after treatment (48h).
Viability (in % of the negative control) of human G112 glioma cells after 48 h incubation with 5-FUrd (positive control) or the derivatives S.18, S.19, S.38, S.98 and S.101 measured by PrestoBlue® assay. Values are given (in % viability of control [incubation with medium alone; = 100 % viability]) as mean ± SEM; **p<0.01, ***p<0.001, significance vs. 0.25 % DMSO control; ###p<0.001 significance vs. 5-FUrd at equal concentration; n=5 independent experiments assayed in quadruplicates.

After the treatment with **5-FUrd** the viability of the human **U251** glioma cells was significantly (p<0.001) reduced by -54.6 % (12.5 µM), -73.8 % (25 µM) and -82.0 % (50 µM) compared to the negative control (Fig.16).

The incubation of the human **U251** glioma cells with **S.18** (25 and 50 µM) revealed a significant (p<0.001) inhibition of the viability by -86.4 % and -98.3 % compared to the negative control. In comparison to 5-FUrd, the treatment with **S.18** (50µM) significantly reduced the viability of the human **U251** glioma cells (p<0.05) by -16.3 % (Fig. 16).

Incubation with derivative **S.19** significantly (p<0.001) decreased the viability of the human **U251** glioma cells by -86.2 % (12.5 µM), - 90.5 % (25 µM) and -91.4 % (50 µM) compared to the negative control. In comparison to 5-FUrd, the treatment with **S.19** significantly inhibited the viability of the human **U251** glioma cells at the concentrations of 12.5 and 25 µM by -31.6 % (p<0.01) and -16.8 % (p<0.05) (Fig. 16).

The incubation of the human **U251** glioma cells with **S.38** (3.12, 6.25, 12.5, 25 or 50 µM) revealed a significant reduction of the viability by -20.5 % (p<0.05), -40.9 %

(p<0.001), -43.9 % (p<0.001), -76.1 % (p<0.001) and -93.2 % (p<0.001) compared to the negative control (Fig.16).

After the treatment of the human **U251** glioma cells with **S.98** (1.56, 3.12, 6.25, 12.5, 25 or 50 µM) the viability was significantly reduced by -43.0 % (p<0.01), -49.3 % (p<0.01), -49.5 % (p<0.001), -70.5 % (p<0.01) -94.7 % (p<0.001) and -95.7 % (p<0.001), respectively, compared to the negative control. In comparison to 5-FUrd, the incubation with **S.98** significantly diminished the viability of the human **U251** glioma cells only at the concentration of 25 µM by -21.0 % (p<0.05) (Fig. 16).

Furthermore, after the treatment with derivative **S.101** the viability of the human **U251** glioma cells was significantly diminished by -40.3 % (6.25 µM, p<0.01), -38.4 % (12.5 µM, p<0.01), -41.5 % (25 µM, p<0.001) and -64.3 % (50 µM, p<0.01) compared to the negative control (Fig.16).

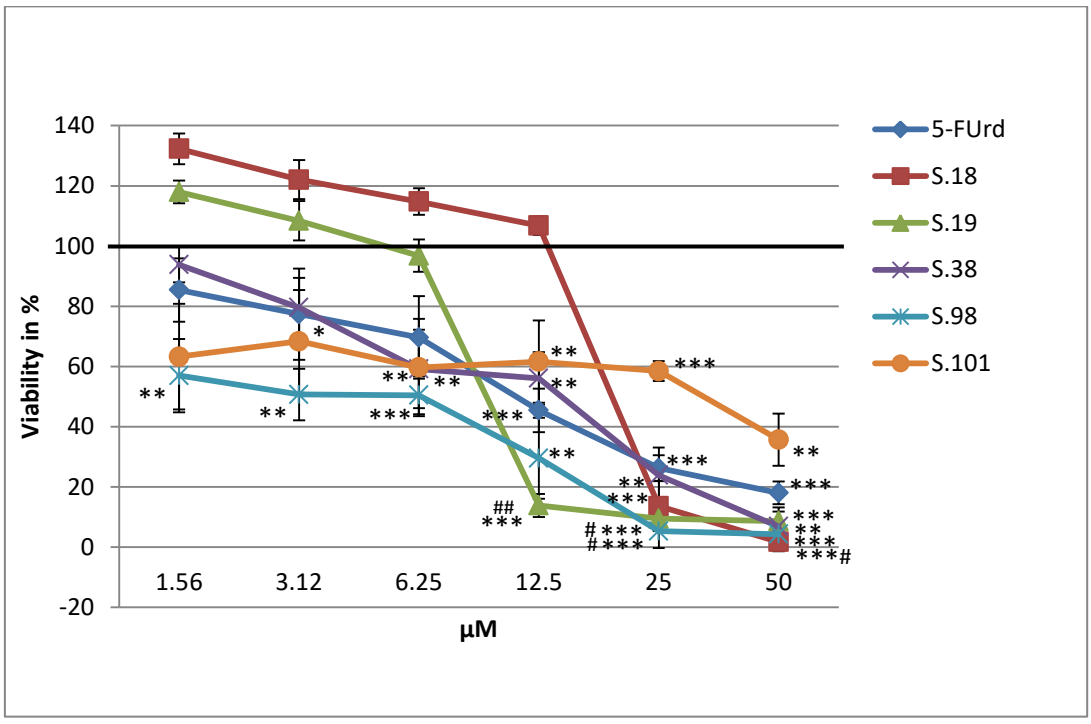

Figure 16: Viability (in %) of human U251 glioma cells after treatment (48h).
Viability (in % of the negative control) of human U251 glioma cells after 48 h incubation with 5-FUrd (positive control) or the derivatives S.18, S.19, S.38, S.98 and S.101 measured by PrestoBlue® assay. Values are given (in % viability of control [incubation with medium alone; = 100 % viability]) as mean ± SEM; *p<0.05, **p<0.01, ***p<0.001, significance vs. 0.25 % DMSO control; $^{\#}$p<0.05, $^{\#\#}$p<0.01 significance vs. 5-FUrd at equal concentration; n=5 independent experiments assayed in quadruplicates.

The incubation of the human **U87** glioma cells with **5-FUrd** revealed at all concentrations a significant ($p<0.001$) inhibition of the viability by -26.2 % (1.56 µM), -37.8 % (3.12 µM), 40.8 % (6.25 µM), 49.1 % (12.5 µM), -61.6 % (25 µM) and -66.0 % (50 µM) compared to the negative control (Fig.17).

The treatment of the human **U87** glioma cells with **S.18** led only at the concentrations of 25 and 50 µM to a significant reduction by -51.2% ($p<0.001$) and -85.0 % ($p<0.01$) in comparison to the negative control (Fig.17).

After the incubation with derivative **S.19** (12.5, 25 and 50 µM) the viability of the human **U87** glioma cells was significantly diminished by -63.5 % ($p<0.01$), -83.6 % ($p<0.001$) and -85.2 % ($p<0.01$), respectively, compared to the negative control. In comparison to 5-FUrd, the treatment with **S.19** significantly reduced the viability of the human **U87** glioma cells at the concentrations 12.5 and 25 µM by -14.3 % ($p<0.05$) and -22.0 % ($p<0.01$) (Fig. 17).

The human **U87** glioma cells showed after the incubation with **S.38** a significant decrease of the viability by -3.5 % (6.25 µM, $p<0.05$), -11.4 % (12.5 µM, $p<0.001$), -46.5 % (25 µM, $p<0.001$) and -88.5 % (50 µM, $p<0.01$) compared to the negative control. In comparison to 5-FUrd, the treatment with **S.38** significantly diminished the viability of the human **U87** glioma cells only at the concentration of 50 µM by -22.5 % ($p<0.05$) (Fig. 17).

After the incubation with **S.98** the human **U87** glioma cells revealed a significant inhibition of the viability by -23.0 % (1.56 µM $p<0.001$), -39.1 % (3.12 µM, $p<0.001$), -51.1 % (6.25 µM, $p<0.001$), -55.3 % (12.5 µM, $p<0.001$), -86.2 % (25 µM, $p<0.01$) and -90.2 % (50 µM, $p<0.01$) compared to the negative control. In comparison to 5-FUrd, the treatment with **S.98** significantly diminished the viability of the human **U87** glioma cells only at the concentrations of 25 and 50 µM by -24.6 % ($p<0.01$) and -24.3 % ($p<0.05$), respectively (Fig. 17).

The treatment of the human **U87** glioma cells with **S.101** (1.56-50 µM) led to a significant inhibition of the viability by -0.9% (1.56 µM, $p<0.001$), -8.2 % (3.12 µM, $p<0.001$),-16.4 % (6.25 µM, $p<0.001$), -32.7 % (12.5 µM, $p<0.01$), -42.0 % (25 µM, $p<0.001$) and -75.2 % (50µM, $p<0.001$) compared to the negative control (Fig.17).

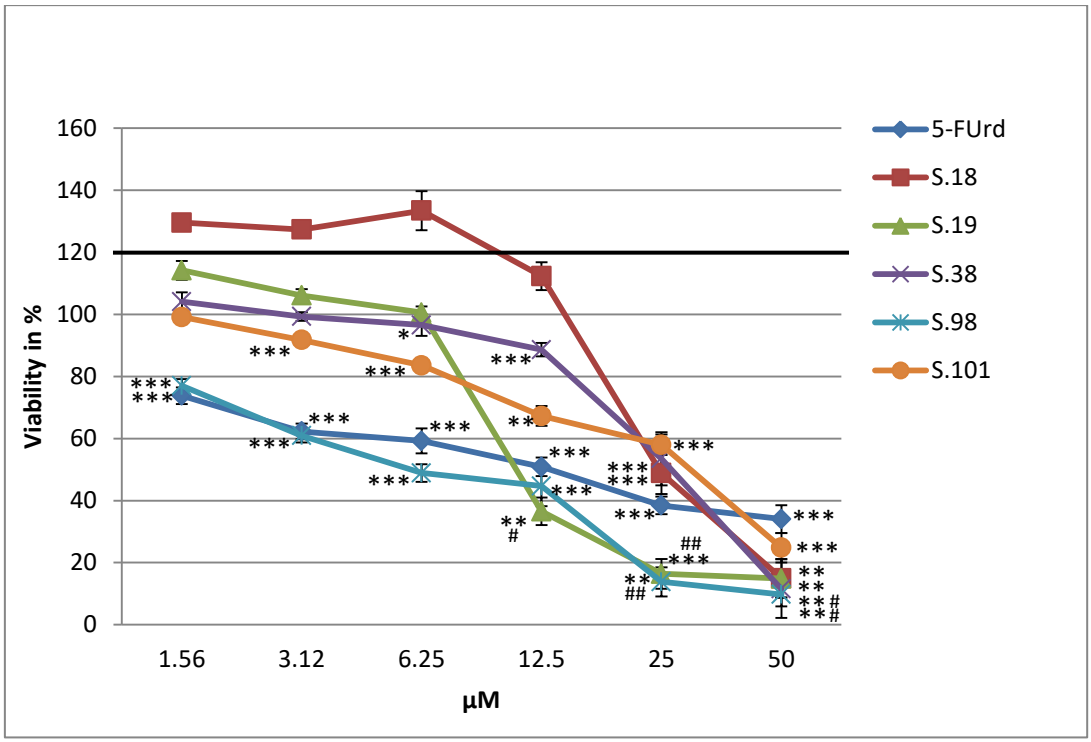

Figure 17: Viability (in %) of human U87 glioma cells after treatment (48h).
Viability (in % of the negative control) of human U87 glioma cells after 48 h incubation with 5-FUrd (positive control) or the derivatives S.18, S.19, S.38, S.98 and S.101 measured by PrestoBlue® assay. Values are given (in % viability of control [incubation with medium alone; = 100 % viability]) as mean ± SEM; *p<0.05, **p<0.01, ***p<0.001, significance vs. 0.25 % DMSO control; $^{\#}$p<0.05, $^{\#\#}$p<0.01 significance vs. 5-FUrd at equal concentration; n=5 independent experiments assayed in quadruplicates.

For the verification of a broad range of activity of these derivatives, we additionally analyzed the effects on the viability of more human tumors cells like colon (HT29), hepato (HepG2), pancreas (Panc-1) and murine renal (RenCa) carcinomas cell lines. The results for these cell lines can be found in the supplements page 147-149, Fig. 23- 26: The figures show the inhibition of the viability depending on the derivative under test, its concentration as well as the specific cell line. Comparing the derivatives, S.19 and S.98 apparently bear the most inhibitive effects on the viability of these tumor cell lines.

4.3. Cytotoxicity of the novel derivatives on different glioma cell lines

For the verification of the results documented via the viability assay, a cytotoxicity assay was performed. The cytotoxicity on all six glioma cell lines (rat **BT4Ca**, human **GOS3**, **G28**, **G112**, **U251** and **U87**) was measured after an incubation of 48 h with the derivatives at concentrations of 1.56-50 µM. All derivatives were solubilized in DMSO; hence a DMSO control was performed using medium with 0.25 % DMSO, corresponding to the concentration of DMSO in 50 µM maximal working concentration of the derivatives under test. No significant cytotoxic effect of the 0.25 % DMSO control on any researched cell type was observed (Fig. 18-23), compared to the negative control (incubation with medium alone). The cytotoxicity is calculated in % of the negative control (= 0 % cytotoxicity) and the significances are given compared to the 0.25 % DMSO control as well as to 5-FUrd.

The incubation of the rat **BT4Ca** glioma cells with **5-FUrd** significantly increased the cytotoxicity by +94.5 % (12.5 µM, $p<0.001$), +96.7 % (25 µM, $p<0.001$) and +97.5 % (50 µM, $p<0.01$) compared to the negative control (Fig. 18).

Treatment of the rat **BT4Ca** glioma cells with **S.18** revealed at the concentration 25 and 50 µM a significant ($p<0.01$) elevation of the cytotoxicity by +39.6 % and +98.3 % compared to the negative control (Fig. 18).

After the incubation with derivative **S.19** the cytotoxicity on the rat **BT4Ca** glioma cells was significantly enhanced at the concentration 12.5, 25 and 50 µM ($p<0.01$) by +43.5 %, +98.1 % and +98.5 % compared to the negative control (Fig. 18).

The treatment of rat **BT4Ca** glioma cells with **S.38** led to a significant elevation of the cytotoxicity by +36.8 % (12.5 µM, $p<0.01$), +83.1 % (25 µM, $p<0.001$) and +98.4 % (50 µM, $p<0.01$) compared to the negative control (Fig. 18).

Incubation with **S.98** significantly raised the cytotoxicity on the rat **BT4Ca** glioma cells ($p<0.01$) by +98.5 % (12.5 µM), +98.5 % (25 µM) and +98.8 % (50 µM) compared to the negative control (Fig. 18). In comparison to 5-FUrd, the treatment with **S.98** 12.5 µM significantly enhanced the cytotoxicity on the rat **BT4Ca** glioma cells ($p<0.05$) by +3.9 % (12.5 µM) (Fig. 18).

After the treatment of the rat **BT4Ca** glioma cells with **S.101** the cytotoxicity was significantly elevated by +25.6 % (12.5 µM, $p<0.01$), +53.3 % (25 µM, $p<0.01$) and +92.7 % (50 µM, $p<0.001$) compared to the negative control (Fig. 18).

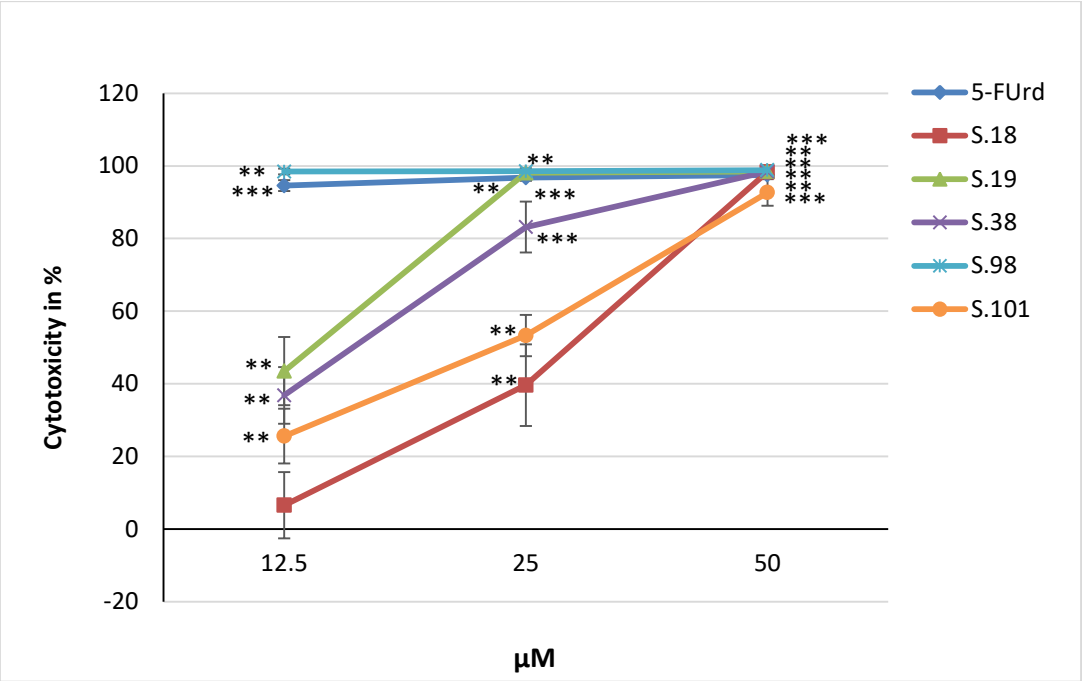

Figure 18: Cytotoxicity on rat BT4Ca glioma cells.
Cytotoxicity (in % of the neg. control) on rat BT4Ca glioma cells after treatment (48 h) with 5-FUrd (positive control) or the derivatives S.18, S.19, S.38, S.98 and S.101 measured by SRB assay. Values are given (in % cytotoxicity of negative control [incubation with medium alone = 0 % cytotoxicity]) as mean ± SEM; **p<0.01, ***p<0.001, significance vs. 0.25 % DMSO control; n=5 independent experiments assayed in quadruplicates.

Due to the treatment with **5-FUrd** the cytotoxicity on the human **GOS3** glioma cells was significantly (p<0.001) increased by +39.0 %, +40.4 % and +42.5 % at all three concentrations (12.5, 25 and 50 µM) compared to the negative control (Fig. 19).

The incubation with **S.18** showed at the concentration of 50 µM a significant raise of the cytotoxicity on the human **GOS3** glioma cells by +62.5 % (p<0.001) compared to the negative control. In comparison to 5-FUrd, the treatment with **S.18** 50 µM led to a significant (p<0.001) increase of the cytotoxicity on the human **GOS3** glioma cells by +20.1 % (Fig. 19).

The human **GOS3** glioma cells revealed after the treatment with 25 and 50 µM **S.19** a significant rise of the cytotoxicity by +89.4 % (p<0.001) and +97.9 % (p<0.01) compared to the negative control. In comparison to 5-FUrd, the incubation with the same concentrations of derivative **S.19** led to a significant increase of the cytotoxicity on the human **GOS3** glioma cells by +49.0 % (25 µM, p<0.001) and +55.4 % (50 µM p<0.01) (Fig. 19).

After the incubation with derivative **S.38** 12.5, 25 and 50 µM the cytotoxicity on the human **GOS3** glioma cells was significantly enhanced by +17.8 % (p<0.001), +23.4 %

(p<0.001) and +96.9 % (p<0.01) compared to the negative control. In comparison to 5-FUrd, only the treatment with **S.38** 50 µM significantly (p<0.01) raised the cytotoxicity on the human **GOS3** glioma cells by +54.1 % (Fig. 19).

Incubation with derivative **S.98** revealed a significant boost of the cytotoxicity on human **GOS3** glioma cells at all three concentrations (12.5, 25 and 50 µM) by +67.1 % (p<0.001), +99.5 % (p<0.01) and +97.8 % (p<0.01) compared to the negative control. In comparison to 5-FUrd, the treatment with **S.98** significantly increased the cytotoxicity on the human **GOS3** glioma cells by +28.1 % (12.5 µM, p<0.001), +59.1 % (25 µM, p<0.01) and +55.3 % (50 µM, p<0.01) (Fig. 19).

The incubation of human **GOS3** glioma cells with **S.101** led to a significant rise of the cytotoxicity by +30.9 % (12.5 µM, p<0.01), +53.0 % (25 µM, p<0.001) and +70.8 % (50 µM, p<0.001) compared to the negative control. In comparison to 5-FUrd, the treatment with **S.101** significantly (p<0.01) enhanced the cytotoxicity on the human **GOS3** glioma cells by +12.6 % (25 µM) and +28.3 % (50 µM) (Fig. 19).

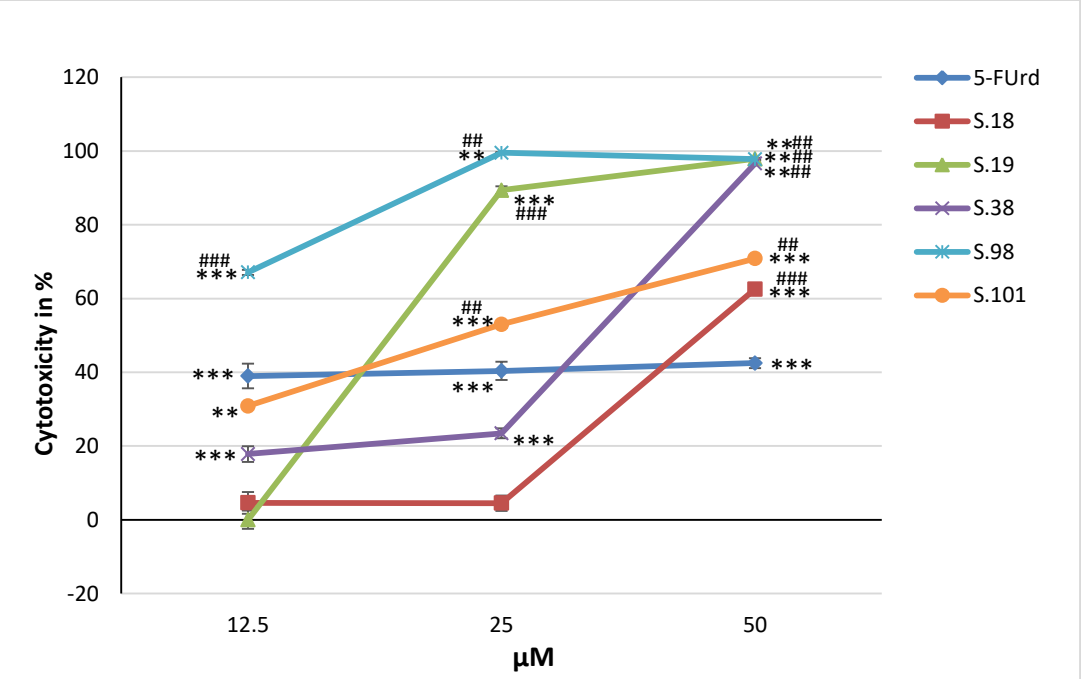

Figure 19: Cytotoxicity on human GOS3 glioma cells.
Cytotoxicity (in % of the neg. control) on human GOS3 glioma cells after treatment (48 h) with 5-FUrd (positive control) or the derivatives S.18, S.19, S.38, S.98 and S.101 measured by SRB assay. Values are given (in % cytotoxicity of negative control [incubation with medium alone = 0 % cytotoxicity]) as mean ± SEM; **p<0.01, ***p<0.001, significance vs. 0.25 % DMSO control; $^{\#\#}$p<0.01, $^{\#\#\#}$p<0.001, significance vs. 5-FUrd at equal concentration; n=5 independent experiments assayed in quadruplicates.

After the treatment with **5-FUrd** the human **G28** glioma cells also showed a significant gain of the cytotoxicity by +15.9 % (12.5 µM, $p<0.01$), +24.9 % (25 µM, $p<0.001$) and +32.1 % (50 µM, $p<0.001$) compared to the negative control (Fig. 20).

Incubation with **S.18** 50 µM revealed a rise of the cytotoxicity on the human **G28** glioma cells by +99.4 % ($p<0.001$) compared to the negative control. In comparison to 5-FUrd, the treatment with **S.18** 50 µM significantly ($p<0.001$) raised the cytotoxicity on the human **G28** glioma cells by +67.3 % (Fig. 20).

Through the treatment with **S.19** the human **G28** glioma cells revealed a significant ($p<0.001$) boost of the cytotoxicity by +91.2 % (12.5 µM), +99.9 % (25 µM) and +99.5 % (50 µM) compared to the negative control. In comparison to 5-FUrd, the incubation with **S.19** (12.5, 25 and 50µM) significantly ($p<0.001$) enhanced the cytotoxicity on the human **G28** glioma cells by +75.3 %, +75.0 % and +67.4 % (Fig. 20).

The human **G28** glioma cells showed after the treatment with **S.38** (25 and 50 µM) a significant ($p<0.001$) enhanced cytotoxicity by +82.8 % and +99.4 % compared to the negative control. In comparison to 5-FUrd, the incubation with **S.38** led at the same concentrations to a significant ($p<0.001$) increase of the cytotoxicity on the human **G28** glioma cells by +58.0 % (25 µM) and +67.2 % (50 µM) (Fig. 20).

After incubation with **S.98**, the human **G28** glioma cells revealed a significant ($p<0.001$) elevated cytotoxicity of +84.7 % (12.5 µM) and +100 % (25 and 50 µM) compared to the negative control. In comparison to 5-FUrd, the treatment with all concentrations of **S.98** (12.5, 25 and 50 µM) significantly ($p<0.001$) raised the cytotoxicity on the human **G28** glioma cells by +68.8 %, +75.5 % and +68.0 % (Fig. 20).

The cytotoxicity on the human **G28** glioma cells was significantly ($p<0.001$) increased by +24.8 %, +58.6 % and +74.1 % after the treatment with **S.101** (12.5, 25 and 50 µM) compared to the negative control. In comparison to 5-FUrd, the incubation with **S.101** revealed a significant elevation of the cytotoxicity on the human **G28** glioma cells by +33.7 % (25 µM, $p<0.01$) and +42.0 % (50 µM, $p<0.001$) (Fig. 20).

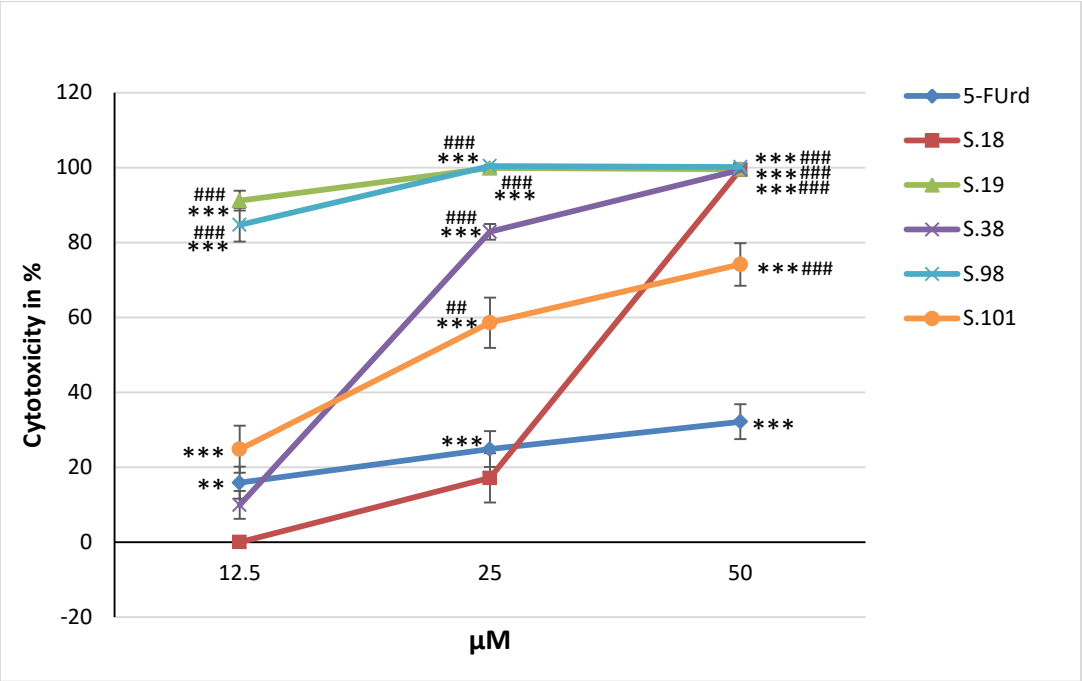

Figure 20: Cytotoxicity on human G28 glioma cells.
Cytotoxicity (in % of the neg. control) of human G28 glioma cells after treatment (48 h) with 5-FUrd (positive control) or the derivatives S.18, S.19, S.38, S.98 and S.101 measured by SRB assay. Values are given (in % cytotoxicity of negative control [incubation with medium alone = 0 % cytotoxicity]) as mean ± SEM; **p<0.01, ***p<0.001, significance vs. 0.25 % DMSO control; $^{\#\#}$p<0.01, $^{\#\#\#}$p<0.001, significance vs. 5-FUrd at equal concentration; n=5 independent experiments assayed in quadruplicates.

After the treatment with **5-FUrd** (12.5, 25 and 50 µM) the human **G112** glioma cells revealed a significant (p<0.001) increase of cytotoxicity by +35.4 %, +48.6 and +55.0% compared to the negative control (Fig. 21).

Incubation with derivative **S.18** significantly (p<0.001) enhanced the cytotoxicity on the human **G112** glioma cells by +31.6 % (25 µM) and +99.5 % (50 µM) compared to the negative control. In comparison to 5-FUrd, the treatment with 50 µM **S.18** significantly increased the cytotoxicity on the human **G112** glioma cells by +44.5 % (p<0.001) (Fig. 21).

After the treatment with **S.19** the human **G112** glioma cells showed a significant (p<0.001) elevated cytotoxicity by +98.0 % (12.5 µM), +100 % (25 µM) and +99.7 % (50 µM) compared to the negative control. In comparison to 5-FUrd, incubation with all three concentrations of **S.19** led to a significant (p<0.001) enhancement of the cytotoxicity on the human **G112** glioma cells by +62.6 %, +51.8 % and +44.6 % (Fig. 21).

After the incubation of the human **G112** glioma cells with **S.38** 25 and 50 µM the cytotoxicity was significantly (p<0.001) raised by +68.9 % and +99.7 % compared to the

negative control. In comparison to 5-FUrd, only the treatment with 50 µM **S.38** significantly ($p<0.001$) increased the cytotoxicity on the human **G112** glioma cells by +44.7 % (Fig. 21).

The treatment with derivative **S.98** 12.5, 25 and 50 µM led to a significant ($p<0.001$) boost of the cytotoxicity on the human **G112** glioma cells by +89.8 %, +100 % and +96.9 % compared to the negative control. In comparison to 5-FUrd, the incubation with all three concentrations of **S.98** significantly ($p<0.001$) raised the cytotoxicity on the human **G112** glioma cells by +54.4 %, +51.5 % and +41.9 % (Fig. 21).

After the treatment with **S.101** the human **G112** glioma cells showed a significant ($p<0.001$) rise of the cytotoxicity by +36.6 % (12.5 µM), +61.6 % (25 µM) and +87.3 % (50µM) compared to the negative control. In comparison to 5-FUrd, only the incubation with 50 µM **S.101** significantly ($p<0.001$) increased the cytotoxicity on the human **G112** glioma cells by +32.3 % (Fig. 21).

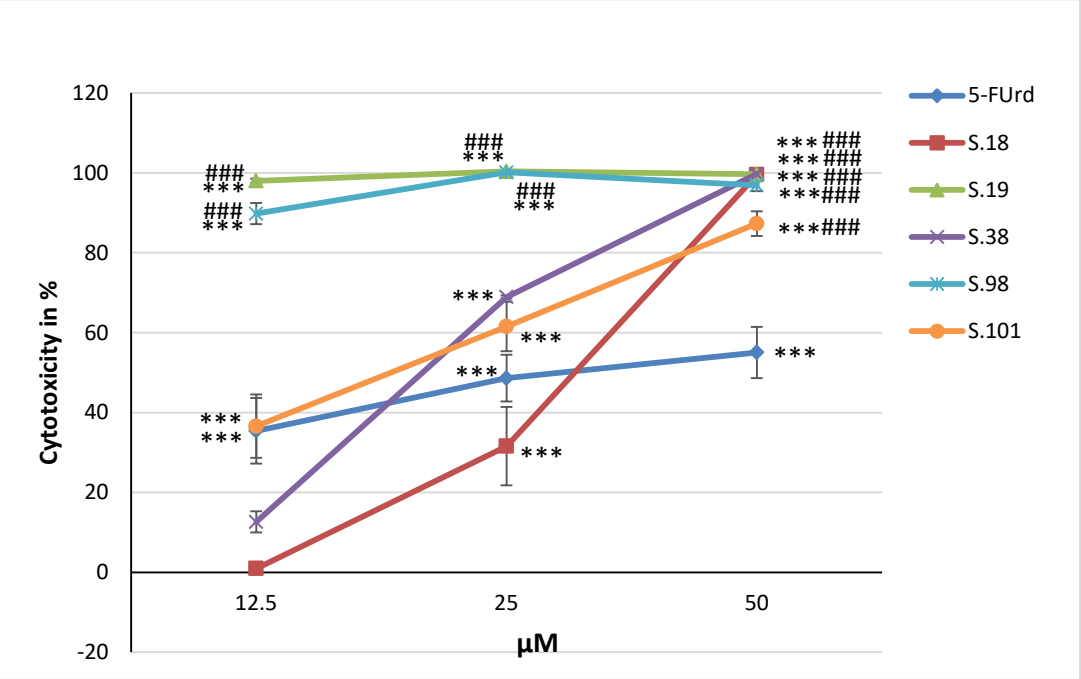

Figure 21: Cytotoxicity on human G112 glioma cells.
Cytotoxicity (in % of the neg. control) on human G112 glioma cells after treatment (48 h) with 5-FUrd (positive control) or the derivatives S.18, S.19, S.38, S.98 and S.101 measured by SRB assay. Values are given (in % cytotoxicity of negative control [incubation with medium alone = 0 % cytotoxicity]) as mean ± SEM; ***$p<0.001$, significance vs. 0.25 % DMSO control; $^{###}p<0.001$, significance vs. 5-FUrd at equal concentration; n=5 independent experiments assayed in quadruplicates.

Through the treatment with **5-FUrd** the cytotoxicity on the human **U251** glioma cells was significantly ($p<0.001$) enhanced by +90.7 % (12.5 µM), +97.4 % (25 µM) and +96.7 % (50 µM) compared to the negative control (Fig. 22).

The human **U251** glioma cells revealed a significant ($p<0.001$) boost of the cytotoxicity by +91.6 % and +93.9% after treatment with 25 or 50 µM of **S.18**, compared to the negative control (Fig. 22).

After the incubation with derivative **S.19** the cytotoxicity on the human **U251** glioma cells was significantly ($p<0.001$) increased by +97.3 % (12.5 µM), +100 % (25 µM) and +99.4 % (50 µM) compared to the negative control (Fig. 22).

The human **U251** glioma cells showed a significant boost of the cytotoxicity by +79.0 % (12.5 µM, $p<0.01$), +100 % (25 µM, $p<0.001$) and +98.8 % (50 µM, $p<0.001$) after the treatment with **S.38**, compared to the negative control (Fig. 22).

The treatment with **S.98** showed a significant ($p<0.001$) enhanced cytotoxicity on the human **U251** glioma cells by +91.4 % (12.5 µM) and +100 % (25 and 50 µM) compared to the negative control (Fig. 22).

Incubation of the human **U251** glioma cells with **S.101** 12.5, 25 and 50 µM led to a significant rise of the cytotoxicity by +69.5 % ($p<0.01$), +95.9% ($p<0.001$) and +95.9 % ($p<0.001$) compared to the negative control (Fig. 22).

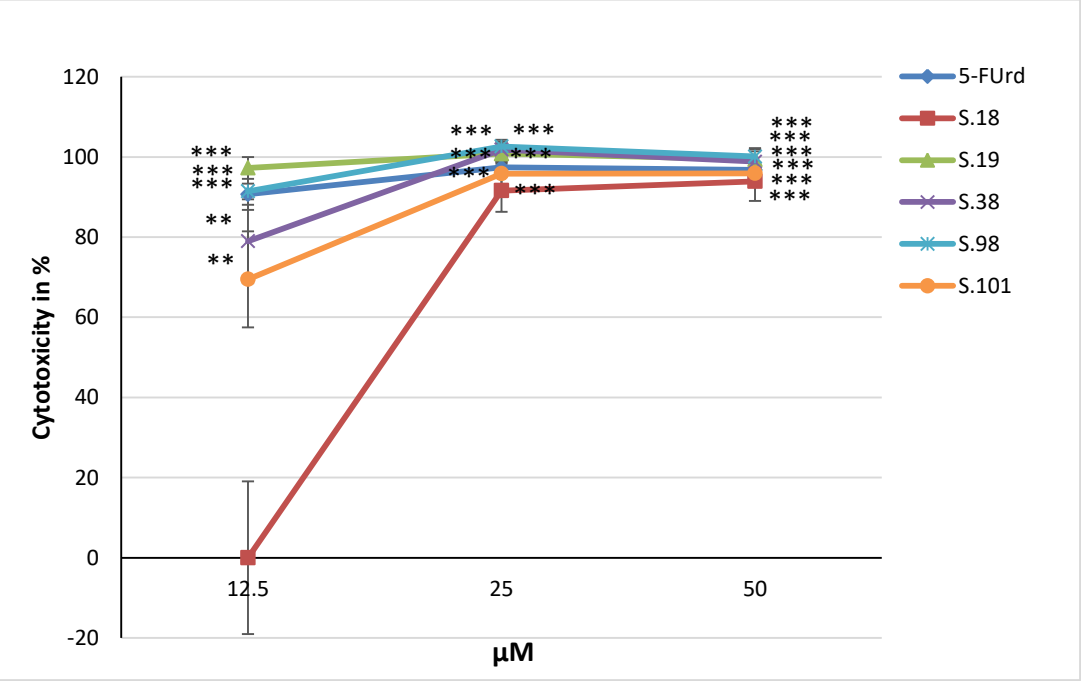

Figure 22: Cytotoxicity on human U251 glioma cells.
Cytotoxicity (in % of the neg. control) on human U251 glioma cells after treatment (48 h) with 5-FUrd (positive control) or the derivatives S.18, S.19, S.38, S.98 and S.101 measured by SRB assay. Values are given (in % cytotoxicity of negative control [incubation with medium alone = 0 % cytotoxicity]) as mean ± SEM; **p<0.01, ***p<0.001, significance vs. 0.25 % DMSO control; n=5 independent experiments assayed in quadruplicates.

The incubation of the human **U87** glioma cells with **5-FUrd** 12.5, 25 and 50 µM resulted in a significant ($p<0.001$) boost of the cytotoxicity by +85.9 %, +92.0 % and +92.4 % compared to the negative control (Fig. 23).

After the treatment with **S.18** the human **U87** glioma cells showed a significant elevation of the cytotoxicity by +8.8 % (12.5 µM, $p<0.05$), +66.8 % (25 µM, $p<0.01$) and +100 % (50 µM, $p<0.001$) compared to the negative control. In comparison to 5-FUrd, only the incubation with 50 µM **S.18** led to a significant ($p<0.01$) increase of the cytotoxicity on the human **U87** glioma cells by +8.4 % (Fig. 23).

The human **U87** glioma cells showed a significant ($p<0.001$) increase of the cytotoxicity by +92.8 % (12.5 µM) and +100 % (25 and 50 µM) after the incubation with **S.19,** compared to the negative control. In comparison to 5-FUrd, the treatment with **S.19** 25 and 50 µM significantly ($p<0.01$) raised the cytotoxicity on the human **U87** glioma cells by +9.1% and +8.7 % (Fig. 23).

After the incubation with derivative **S.38** (12.5, 25 and 50 µM) the cytotoxicity was significantly increased by +26.9 % ($p<0.01$), +69.5 % ($p<0.01$) and +100 % ($p<0.001$) compared to the negative control. In comparison to 5-FUrd, only the treatment with 50 µM **S.38** significantly enhanced the cytotoxicity on the human **U87** glioma cells by +8.7 % ($p<0.01$) (Fig. 23).

The treatment of the human **U87** glioma cells with **S.98** revealed a significant ($p<0.001$) elevation of the cytotoxicity by +88.4 % (12.5 µM) and +100 % (25 and 50 µM) compared to the negative control. In comparison to 5-FUrd, incubation with **S.98** 25 and 50 µM significantly ($p<0.01$) increased the cytotoxicity on the human **U87** glioma cells by +9.2% and +8.4 % (Fig. 23).

After the treatment with **S.101** the human **U87** glioma cells revealed a significant ($p<0.001$) enhancement of the cytotoxicity by +64.8 (12.5 µM), +80.2 % (25 µM) and +95.8 % (50 µM) compared to the negative control (Fig. 23).

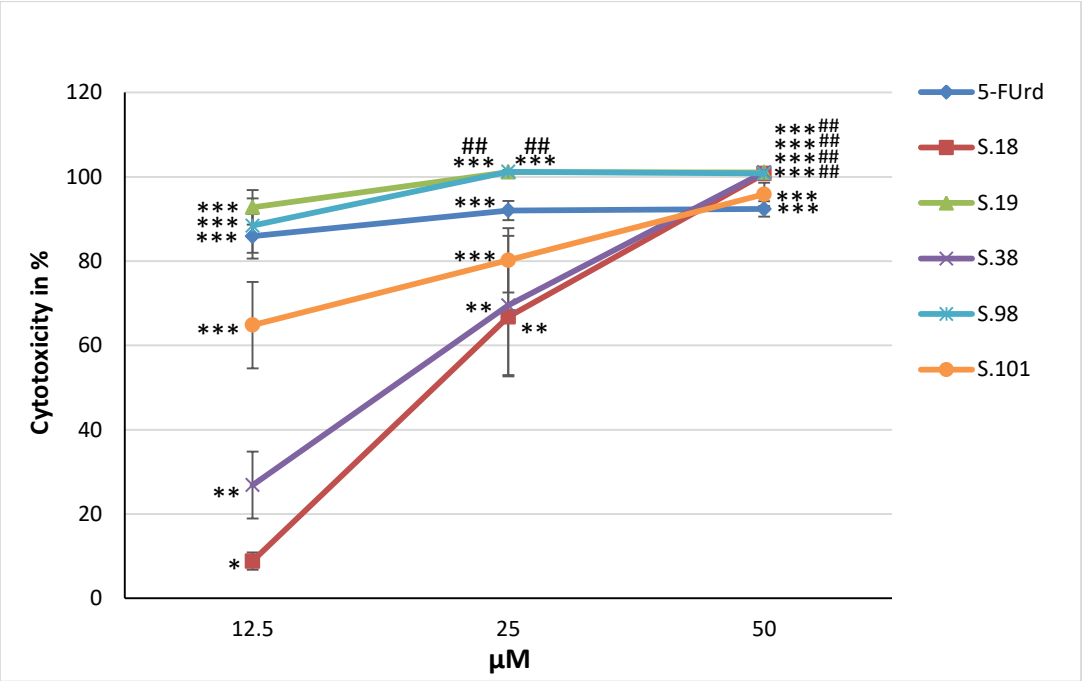

Figure 23: Cytotoxicity on human U87 glioma cells.
Cytotoxicity (in % of the neg. control) on human U87 glioma cells after treatment (48 h) with 5-FUrd (positive control) or the derivatives S.18, S.19, S.38, S.98 and S.101 measured by SRB assay. Values are given (in % cytotoxicity of negative control [incubation with medium alone = 0 % cytotoxicity]) as mean ± SEM; as mean ± SEM; *p<0.05, **p<0.01, ***p<0.001, significance vs. 0.25 % DMSO control; ##p<0.01 significance vs. 5-FUrd at equal concentration; n=5 independent experiments assayed in quadruplicates.

4.4. Effects of the novel derivatives on the induction of apoptosis or necrosis

4.4.1. Effects of the novel derivatives on the rate of apoptotic and necrotic cells

For the analysis of the induction of apoptosis or necrosis a triple staining with YO-PRO®-1, propidium iodine (PI) and Hoechst 33342 (H) was performed. The induction of apoptosis and necrosis in rat **BT4Ca** glioma cells was measured after an incubation of 48 h with the derivatives under test at a concentration range of 12.5-50 µM; the pro-apoptotic camptothecin (1 µM) was used as a positive control.

All derivatives were solubilized in DMSO; hence a DMSO control was performed using medium with 0.25 % DMSO, corresponding to the concentration of DMSO in 50 µM maximal working concentration of the derivatives under test.

Incubation of rat **BT4Ca** glioma cells with 0.25 % DMSO did not significantly affect the cell amount compared to the negative control (incubation with medium alone) (Fig. 24). The incubation of the rat **BT4Ca** glioma cells with 1 µM camptothecin resulted in a

significant decrease of the cell amount by -48.5 % (p<0.001) compared to the negative control (Fig. 24). The treatment with **5-FUrd** 12.5, 25 and 50 µM revealed a significant (p<0.001) loss of the rat **BT4Ca** glioma cells by -67.4 %, -69.6 % and -71.1 % compared to the negative control. In comparison to camptothecin (apoptosis positive control), the incubation with **5-FUrd** significantly reduced the amount of the rat **BT4Ca** glioma cells by -18.9 % (12.5µM, p<0.01), -21.1 % (25µM, p<0.001) and -22.6 % (50µM, p<0.001) (Fig. 24).

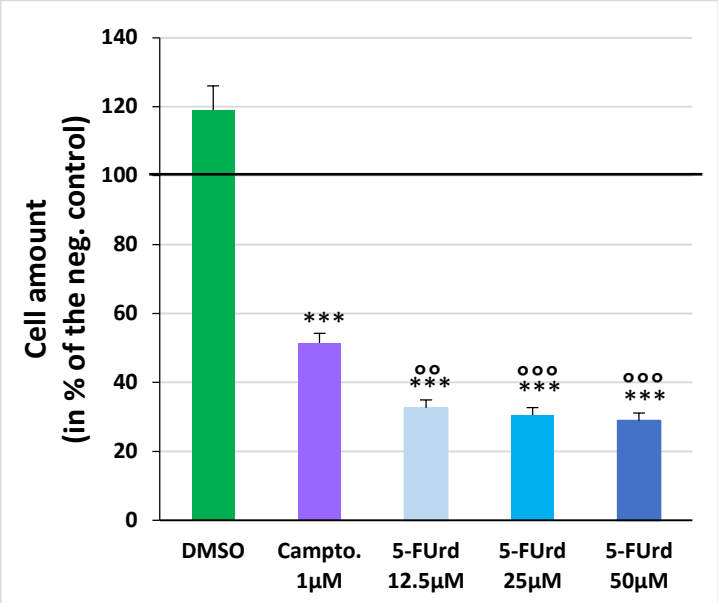

Figure 24: Cell amount of rat BT4Ca glioma cells after treatment with 5-FUrd.
Cell amount of rat BT4Ca glioma cells after 48 h incubation with 5-FUrd, DMSO 0.25 % and camptothecin, determined by measuring the Hoechst fluorescence at Ex.355/Em.465 nm. Values are given (in % cells of neg. control [incubation with medium alone; = 100 %]) as mean +SEM; ***p<0.001 significance vs. 0.25 % DMSO control; °°p<0.01, °°°p<0.001 significance vs. 1µM camptothecin (apoptosis positive control); n=5 independent experiments assayed in quadruplicates

Incubation of rat **BT4Ca** glioma cells with 0.25 % DMSO did not significantly affect the apoptotic cell rate compared to the negative control (Fig. 25). The incubation of rat **BT4Ca** glioma cells with the camptothecin (1 µM) induced a significant (p<0.01) +2.15-fold increase of the apoptotic cell rate compared to the negative control (Fig. 25). The incubation of the rat **BT4Ca** glioma cells with **5-FUrd** 12.5, 25 and 50 µM revealed a significant boost of the apoptotic cell rate by +3.08- (p<0.001), +3.31- (p<0.001) and +3.42-fold (p<0.01) compared to the negative control. In comparison to camptothecin, the treatment with 25 and 50 µM **5-FUrd** significantly (p<0.05) raised the rate of apoptotic rat **BT4Ca** glioma cells by +1.54- and +1.60-fold (Fig. 25).

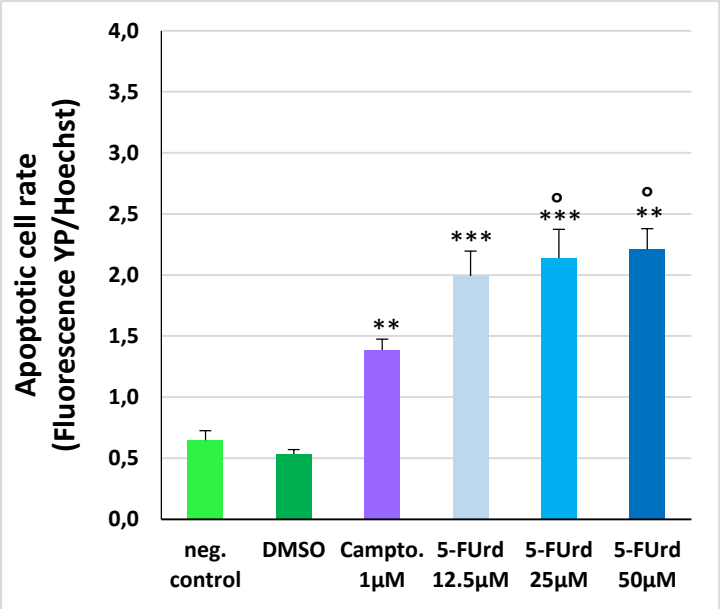

Figure 25: Apoptotic cell rate of rat BT4Ca glioma cells after treatment with 5-FUrd.
Rate of apoptotic cells measured by fluorometric quantification of YO-PRO®-1 normalized with Hoechst in rat BT4Ca glioma cells after 48 h treatment with 5-FUrd, DMSO 0.25 % and camptothecin. Values are given in fluorescence intensity ratio of YO-PRO®-1 (Ex.535/Em.617 nm) / Hoechst (Ex.355/Em.465 nm) as mean + SEM; **p<0.01, ***p<0.001 significance vs. 0.25 % DMSO control; °p<0.05 significance vs. 1µM camptothecin (apoptosis positive control); n=5 independent experiments assayed in quadruplicates.

Incubation of rat **BT4Ca** glioma cells with 0.25 % DMSO did not significantly affect the necrotic cell rate compared to the negative control (incubation with medium alone) (Fig. 26). The incubation with camptothecin (1 µM) showed a significant ($p<0.05$) increase of the necrotic rat **BT4Ca** glioma cell rate by +3.75-fold compared to the negative control (Fig. 26). The treatment of the rat **BT4Ca** glioma cells with 12.5, 25 or 50 µM **5-FUrd** led to a significant increase of the necrotic cell rate by +4.16- ($p<0.001$), +4.45- ($p<0.01$) and +5.52-fold ($p<0.001$) compared to the negative control. Moreover, incubation of rat **BT4Ca** glioma cells with 50 µM **5-FUrd** significantly ($p<0.01$) raised the rate of necrotic cells +1.47-fold in comparison to camptothecin (Fig. 26).

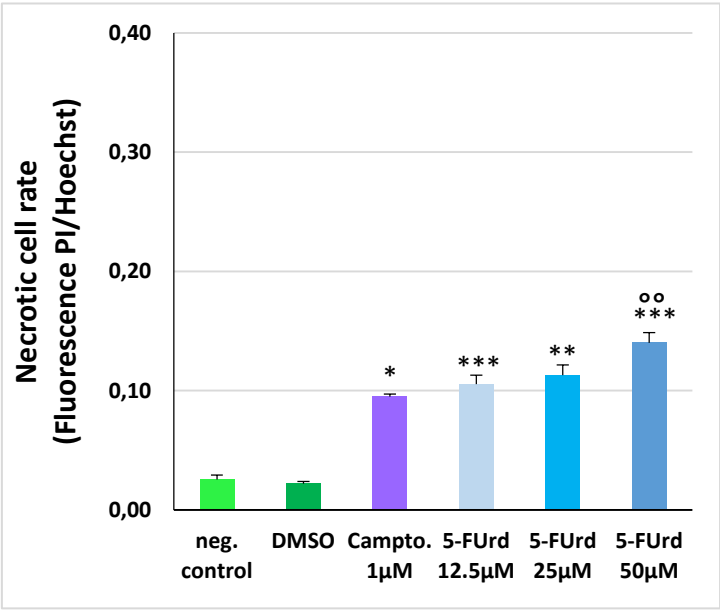

Figure 26: Necrotic cell rate of rat BT4Ca glioma cells after treatment with 5-FUrd.
Rate of necrotic cells measured by fluorometric quantification of PI normalized with Hoechst in rat BT4Ca glioma cells after treatment with 5-FUrd, DMSO 0.25 % and camptothecin. Values are given in fluorescence intensity ratio of PI (Ex.350/Em.462 nm) / Hoechst (Ex.355/Em.465 nm) as mean + SEM; *p<0.05, **p<0.01, ***p<0.001 significance vs. 0.25 % DMSO control; °°p<0.01 significance vs. 1µM camptothecin (apoptosis positive control); n=5 independent experiments assayed in quadruplicates.

The treatment of the rat **BT4Ca** glioma cells with **S.18** 25 or 50 µM significantly ($p<0.001$) decreased the cell amount by -50.7 %, and -72.8 % compared to the negative control. The incubation with 12.5 µM **S.18** did not show any significant effects on the rat **BT4Ca** glioma cells. In comparison to camptothecin, only the treatment of rat **BT4Ca** glioma cells with 50µM **S.18** significantly ($p<0.05$) reduced the cell amount by -24.3 % (Fig. 27).

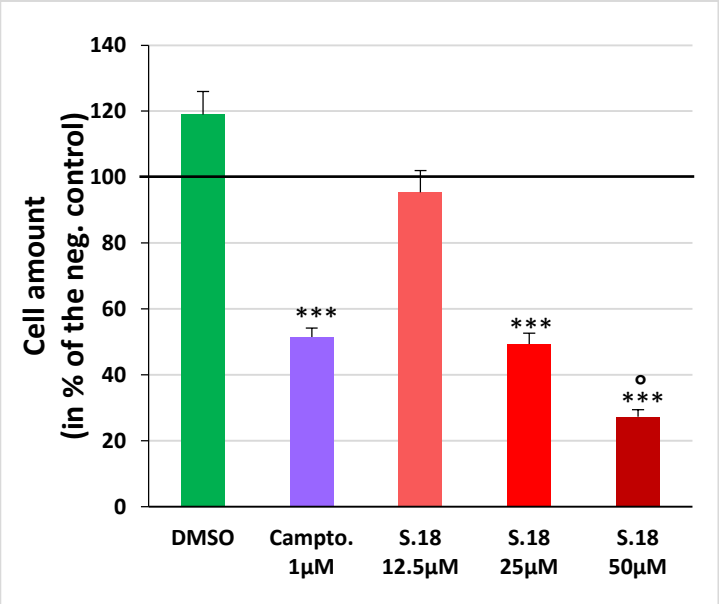

Figure 27: Cell amount in rat BT4Ca glioma cells after treatment with S.18.
Cell amount of rat BT4Ca glioma cells after 48 h incubation with S.18, DMSO 0.25 % and camptothecin, determined by measuring the Hoechst fluorescence at Ex.355/Em.465 nm. Values are given (in % cells of neg. control [incubation with medium alone; = 100 %]) as mean +SEM; ***$p<0.001$ significance vs. 0.25 % DMSO control; °°$p<0.01$, °°°$p<0.001$ significance vs. 1µM camptothecin (apoptosis positive control); n=5 independent experiments assayed in quadruplicates

Treatment of the rat **BT4Ca** glioma cells with **S.18** 25 and 50 µM showed a significant increase of the apoptotic cell rate by +2.03- ($p<0.01$) and +3.64-fold ($p<0.001$) compared to the negative control. The incubation with 12.5 µM **S.18** did not show any significant effects on the rat **BT4Ca** glioma cells. In comparison to camptothecin the treatment of the rat **BT4Ca** glioma cells with **S.18** raised only at the concentrations of 50 µM the rate of apoptotic cells significantly ($p<0.001$) by +1.7-fold (Fig. 28).

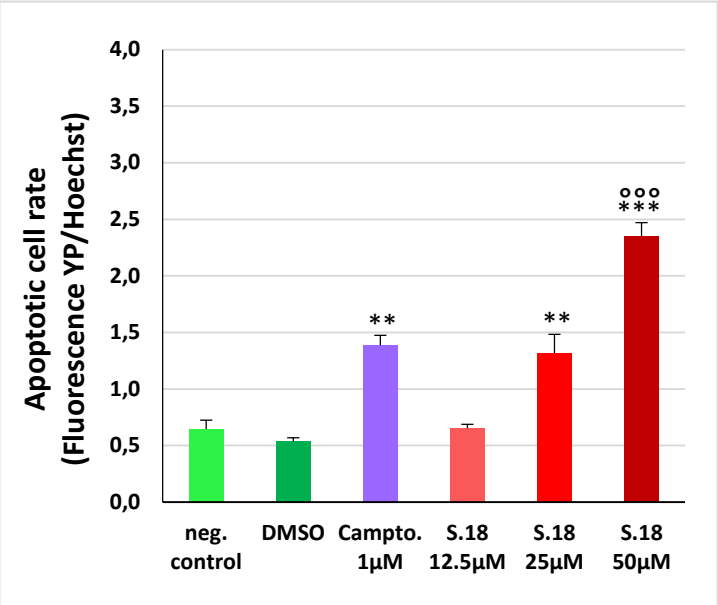

Figure 28: Apoptotic cell rate of rat BT4Ca glioma cells after treatment with S.18.
Rate of apoptotic cells measured by fluorometric quantification of YO-PRO®-1 normalized with Hoechst in rat BT4Ca glioma cells after 48 h treatment with S.18, DMSO 0.25 % and camptothecin. Values are given in fluorescence intensity ratio of YO-PRO®-1 (Ex.535/Em.617 nm) / Hoechst (Ex.355/Em.465 nm) as mean + SEM; **p<0.01, ***p<0.001 significance vs. 0.25 % DMSO control; °p<0.05 significance vs. 1µM camptothecin (apoptosis positive control); n=5 independent experiments assayed in quadruplicates.

The incubation of the rat **BT4Ca** glioma cells with **S.18** 25 and 50 µM induced a significant boost of the necrotic rate by +2.27- (p<0.01) and +6.15-fold (p<0.001) compared to the negative control. The treatment with 12.5 µM **S.18** did not show any significant effects on the rat **BT4Ca** glioma cells. In comparison to camptothecin, the incubation of the rat **BT4Ca** glioma cells with **S.18** showed at the concentrations of 50 µM a significant (p<0.001) rise of the necrotic rate by +1.64-fold (Fig. 29).

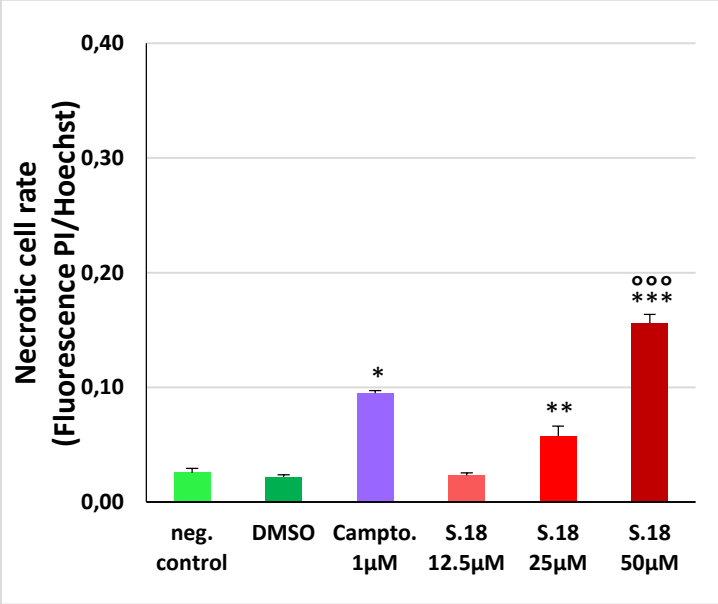

Figure 29: Necrotic cell rate of rat BT4Ca glioma cells after treatment with S.18.
Rate of necrotic cells measured by fluorometric quantification of PI normalized with Hoechst in rat BT4Ca glioma cells after treatment with 5-FUrd, DMSO 0.25 % and camptothecin. Values are given in fluorescence intensity ratio of PI (Ex.350/Em.462 nm) / Hoechst (Ex.355/Em.465 nm) as mean + SEM; *p<0.05, **p<0.01, ***p<0.001 significance vs. 0.25 % DMSO control; °°p<0.01 significance vs. 1µM camptothecin (apoptosis positive control); n=5 independent experiments assayed in quadruplicates.

The incubation of the rat **BT4Ca** glioma cells with **S.19** 12.5, 25 and 50 µM revealed a significant (p<0.001) loss of the cell amount by -40.3 %, -72.4 % and -62.3 % compared to the negative control. In comparison to camptothecin, only the treatment of the rat

BT4Ca glioma cells with 25 µM **S.19** significantly (p<0.001) decreased the cell amount by -23.9 % (Fig. 30).

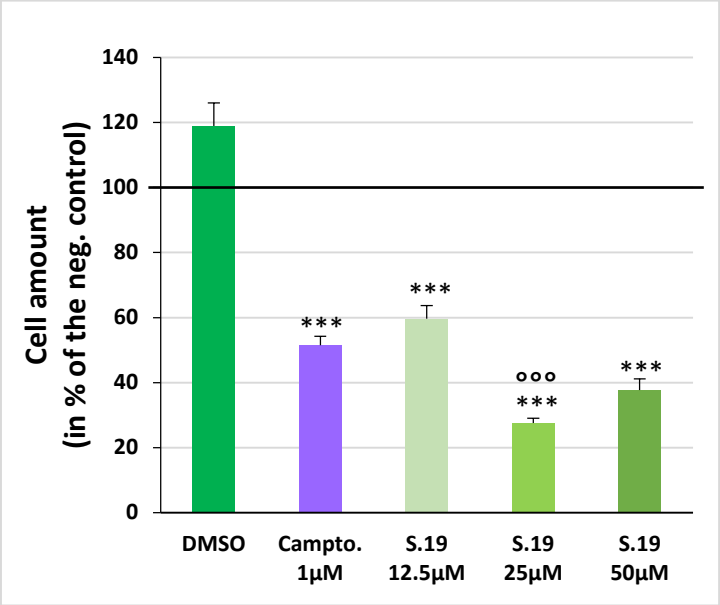

Figure 30: Cell amount in rat BT4Ca glioma cells after treatment with S.19.
Cell amount of rat BT4Ca glioma cells after 48 h incubation with S.19, DMSO 0.25 % and camptothecin, determined by measuring the Hoechst fluorescence at Ex.355/Em.465 nm. Values are given (in % cells of neg. control [incubation with medium alone; = 100 %]) as mean +SEM; ***p<0.001 significance vs. 0.25 % DMSO control; °°p<0.01, °°°p<0.001 significance vs. 1µM camptothecin (apoptosis positive control); n=5 independent experiments assayed in quadruplicates

The treatment of the rat **BT4Ca** glioma cells with **S.19** 12.5, 25 and 50 µM raised the apoptotic rate significantly by +1.80- (p<0.05), +3.85- (p<0.001) and +2.68-fold (p<0.001) compared to the negative control. In comparison to camptothecin, incubation with **S.19** (25 and 50 µM) significantly (p<0.05) enhanced the rate of the apoptotic rat **BT4Ca** glioma cells by +1.79- and +1.25-fold (Fig. 31).

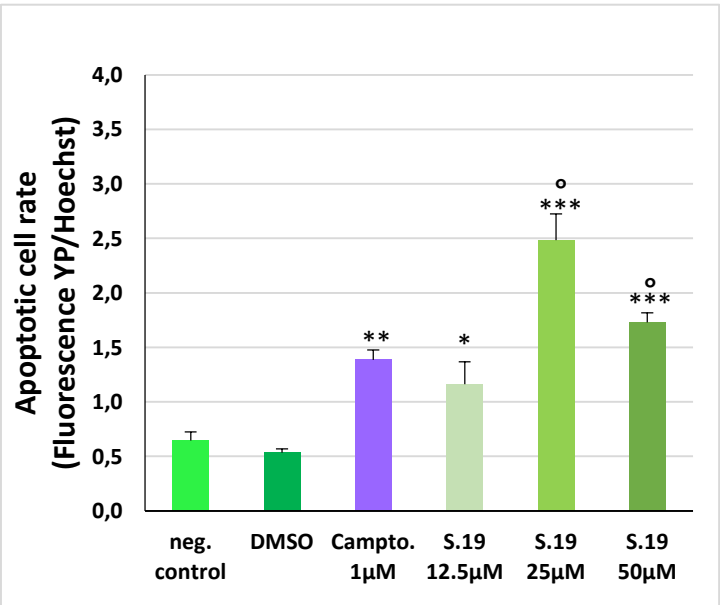

Figure 31: Apoptotic cell rate of rat BT4Ca glioma cells after treatment with S.19.
Rate of apoptotic cells measured by fluorometric quantification of YO-PRO®-1 normalized with Hoechst in rat BT4Ca glioma cells after 48 h treatment with S.19, DMSO 0.25 % and camptothecin. Values are given in fluorescence intensity ratio of YO-PRO®-1 (Ex.535/Em.617 nm) / Hoechst (Ex.355/Em.465 nm) as mean + SEM; **p<0.01, ***p<0.001 significance vs. 0.25 % DMSO control; °p<0.05 significance vs. 1µM camptothecin (apoptosis positive control); n=5 independent experiments assayed in quadruplicates.

The incubation of the rat **BT4Ca** glioma cells with **S.19** 25 and 50 µM induced a significant boost of the necrotic rate by +9.45- ($p<0.001$) and +5.89-fold ($p<0.01$) compared to the negative control. The treatment with 12.5 µM **S.19** did not show any significant effects on the rat **BT4Ca** glioma cells. In comparison to camptothecin, incubation of the rat **BT4Ca** glioma cells with **S.19** (25 and 50 µM) revealed a significant increase of the necrotic rate by +2.52- ($p<0.001$) and +1.57-fold ($p<0.05$). Additionally, compared to 5-FUrd the incubation with **S.19** 25 µM led to a significant ($p<0.001$) enhancement of the necrotic rate of the rat **BT4Ca** glioma cells by +2.12-fold (Fig. 32).

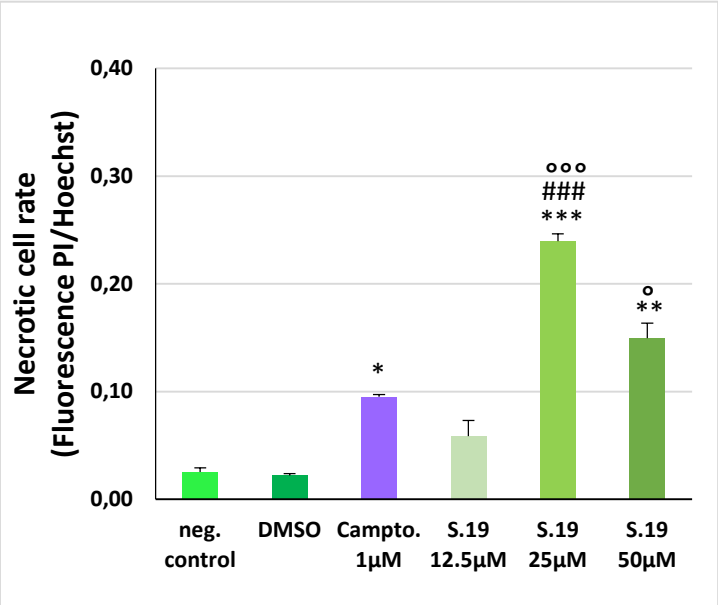

Figure 32: Necrotic cell rate of rat BT4Ca glioma cells after treatment with S.19.
Rate of necrotic cells measured by fluorometric quantification of PI normalized with Hoechst in rat BT4Ca glioma cells after treatment with 5-FUrd, DMSO 0.25 % and camptothecin. Values are given in fluorescence intensity ratio of PI (Ex.350/Em.462 nm) / Hoechst (Ex.355/Em.465 nm) as mean + SEM; *$p<0.05$, **$p<0.01$, ***$p<0.001$ significance vs. 0.25 % DMSO control; °°$p<0.01$ significance vs. 1µM camptothecin (apoptosis positive control); n=5 independent experiments assayed in quadruplicates.

The incubation of the rat **BT4Ca** glioma cells with **S.38** 25 and 50 µM showed a significant decrease of the cell amount by -53.9 % ($p<0.01$) and -74.8 % ($p<0.001$) compared to the negative control. The treatment with 12.5 µM **S.38** did not show any significant effects on the rat **BT4Ca** glioma cells. In comparison to camptothecin, only the incubation with 50 µM **S.38** significantly ($p<0.001$) lowered the cell amount of the rat **BT4Ca** glioma cells by -26.3 % (Fig. 33).

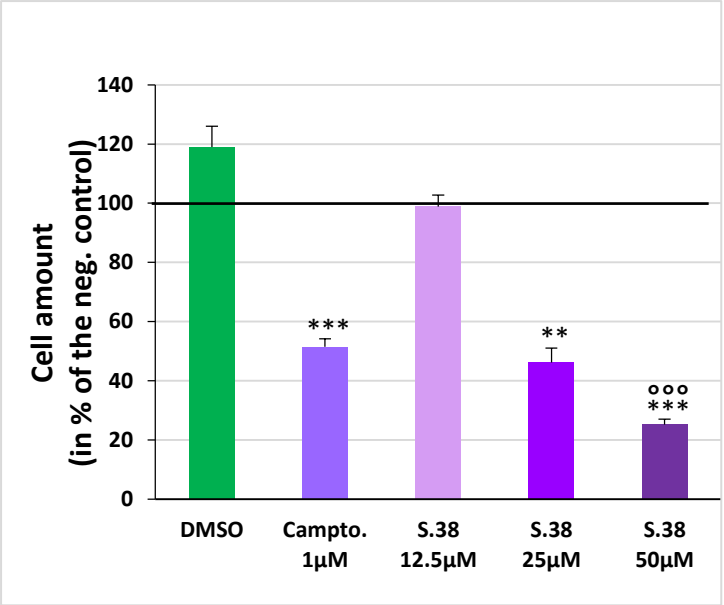

Figure 33: Cell amount in rat BT4Ca glioma cells after treatment with S.38.
Cell amount of rat BT4Ca glioma cells after 48 h incubation with S.38, DMSO 0.25 % and camptothecin, determined by measuring the Hoechst fluorescence at Ex.355/Em.465 nm. Values are given (in % cells of neg. control [incubation with medium alone; = 100 %]) as mean +SEM; ***p<0.001 significance vs. 0.25 % DMSO control; °°p<0.01, °°°p<0.001 significance vs. 1µM camptothecin (apoptosis positive control); n=5 independent experiments assayed in quadruplicates

The treatment of the rat **BT4Ca** glioma cells with **S.38** 25 and 50 µM significantly raised the apoptotic rate by +2.47- ($p<0.05$) and +4.01-fold ($p<0.01$) compared to the negative control. Incubation with 12.5 µM **S.38** did not show any significant effects on the rat **BT4Ca** glioma cells. In comparison to camptothecin, the treatment with **S.38** significantly ($p<0.01$) increased only at the concentrations of 50 µM the rate of apoptotic rat **BT4Ca** glioma cells by +1.87-fold (Fig. 34).

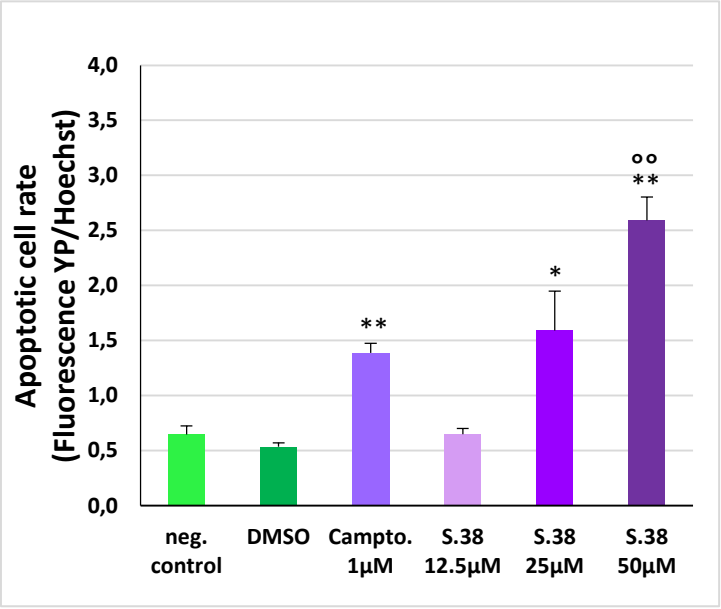

Figure 34: Apoptotic cell rate of rat BT4Ca glioma cells after treatment with S.38.
Rate of apoptotic cells measured by fluorometric quantification of YO-PRO®-1 normalized with Hoechst in rat BT4Ca glioma cells after 48 h treatment with S.38, DMSO 0.25 % and camptothecin. Values are given in fluorescence intensity ratio of YO-PRO®-1 (Ex.535/Em.617 nm) / Hoechst (Ex.355/Em.465 nm) as mean + SEM; **p<0.01, ***p<0.001 significance vs. 0.25 % DMSO control; °p<0.05 significance vs. 1µM camptothecin (apoptosis positive control); n=5 independent experiments assayed in quadruplicates.

The incubation of the rat **BT4Ca** glioma cells with **S.38** 50 µM induced a significant boost of the necrotic rate by +9.54-fold ($p<0.01$) compared to the negative control. The treatment with 12.5 and 25 µM **S.38** did not show any significant effects on the rat **BT4Ca** glioma cells. In comparison to camptothecin, incubation with **S.38** 50µM revealed a significant enhancement of the necrotic rate of the rat **BT4Ca** glioma cells by +2.55-fold ($p<0.001$). Additionally, compared to 5-FUrd (Fig. 26), the treatment with **S.38** 50 µM led to a significant ($p<0.001$) increase of the necrotic rate of the rat **BT4Ca** glioma cells by +1.73-fold (Fig. 35).

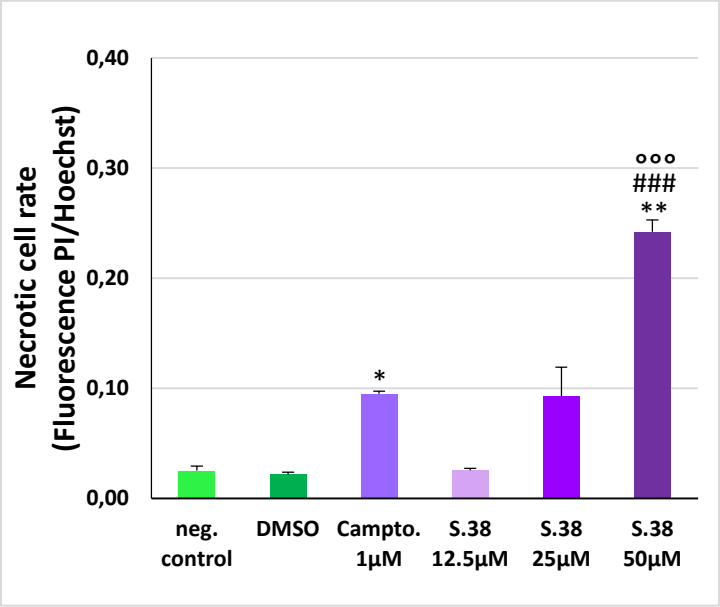

Figure 35: Necrotic cell rate of rat BT4Ca glioma cells after treatment with S.38.
Rate of necrotic cells measured by fluorometric quantification of PI normalized with Hoechst in rat BT4Ca glioma cells after treatment with 5-FUrd, DMSO 0.25 % and camptothecin. Values are given in fluorescence intensity ratio of PI (Ex.350/Em.462 nm) / Hoechst (Ex.355/Em.465 nm) as mean + SEM; *$p<0.05$, **$p<0.01$, ***$p<0.001$ significance vs. 0.25 % DMSO control; °°$p<0.01$ significance vs. 1µM camptothecin (apoptosis positive control); n=5 independent experiments assayed in quadruplicates.

The incubation of the rat **BT4Ca** glioma cells with **S.98** 12.5, 25 and 50 µM revealed a significant ($p<0.001$) loss of the cell amount by -63.6 %, -77.1 % and -76.2 % compared to the negative control. In comparison to camptothecin, the treatment with **S.98** (12.5, 25 and 50 µM) significantly decreased the cell amount of the rat **BT4Ca** glioma cells by -15.1 % ($p<0.05$), -28.6 % ($p<0.001$) and -27.7 % ($p<0.001$) (Fig. 36). Moreover, compared to 5-FUrd, (Fig. 24) incubation with **S.98** 25 µM led to a significant ($p<0.001$) decrease of cell amount of the rat **BT4Ca** glioma cells by -7.5 % (Fig. 36).

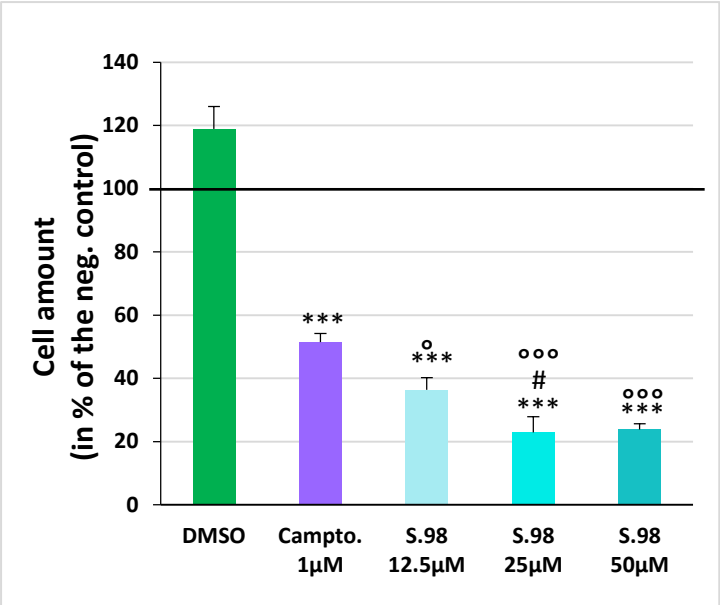

Figure 36: Cell amount in rat BT4Ca glioma cells after treatment with S.98.
Cell amount of rat BT4Ca glioma cells after 48 h incubation with S.98, DMSO 0.25 % and camptothecin, determined by measuring the Hoechst fluorescence at Ex.355/Em.465 nm. Values are given (in % cells of neg. control [incubation with medium alone; = 100 %]) as mean +SEM; ***p<0.001 significance vs. 0.25 % DMSO control; °°p<0.01, °°°p<0.001 significance vs. 1µM camptothecin (apoptosis positive control); n=5 independent experiments assayed in quadruplicates

The treatment of the rat **BT4Ca** glioma cells with **S.98** 12.5, 25 and 50 µM led to a significant rise of the apoptotic rate by +3.19- (p<0.01), +4.67- (p<0.001) and +4.47-fold (p<0.001) compared to the negative control. In comparison to camptothecin, the incubation with 25 and 50 µM **S.98** significantly (p<0.05) increased the rate of apoptotic rat **BT4Ca** glioma cells by +2.17- and +2.08-fold (Fig. 37).

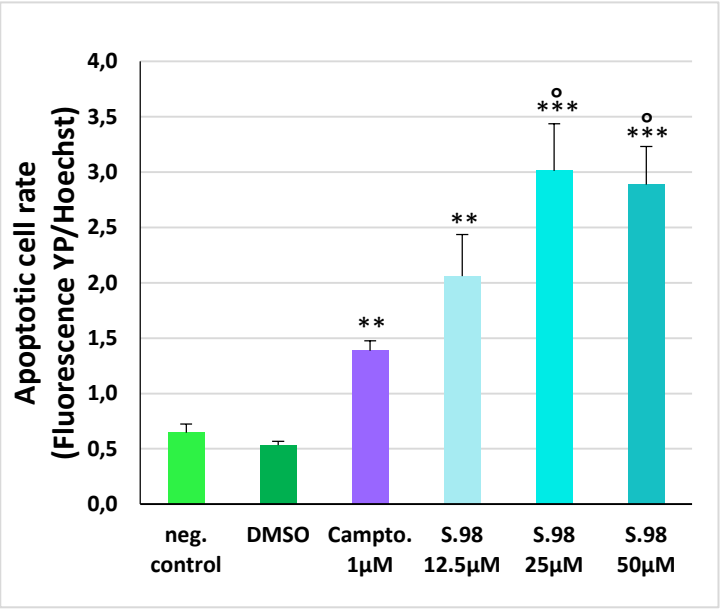

Figure 37: Apoptotic cell rate of rat BT4Ca glioma cells after treatment with S.98.
Rate of apoptotic cells measured by fluorometric quantification of YO-PRO®-1 normalized with Hoechst in rat BT4Ca glioma cells after 48 h treatment with S.98, DMSO 0.25 % and camptothecin. Values are given in fluorescence intensity ratio of YO-PRO®-1 (Ex.535/Em.617 nm) / Hoechst (Ex.355/Em.465 nm) as mean + SEM; **p<0.01, ***p<0.001 significance vs. 0.25 % DMSO control; °p<0.05 significance vs. 1µM camptothecin (apoptosis positive control); n=5 independent experiments assayed in quadruplicates.

The incubation of the rat **BT4Ca** glioma cells with **S.98** 12.5, 25 and 50 µM revealed a significant boost of the necrotic rate by +7.78- ($p<0.001$), +10.98- ($p<0.001$) and +11.78-fold ($p<0.01$) compared to the negative control. In comparison to camptothecin, the treatment of the rat **BT4Ca** glioma cells with **S.98** revealed at all three concentrations (12.5, 25 and 50 µM) a significant rise of the necrotic rate by +2.08- ($p<0.05$), +2.93- ($p<0.001$) and +3.14-fold ($p<0.05$). Additionally, compared to 5-FUrd (Fig. 26), the incubation with **S.98** (12.5, 25 and 50 µM) led to a significant ($p<0.001$) increase of the necrotic rate of the rat **BT4Ca** glioma cells by +1.87- ($p<0.05$), +2.47- ($p<0.001$) and +2.13-fold ($p<0.001$) (Fig. 38).

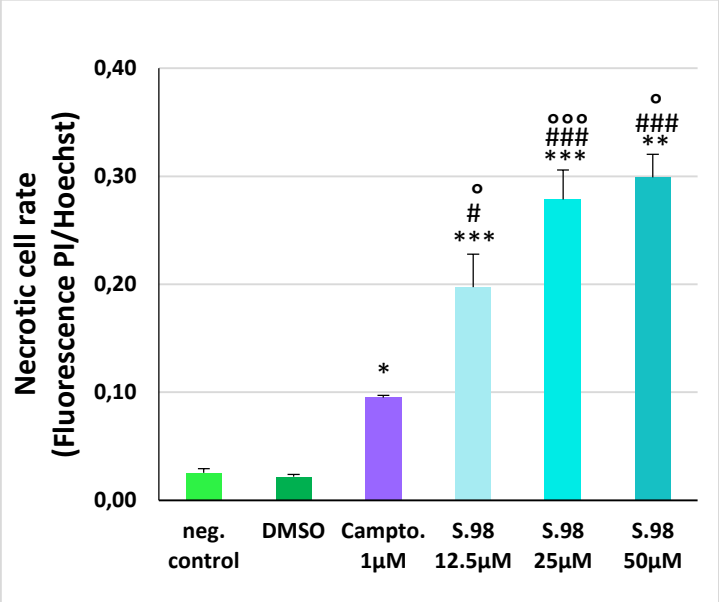

Figure 38: Necrotic cell rate of rat BT4Ca glioma cells after treatment with S.98.
Rate of necrotic cells measured by fluorometric quantification of PI normalized with Hoechst in rat BT4Ca glioma cells after treatment with 5-FUrd, DMSO 0.25 % and camptothecin. Values are given in fluorescence intensity ratio of PI (Ex.350/Em.462 nm) / Hoechst (Ex.355/Em.465 nm) as mean + SEM; *$p<0.05$, **$p<0.01$, ***$p<0.001$ significance vs. 0.25 % DMSO control; °°$p<0.01$ significance vs. 1µM camptothecin (apoptosis positive control); n=5 independent experiments assayed in quadruplicates.

The treatment of the rat **BT4Ca** glioma cells with **S.101** 12.5, 25 and 50 µM led to a significant decrease of the cell amount by -19.4 % ($p<0.01$), -41.2 % ($p<0.001$) and -60.0 % ($p<0.001$) compared to the negative control. In comparison to camptothecin, only incubation with 50 µM **S.101** showed a significant loss of the rat **BT4Ca** glioma cells by -11.5 % ($p<0.05$) (Fig. 39).

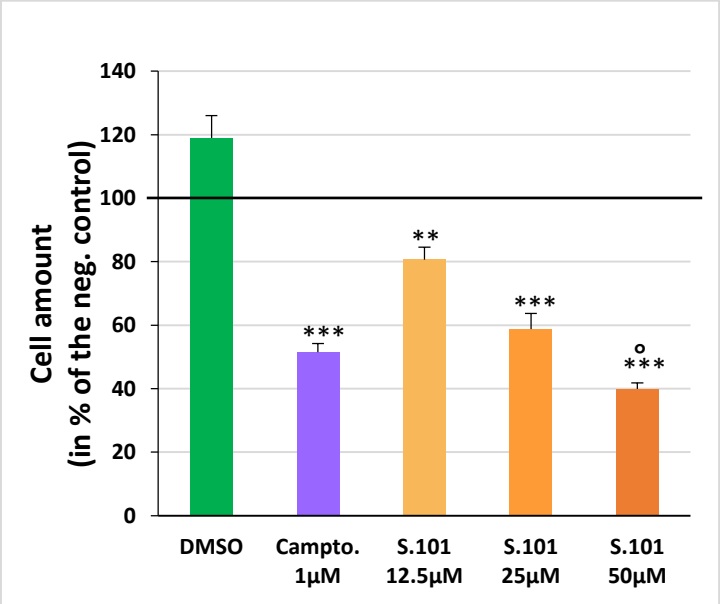

Figure 39: Cell amount in rat BT4Ca glioma cells after treatment with S.101.
Cell amount of rat BT4Ca glioma cells after 48 h incubation with S.101, DMSO 0.25 % and camptothecin, determined by measuring the Hoechst fluorescence at Ex.355/Em.465 nm. Values are given (in % cells of neg. control [incubation with medium alone; = 100 %]) as mean +SEM; ***p<0.001 significance vs. 0.25 % DMSO control; °°p<0.01, °°°p<0.001 significance vs. 1µM camptothecin (apoptosis positive control); n=5 independent experiments assayed in quadruplicates

The incubation of the rat **BT4Ca** glioma cells with **S.101** 12.5, 25 and 50 µM showed a significant (p<0.001) boost of the apoptotic rate by +1.25-, +1.74- and +2.49-fold compared to the negative control. In comparison to camptothecin, the treatment with **S.101** (12.5, 25 and 50 µM did not show any significant effects on the rat **BT4Ca** glioma cells (Fig. 40).

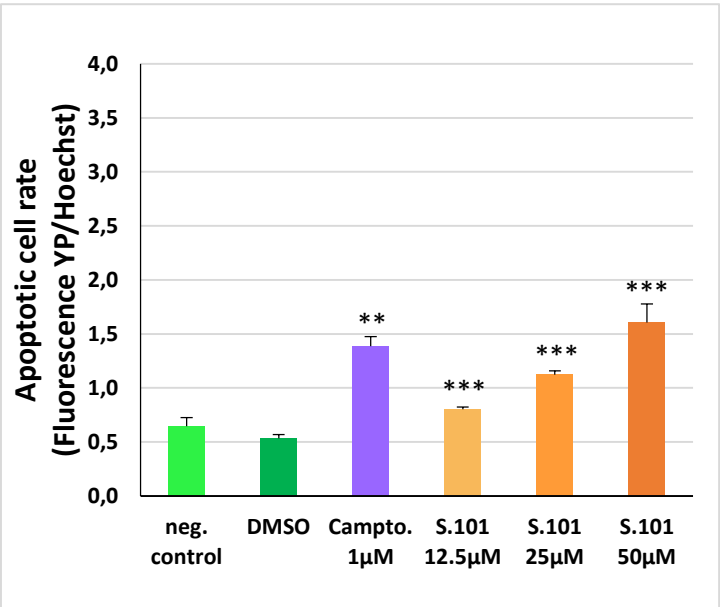

Figure 40: Apoptotic cell rate of rat BT4Ca glioma cells after treatment with S.101.
Rate of apoptotic cells measured by fluorometric quantification of YO-PRO®-1 normalized with Hoechst in rat BT4Ca glioma cells after 48 h treatment with S.101, DMSO 0.25 % and camptothecin. Values are given in fluorescence intensity ratio of YO-PRO®-1 (Ex.535/Em.617 nm) / Hoechst (Ex.355/Em.465 nm) as mean + SEM; **p<0.01, ***p<0.001 significance vs. 0.25 % DMSO control; °p<0.05 significance vs. 1µM camptothecin (apoptosis positive control); n=5 independent experiments assayed in quadruplicates.

The treatment of the rat **BT4Ca** glioma cells with **S.101** 12.5, 25 and 50 µM revealed a significant increase of the necrotic rate by +1.20- ($p<0.05$), +1.62- ($p<0.001$) and +2.26-fold ($p<0.05$) compared to the negative control. In comparison to camptothecin, incubation with **S.101** had no significant effects on the necrotic rate of the rat **BT4Ca** glioma cells at all three concentrations (12.5, 25 and 50 µM) (Fig. 41).

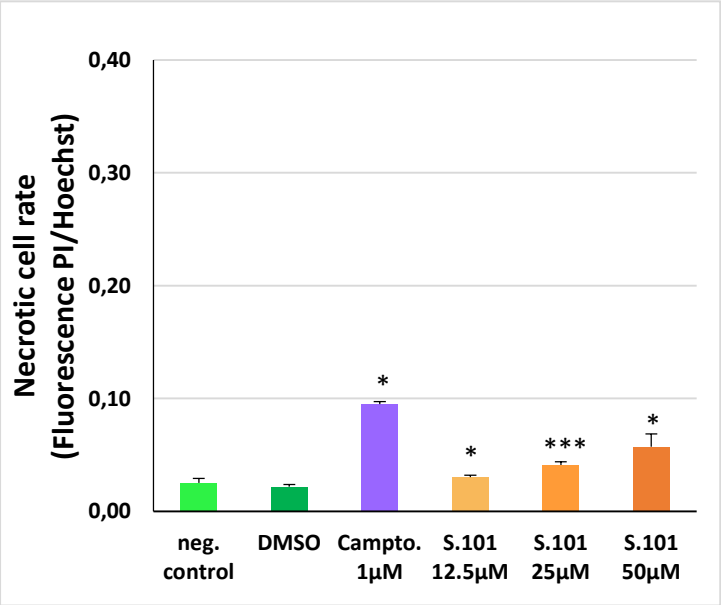

Figure 41: Necrotic cell rate rat BT4Ca glioma cells after treatment with S.101.
Rate of necrotic cells measured by fluorometric quantification of PI normalized with Hoechst in rat BT4Ca glioma cells after treatment with 5-FUrd, DMSO 0.25 % and camptothecin. Values are given in fluorescence intensity ratio of PI (Ex.350/Em.462 nm) / Hoechst (Ex.355/Em.465 nm) as mean + SEM; *p<0.05, **p<0.01, ***p<0.001 significance vs. 0.25 % DMSO control; °°p<0.01 significance vs. 1µM camptothecin (apoptosis positive control); n=5 independent experiments assayed in quadruplicates.

The pictures and evaluation of the second measuring technique (see description methods 3.3.1), showing that the measurements of the cytation are confirmed, can be found in the supplements S.150- 163 (Fig. 27-39).

4.4.2. Effects of the novel derivatives on the active caspase 3 activity

For the characterization of the induction of apoptosis, the activity of the key protein caspase 3 was determined. Hence the activity of caspase 3 in the rat **BT4Ca** glioma cells was estimated after an incubation of 48 h with the derivatives at a concentration range of 12.5-50 µM. The pro-apoptotic camptothecin (1 µM) was used as positive control.

At the end of the treatment (48 h) the rat **BT4Ca** glioma cells were additionally counterstained with Hoechst 33342 without exchanging the medium, so no apoptotic cells were lost. The fluorescence was measured at 350 nm excitation/462 nm emission. The detected DEVD fluorescence was normalized against the Hoechst 33342 fluorescence

and the caspase activity was calculated in % of the negative control (= 0 % activity). All derivatives were solubilized in DMSO; hence a DMSO control was performed using medium with 0.25 % DMSO, corresponding to the concentration of DMSO in 50 µM maximal working concentration of the derivatives under test.

After the incubation of the rat **BT4Ca** glioma cells with 0.25 % DMSO no significant effect on the activation of caspase 3 was observed, compared to the negative control (incubation with medium alone = 0 % activity of caspase 3) (Fig. 42-47).

The treatment of the rat **BT4Ca** cells with **1 µM camptothecin** significantly ($p<0.05$) increased the caspase 3 activity by +50.8 % compared to the negative control (Fig. 42).

The treatment of rat **BT4Ca** glioma cells with 12.5, 25 or 50 µM **5-FUrd** revealed a significant ($p<0.001$) increase of the caspase 3 activity by +82.3 %, +90.8 % and +91.0 % compared to the negative control. Incubation of rat **BT4Ca** glioma cells with 12.5, 25 or 50 µM 5-FUrd showed also a significant ($p<0.001$) increase of the caspase 3 activity by +31.5 %, +39.9 % and +40.2 % compared to camptothecin (Fig. 42).

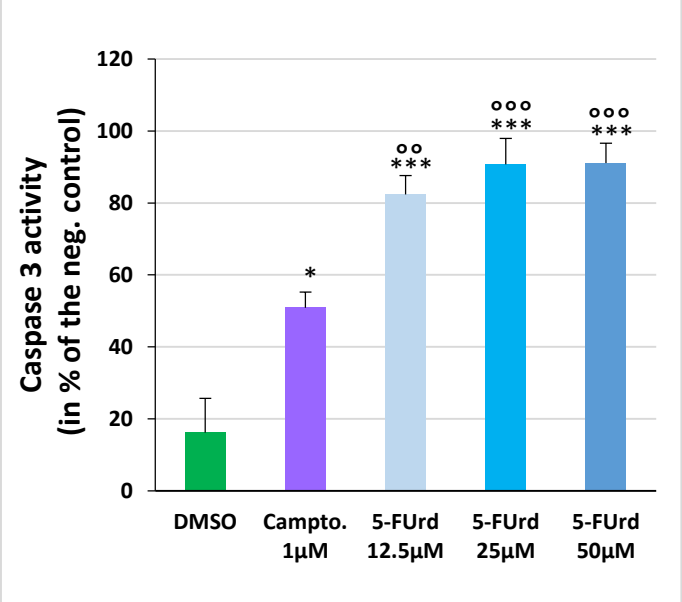

Figure 42: Caspase 3 activity of rat BT4Ca glioma cells after treatment with 5-FUrd.
Caspase 3 activity measured by fluorometric quantification of DEVD (Ex.502/Em.530 nm) normalized with Hoechst (Ex.355/Em.465 nm) in rat BT4Ca glioma cells after 48 h incubation with 5-FUrd, DMSO 0.25 % and camptothecin. Values are given (in % activity of neg. control [incubation with medium alone; = 0 % activity]) as mean + SEM; *$p<0.05$, ***$p<0.001$, significance vs. 0.25 % DMSO control, °°$p<0.01$, °°°$p<0.001$, significance vs. 1µM camptothecin (apoptosis positive control); n=5 independent experiments assayed in quadruplicates.

After the incubation of the rat **BT4Ca** glioma cells with 50 µM **S.18** the activity of caspase 3 was significantly increased by +57.3 % ($p<0.05$) compared to the negative control. The treatment with 12.5 and 25 µM **S.18** did not reveal any significant effects on the caspase 3 activity in the rat **BT4Ca** glioma cells. Compared to camptothecin, incubation with **S.18** did not show any significant effects (Fig. 43) on the caspase 3 activity in the rat **BT4Ca** glioma cells.

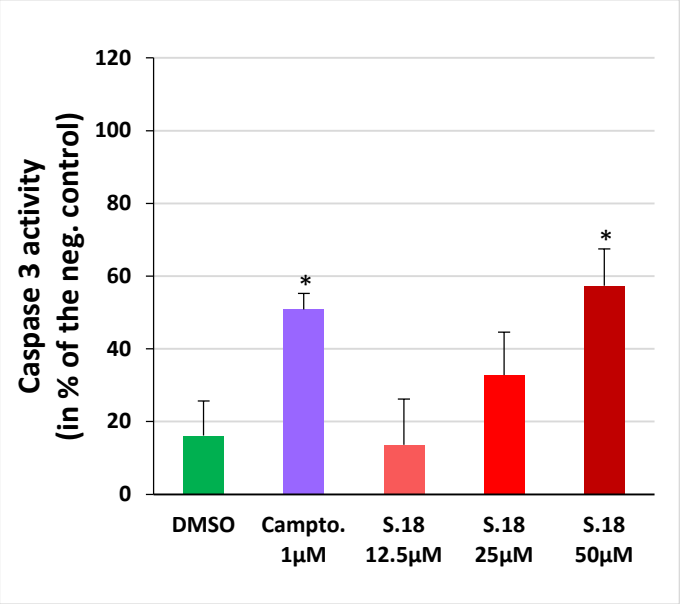

Figure 43: Caspase 3 activity of rat BT4Ca glioma cells after treatment with S.18.
Caspase 3 activity measured by fluorometric quantification of DEVD (Ex.502/Em.530 nm) normalized with Hoechst (Ex.355/Em.465 nm) in rat BT4Ca glioma cells after 48 h incubation with S.18, DMSO 0.25 % and camptothecin. Values are given (in % activity of neg. control [incubation with medium alone; = 0 % activity]) as mean + SEM; *$p<0.05$, ***$p<0.001$, significance vs. 0.25 % DMSO control; n=5 independent experiments assayed in quadruplicates.

The treatment of the rat **BT4Ca** glioma cells with **S.19** significantly ($p<0.05$) raised the caspase 3 activity by +54.8 % (25 µM) and +41.4 % (50 µM) compared to the negative control. Incubation with 12.5 µM **S.19** did not show any significant effects on the rat **BT4Ca** glioma cells. Compared to camptothecin, the treatment with none of the concentration of **S.19** led to a significant boost of the caspase 3 activity in the rat **BT4Ca** glioma cells (Fig. 44).

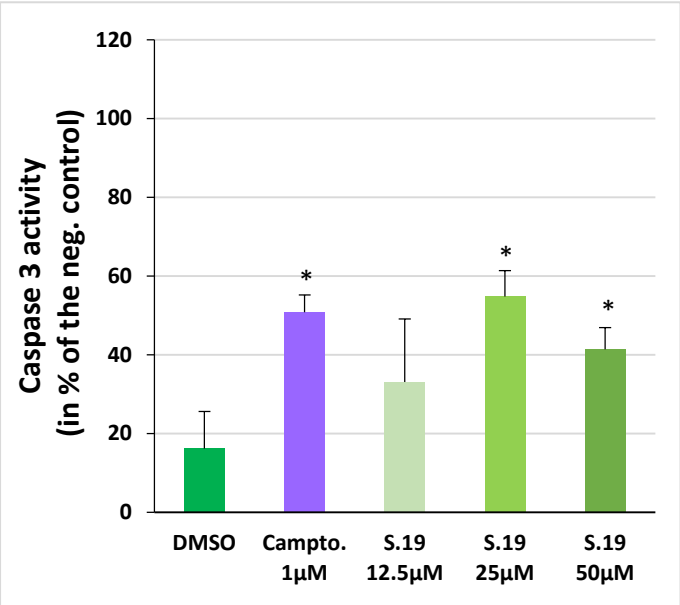

Figure 44: Caspase 3 activity of rat BT4Ca glioma cells after treatment with S.19.
Caspase 3 activity in relation to cell Caspase 3 activity measured by fluorometric quantification of DEVD (Ex.502/Em.530 nm) normalized with Hoechst (Ex.355/Em.465 nm) in rat BT4Ca glioma cells after 48 h incubation with S.19, DMSO 0.25 % and camptothecin. Values are given (in % activity of neg. control [incubation with medium alone; = 0 % activity]) as mean + SEM; *p<0.05, ***p<0.001, significance vs. 0.25 % DMSO control; n=5 independent experiments assayed in quadruplicates.

The treatment of the rat **BT4Ca** glioma cells with 50 µM **S.38** revealed a significant increase ($p<0.01$) of the caspase 3 activity by + 56.2 % compared to the negative control. Incubation with 12.5 and 25 µM **S.38** did not show any significant effects on the rat **BT4Ca** glioma cells. Compared to camptothecin, the treatment with none of the concentration of **S.38** showed a significant increase of the caspase 3 activity in the rat **BT4Ca** glioma cells (Fig. 45).

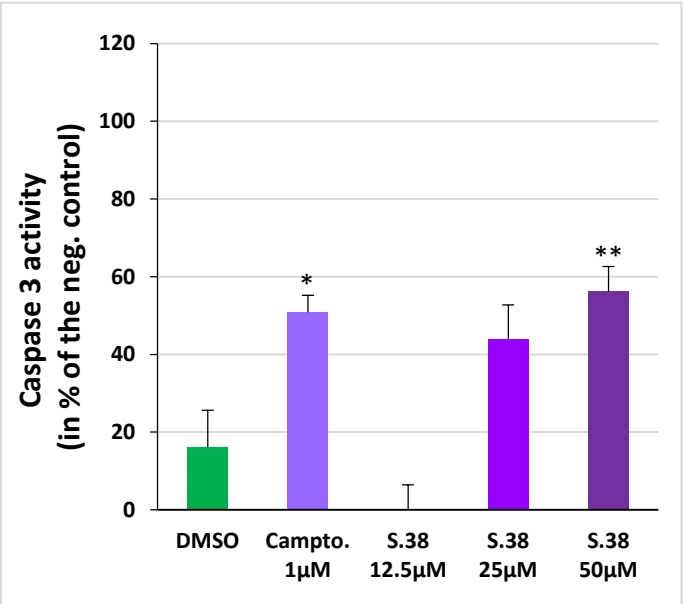

Figure 45: Caspase 3 activity of rat BT4Ca glioma cells after treatment with S.38.
Caspase 3 activity measured by fluorometric quantification of DEVD (Ex.502/Em.530 nm) normalized with Hoechst (Ex.355/Em.465 nm) in rat BT4Ca glioma cells after 48 h incubation with S.38, DMSO 0.25 % and camptothecin. Values are given (in % activity of neg. control [incubation with medium alone; = 0 % activity]) as mean + SEM; *p<0.05, ***p<0.001, significance vs. 0.25 % DMSO control; n=5 independent experiments assayed in quadruplicates.

The treatment of the rat **BT4Ca** glioma cells with **S.98** (12.5, 25 and 50 µM) led to a significant increase of the caspase 3 activity by + 52.9 % ($p<0.01$), +75.9 % ($p<0.001$) and +61.7 % ($p<0.01$) compared to the negative control. In comparison to camptothe-

cin, incubation with 25 µM **S.98** significantly raised the caspase 3 activity by + 25.1 % ($p<0.05$) in the rat **BT4Ca** glioma cells (Fig. 46).

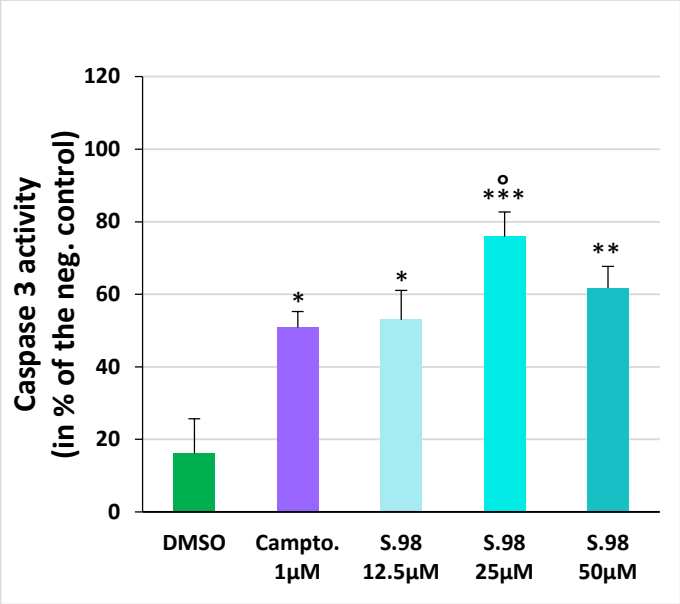

Figure 46: Caspase 3 activity of rat BT4Ca glioma cells after treatment with S.98.
Caspase 3 activity measured by fluorometric quantification of DEVD (Ex.502/Em.530 nm) normalized with Hoechst (Ex.355/Em.465 nm) in rat BT4Ca glioma cells after 48 h incubation with S.98, DMSO 0.25 % and camptothecin. Values are given (in % activity of neg. control [incubation with medium alone; = 0 % activity]) as mean + SEM; *p<0.05, ***p<0.001, significance vs. 0.25 % DMSO control, °p<0.05, significance vs. 1µM camptothecin (apoptosis positive control); n=5 independent experiments assayed in quadruplicates.

The treatment of the rat **BT4Ca** glioma cells with 50 µM **S.101** revealed a significant increase ($p<0.01$) of the caspase 3 activity by + 70.9 % compared to the negative control. Incubation with 12.5 and 25 µM **S.101** did not show any significant effects on the rat **BT4Ca** glioma cells. Compared to camptothecin, the treatment with none of the concentration of **S.101** revealed a significant increase of the caspase 3 activity in the rat **BT4Ca** glioma cells (Fig.47).

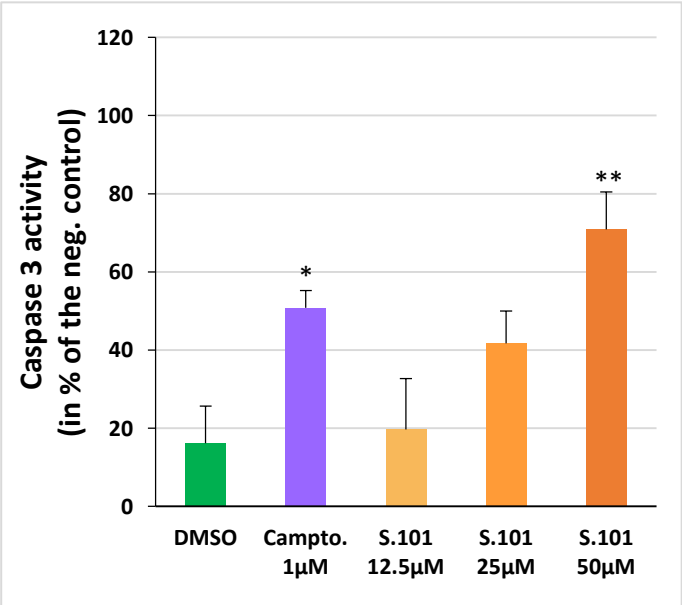

Figure 47: Caspase 3 activity of rat BT4Ca glioma cells after treatment with S.101.
Caspase 3 activity measured by fluorometric quantification of DEVD (Ex.502/Em.530 nm) normalized with Hoechst (Ex.355/Em.465 nm) in rat BT4Ca glioma cells after 48 h incubation with 5-FUrd, DMSO 0.25 % and camptothecin. Values are given (in % activity of neg. control [incubation with medium alone; = 0 % activity]) as mean + SEM; *p<0.05, ***p<0.001, significance vs. 0.25 % DMSO control; n=5 independent experiments assayed in quadruplicates.

4.5. Effects of the novel derivatives on the proliferation

4.5.1. Effects of the novel derivatives on the amount of proliferating cell nuclear antigen (PCNA)

For the analysis of the effects of the derivatives on the proliferation the amount of PCNA in rat **BT4Ca** glioma cells was estimated after an incubation of 24 h with the derivatives at a concentrations of 12.5 and 25 µM. For every experiment a DMSO control was done, to check the influence of the solvent DMSO. Compared to the negative control (incubation with medium alone = 100 %), no significant effects on the amount of PCNA for the used 0.063 % and 0.125 % DMSO control were observed. The PCNA amount was calculated in % of the negative control (= 100 %) and the significances are given compared to the according DMSO control as well as to 5-FUrd.

After the treatment of the rat **BT4Ca** glioma cells with **5-FUrd** an insignificant increase of the PCNA levels by +29.9 % (12.5 µM) and +24.7 % (25 µM) were observed compared to the negative control (Fig. 51).

Through the treatment of rat **BT4Ca** glioma cells with 12.5 µM **S.18** an insignificant reduction of the PCNA content by -38.9 % was detected compared to the negative control.

Whereas the incubation of rat **BT4Ca** glioma cells with 25 µM **S.18** significantly ($p<0.05$) lowered the amount of PCNA by -66.6 % compared to the negative control. Additionally, compared to 5-FUrd, the treatment of the rat **BT4Ca** glioma cells with 25 µM **S.18** significantly ($p<0.05$) reduced the content of PCNA by -91.3 % (Fig. 51).

After the incubation with 12.5 µM **S.19** the level of PCNA in the rat **BT4Ca** glioma cells was insignificantly diminished by -43.0 % compared to the negative control.

In contrast, the treatment with **S.19** (25 µM) led to a significant ($p<0.05$) decrease of PCNA content in the rat **BT4Ca** glioma cells by -59.2 % compared to the negative control. Whereas, compared to 5-FUrd, the incubation of the rat **BT4Ca** glioma cells with both concentrations of **S.19** (12.5 or 25 µM) significantly ($p<0.05$) diminished the level of PCNA by -72.2 % and -83.9 % (Fig. 51).

Compared to the negative control, the treatment of the rat **BT4Ca** glioma cells with **S.38** 12.5 or 25 µM revealed an insignificant decrease of the PCNA amount by -56.0 %

and -70.3 %. But compared to 5-FUrd the incubation of the rat **BT4Ca** glioma cells with **S.38** 25 µM revealed a significant ($p<0.05$) reduction of PCNA level by -95.0 % (Fig. 51). Through the incubation of the rat **BT4Ca** glioma cells with 12.5 µM **S.98** the PCNA content was insignificantly decreased by -30.0 % compared to the negative control. Whereas, after the treatment with **S.98** (25 µM) the PCNA level in the rat **BT4Ca** glioma cells was significantly ($p<0.05$) lowered by -96.4 % compared to the negative control. Moreover, compared to 5-FUrd, incubation of the rat **BT4Ca** glioma cells with 25 µM **S.98** showed also a significant ($p<0.05$) reduction of the PCNA level by -121.1 % (Fig. 51).

The treatment of the rat **BT4Ca** glioma cells with 12.5 µM **S.101** revealed an insignificant decrease of the PCNA level by -66.3 % compared to the negative control. However, compared to 5-FUrd, incubation of the rat **BT4Ca** glioma cells with 12.5 µM **S.101** led to a significant ($p<0.05$) decrease of the PCNA level by -95.5 %.

In contrast, the treatment with 25 µM **S.101** insignificantly increased the PCNA content in the rat **BT4Ca** glioma by +29.1 % compared to the negative control (Fig. 51).

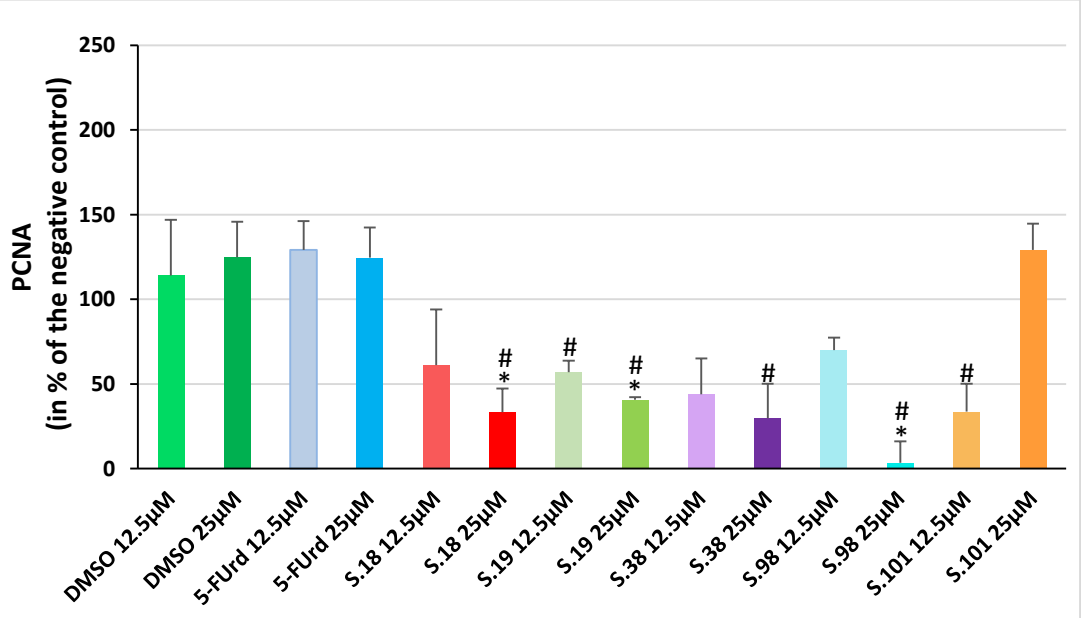

Figure 48: PCNA content of rat BT4Ca glioma cells after treatment.
PCNA content of rat BT4Ca glioma cells after 24 h incubation with DMSO, 5-FUrd, S.18, S.19, S.38, S.98 or S.101 at the concentrations of 12.5 and 25 µM. Values are given (in % of neg. control [incubation with medium alone; = 100 %]) as mean + SEM; *$p<0.05$, significance vs. 0.625 % and 0.125 % DMSO, #$p<0.05$, significance vs. 5-FUrd at equal concentration; n=3 independent experiments assayed in duplicates.

4.6. Effects of the novel derivatives on the induction of oxidative stress

4.6.1. Effects of the novel derivatives on the production of ROS

We used this assay to determine the amount of generated ROS in rat **BT4Ca** glioma cells after treatment with the derivatives of interest at the concentrations of 12.5, 25 and 50 µM.

For every experiment a DMSO control was done, to check the effect of the solvent DMSO. Incubation of the rat **BT4Ca** glioma cells with 0.25% DMSO (DMSO control) for 30 min, 1, 2, 3, 4, 5, 24 and 48 h showed no significant effects on the formation of ROS compared to the rat **BT4Ca** glioma cells incubated with medium alone (negative control) (Fig. 48).

The treatment of the rat **BT4Ca** glioma cells with **S.18** 50 µM revealed a significant ($p<0.05$) boost of the ROS production after 24 and 48 h by +1.71- and +2.15-fold compared to the negative control. Additionally, compared to 5-FUrd, the incubation of in the rat **BT4Ca** glioma cells with **S.18** 50 µM significantly ($p<0.05$) raised the ROS production at the same time points (24 and 48 h) by +1.66- and 2.04-fold (Fig. 48).

Incubation with derivative **S.38** (50 µM) significantly ($p<0.05$) increased the ROS production in the rat **BT4Ca** glioma cells after 24 and 48 h by +1.29- and 1.66-fold compared to the negative control, but no significances against 5-FUrd were found (Fig. 48).

The incubation of the rat **BT4Ca** glioma cells with 50 µM **S.98** showed after 48 h a significant ($p<0.05$) increase of the ROS production by +1.86-fold compared to the negative control. In comparison to 5-FUrd, the treatment with 50 µM **S.98** significantly ($p<0.05$) increased the ROS production after 48 in the rat **BT4Ca** glioma cells by +1.77-fold (Fig. 48).

The incubation with other derivatives under test, **5-FUrd**, **S.19** and **S.101**, did not lead to any significant changes in the ROS production of the rat **BT4Ca** glioma cells compared to the negative control or 5-FUrd (Fig. 48).

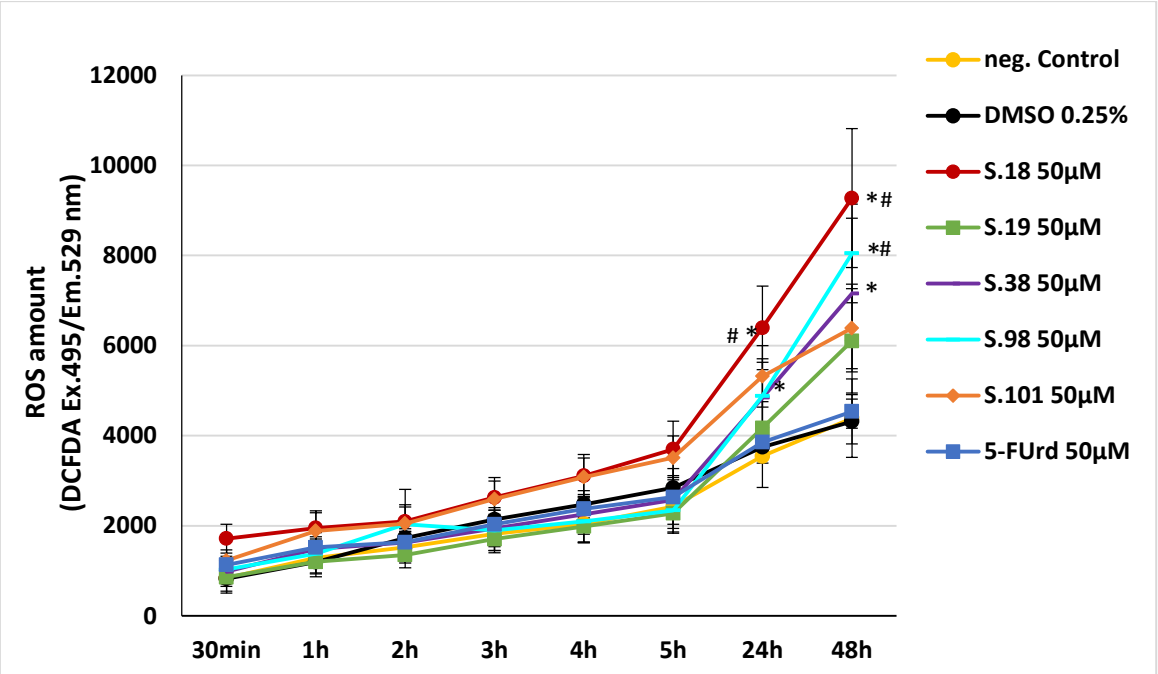

Figure 49: ROS amount of rat BT4Ca glioma cells after treatment.
ROS amount of rat BT4Ca glioma cells during the incubation (48 h) with 5-FUrd, S.18, S.19, S.38, S.98, and S.101 50 µM. Values are given as fluorescence-intensity of DCFDA (Ext.495nm/Em.529nm) as mean ± SEM; *p<0.05 significance vs. 0.25 % DMSO control; $^{\#}$p<0.05 significance vs. 5-FUrd at equal concentration; n=5 independent experiments assayed in quadruplicates.

After the treatment of the rat **BT4Ca** glioma cells with each derivative at lower concentrations (12.5 and 25 µM), no further significant effects on the production of ROS were measured, compared to the negative control. The results for the concentrations 12.5 and 25 µM for each of the five derivatives can be found in the supplements page 164-167 (Fig. 40-45).

In addition to the kinetics of the production of ROS, we also examined the ROS amount compared to the cell amount at the end of the treatment (48 h) (Fig. 49). Although, after the treatment with the derivatives the amount of ROS is increased in the rat **BT4Ca** glioma cells, the cell amount is simultaneously decreased, compared to the negative control (Fig. 49).

The treatment of the rat **BT4Ca** glioma cells with derivative 50 µM **S.18** significantly raised the total ROS amount after 48 h by 2.15-fold ($p<0.05$) and led simultaneously to a significant ($p<0.001$) decrease of the cell amount by -3.62-fold compared to the negative control.

The incubation of rat **BT4Ca** glioma cells with 50 µM **S.38** significantly ($p<0.05$) enhanced the total ROS amount by +1.66-fold and significantly ($p<0.001$) lowered the cell amount by -3.35-fold compared to the negative control.

The treatment of the rat **BT4Ca** glioma cells with derivative 50 µM **S.98** revealed a significant ($p<0.05$) boost of the total ROS amount by +1.86-fold after 48 h and showed a significant ($p<0.001$) reduction of the cell amount by -3.73-fold compared to the negative control.

The incubation of the rat **BT4Ca** glioma cells with the other derivatives, **S.19**, **S.101** and **5-FUrd** (50 µM) did not significantly change the total amount of ROS compared to the negative control. However, the treatment of the rat **BT4Ca** glioma cells with 50 µM **S.19**, **S.101** and **5-FUrd** significantly decreased the cell amount by -2.48- ($p<0.001$), -2.27- ($p<0.01$) and -3.21-fold ($p<0.001$) compared to the negative control. Hence, all derivatives raised the ROS production per cell (Fig. 49) and thus induced oxidative stress.

Moreover, compared to 5-FUrd, the incubation of the rat **BT4Ca** glioma cells with 50 µM **S.18** or **S.98** significantly ($p<0.05$) increased the ROS amount by +2.04 and +1.77 (Fig.49).

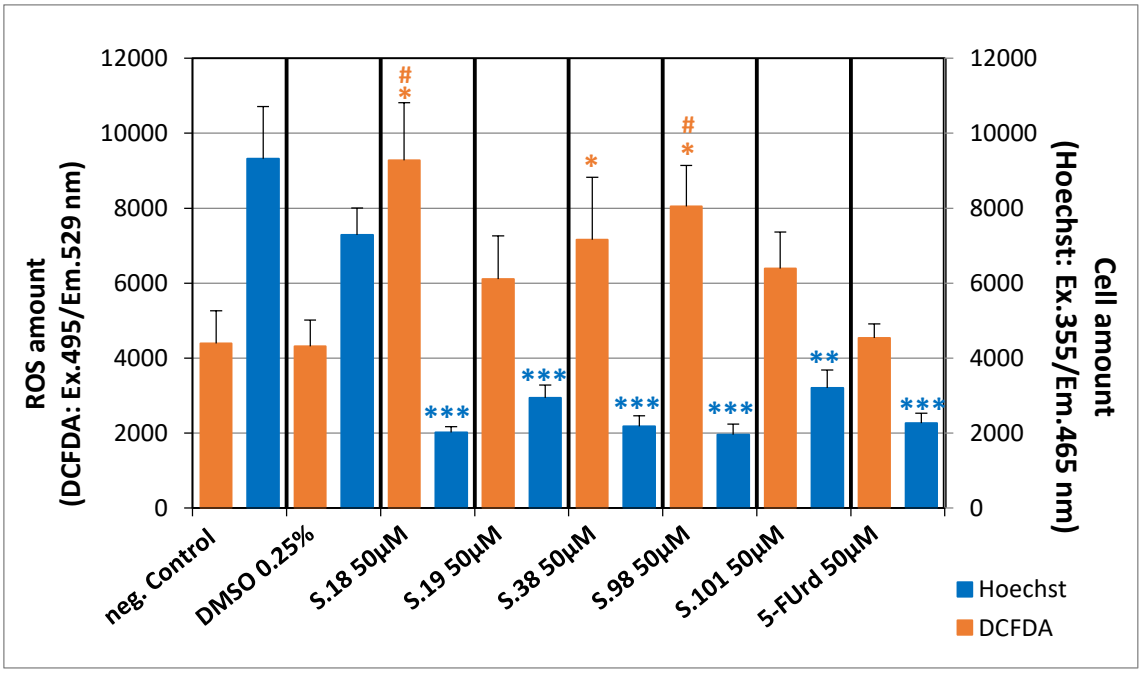

Figure 50: ROS and cell amount of rat BT4Ca glioma cells after 48 h treatment.
ROS and cell amount of rat BT4Ca glioma cells after the incubation (48 h) with 5-FUrd, S.18, S.19, S.38, S.98, S.101 50 µM and 0.25 % DMSO. Values are given as fluorescence-intensity as mean ± SEM; *p<0.05, **p<0.01, ***p<0.001, significance vs. 0.25 % DMSO; #p<0.05 significance vs. 5-FUrd at equal concentration; n=5 independent experiments assayed in quadruplicates.

4.6.2. Effects of the novel derivatives on the ratio of rGSH/GSSG

Based on the results of the ROS assay, the rGSH/GSSG assay was performed, to determine if the GSH system is buffering the emerging ROS. The proportion of GSH and GSSG was determined by using spectrophotometry (Rahman, Kode & Biswas, 2006).
Hence the amount of the reduced and oxidized form of GSH in rat **BT4Ca** glioma cells was estimated after an incubation of 48 h with the derivatives at a concentrations of 6.25 and 12.5 µM. For every experiment a DMSO control accordingly to derivative solution was done, to check for the effect of the solvent DMSO on the intracellular redox state. Compared to the negative control (incubation with medium alone), no significant effects on the ratio of rGSH/GSSG for the used 0.032 % and 0.063 % DMSO controls were observed. The ratio of rGSH/GSSG was calculated in % of the negative control (= 100%) and the significances are given compared to the according DMSO control as well as to 5-FUrd.

The treatment of the rat **BT4Ca** glioma cells with 12.5 µM **5-FUrd** revealed a significant ($p<0.05$) reduction of the rGSH/GSSG ratio by -55.9 % compared to the negative control. The incubation of the rat **BT4Ca** glioma cells with **5-FUrd** at the concentrations of 6.25 µM did not show a significant effect on the ratio of rGSH/GSSG compared to the negative control (Fig. 50).
After treatment of the rat **BT4Ca** glioma cells with 12.5 µM **S.98** the ratio of rGSH/GSSH was significantly ($p<0.001$) decreased by -95.6 % compared to the negative control. Additionally, compared to 5-FUrd, incubation of the rat **BT4Ca** glioma cells with 12.5 µM **S.98** significantly ($p<0.001$) lowered the ratio of rGSH/GSSG by -39.7 % (Fig. 50).
Moreover, the incubation of the rat **BT4Ca** glioma cells with 12.5 µM **S.101** also led to a significant ($p<0.05$) decrease of the rGSH/GSSG ratio by -45.3 % compared to the negative control (Fig. 50).
Through treatment with the other derivatives under test, **S.18**, **S.19** and **S.38**, no significant changes in the ratio of rGSH/GSSG in the rat **BT4Ca** glioma cells were observed, compared to the negative control or 5-FUrd (Fig. 50).

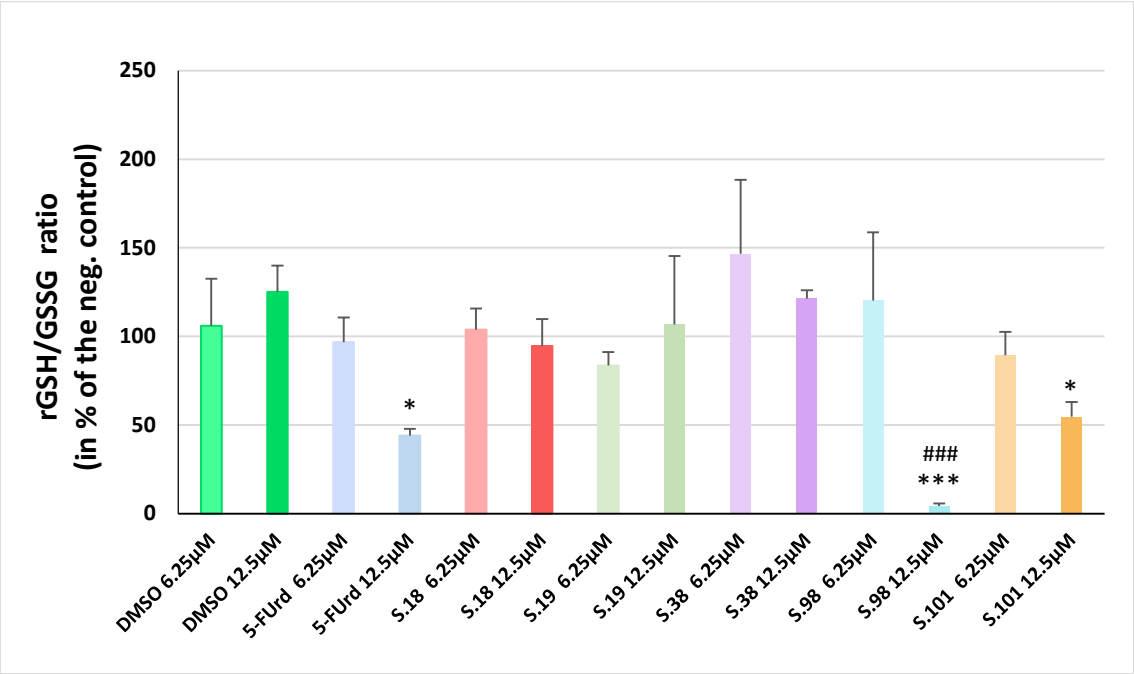

Figure 51: rGSH/GSSG ratio in rat BT4Ca glioma cells after treatment.
Ratio of the reduced GSH (rGSH) and GSSG in rat BT4Ca glioma cells after 24 h incubation with DMSO, 5-FUrd, S.18, S.19, S.38, S.98 and S.101 at the concentrations of 6.25 and 12.5 µM. Values are given (in % of neg. control [incubation with medium alone; = 100 %]) as mean + SEM; *p<0.05, ***p<0.001, significance vs. 0.032 % and 0.063 % DMSO control, $^{###}$p<0.001, significance vs. 5-FUrd at equal concentration; n=3 independent experiments assayed in duplicates.

4.7. Effects of the novel derivatives on the activation of NFκB

4.7.1. Effects of the novel derivatives on the localization of NFκB p65

This assay is primarily used to determine whether the NFκB signal pathway has been activated. Therefore the intracellular localization, nuclear or cytoplasmic, of the NFκB-p65 subunit is analyzed by immunofluorescence. The localization of NFκB-p65 in rat **BT4Ca** glioma cells was estimated after an incubation of 24 h with the derivatives at concentrations of 12.5 and 25 µM. For every experiment a DMSO control was done to check the influence of the solvent DMSO. Compared to the negative control (incubation with medium alone), no significant effects of 0.0625 % or 0.125 % DMSO on the localization of NFκB-p65 was detected.

Moreover, after treatment (24 h) of the rat **BT4Ca** glioma cells with any of the five derivatives or 5-FUrd no nuclear translocation of the subunit p65 was observed (see supplements page 168-173, Fig. 46-51).

Following, the localization of p65 after incubation with 25 µM **S.98** compared to the incubation with medium (negative control) is shown as an example (Fig 52).

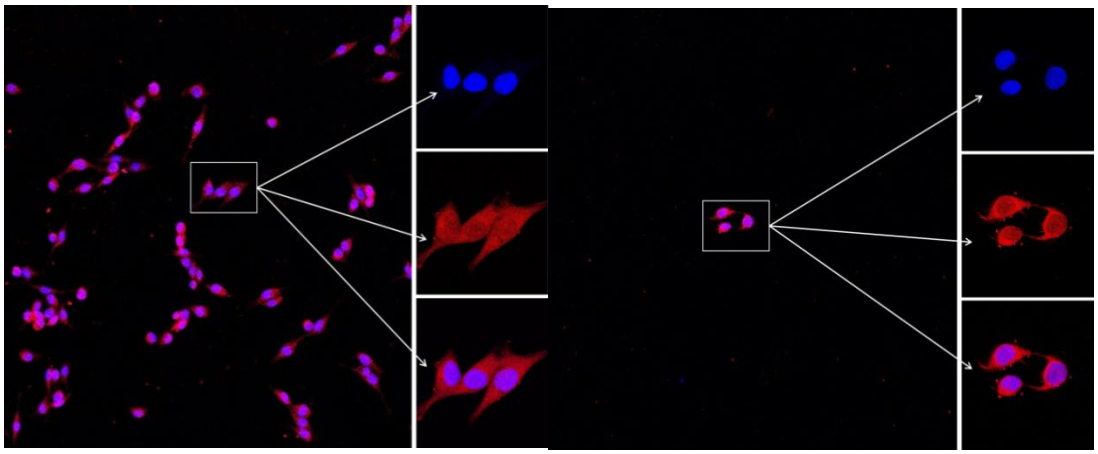

4.8. Effects of the novel derivatives on the migration

4.8.1. Effects of the novel derivatives on the wound healing capac

4.8. Effects of the novel derivatives on the migration

4.8.1. Effects of the novel derivatives on the wound healing capacity

This assay is used to determine the migratory capacity of the cells. Therefore “wounding” was performed by scratching of a cell monolayer at the bottom of the well. The “wound” was photographed at time 0 and after 6 h of the treatment at the same location. Hence, the migration was plotted as a percentage of wound closure (Fig. 53).

The migration of rat **BT4Ca** glioma cells was estimated during an incubation of 6 h with the derivatives at concentrations of 12.5 and 25 µM. For every experiment a solution control was done, to check for the influence of the solvent DMSO. Compared to the negative control (incubation with medium alone), no significant effects on the migration were observed for the used DMSO concentrations 0.063 % and 0.13 % (equal concentration of DMSO to 12.5 and 25 µM substance solution). Below the wound at time point 0 and after 6 h of treatment with medium (neg. control) or 25µM S.98 are illustrated as representative images.

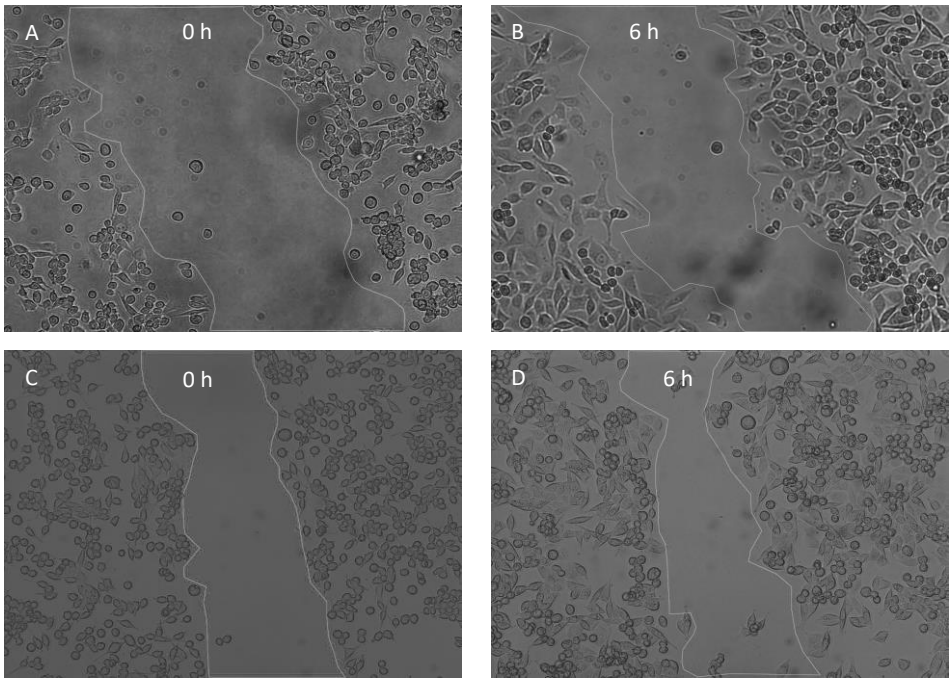

Figure 53: Wound healing of BT4Ca glioma cells
Representative images of the Scratch or wound healing assay of rat BT4Ca glioma cells after 0h and 6h cultured with medium alone (A and B) and after treatment with S.98 25 µM (C and D) (magnification 100x).

With this assay we investigated the influence of the derivatives of interest on the migratory capacity of the rat **BT4Ca** glioma cells after treatment. No difference between the migration ability after 6 h with e.g. **S.98** 25 µM compared to the negative control was observed (Fig 53). The other derivatives (S.18, S.19, S.38 and S.101) did not significantly lower the migration ability of the rat BT4Ca glioma cells as well (Fig 54).

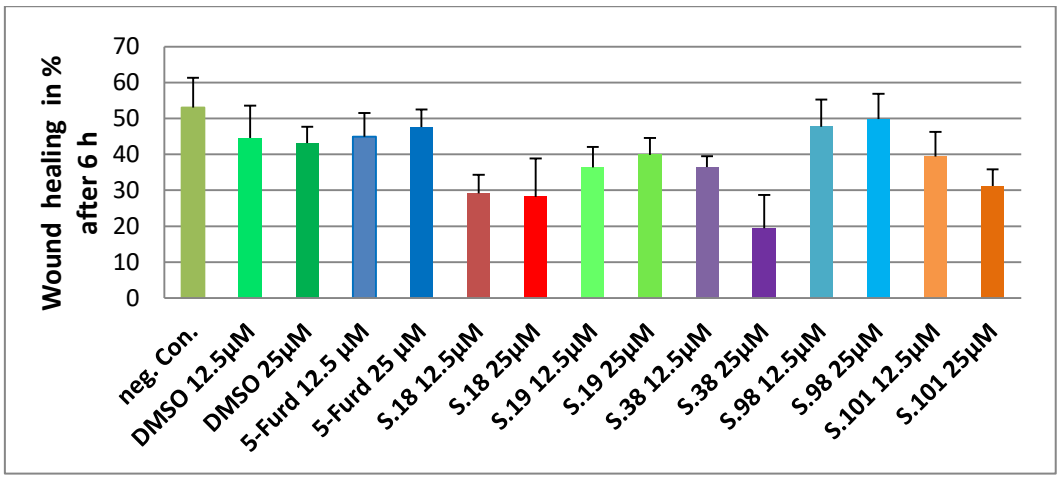

Figure 54: Wound healing of rat BT4Ca glioma cells after treatment.
Wound healing of rat BT4Ca glioma cells after 6 h during the incubation with medium (= neg. control) or DMSO, 5-FUrd, S.18, S.19, S.38, S.98 and S.101 at the concentrations of 12.5 and 25 µM. Values are given (in % of wound size at 0 h = 100 %) as mean + SEM; n=3 independent experiments.

5. Discussion

In 2018, 18.1 million cancer cases were registered worldwide. With an estimated number of 9.6 million deceased patients, cancer was the second leading cause of death around the world (GLOBOCAN 2018). Nowadays, the clinics use chemotherapy as a standard technique for the treatment of cancer (Longley et al., 2003). 5-Fluorouracil (5-FU), developed by Charles Heidelberger in the 1950's (Heidelberger et al., 1957), is a chemotherapeutic agent widely used against a variety of malignant tumors (Tanaka et al., 2000) especially colon and breast cancer (Longley et al., 2003b; Yoon, 2005). But, besides its anti-cancer-impact as an effective antimetabolite, it carries along a wide range of unpleasant side effects (Focaccetti et al., 2015). 5-FU belongs to the fraction of molecules with low molecular weight. This class of molecules includes lipids, monosaccharides, second messengers or other natural products and metabolites as well as drugs and other xenobiotics and differs from macromolecules such as proteins (Nature, 2019). Because of their low molecular weight, these substances are able to pass through the cell membrane easily. Once they have entered a cell, they can damage molecules, like proteins, the DNA or RNA and trigger cytotoxicity of cancer cells. (NIH, National Cancer Institute, 2019). Nevertheless, anticancer drugs with a small molecular weight still have several limitations such as adverse side effects, increased metabolism and nonspecific cytotoxicity, severe multidrug resistance and low bioavailability (Jahangirian et al., 2019). Beside this, the penetration of the cell membrane is not only related to the size of the molecules but also depends on their polarity, lipophilicity, hydrophilicity, polar surface area, hydrogen bonding and charge (Lipinski et al., 2001; Yang & Hinner, 2016). Under the application of the rules of five (Lipinski et al., 2001) and based on the structure of the well-known 5-FU derivative 5-Fluorouridine (5-FUrd), as well as the nucleosides adenosine, cladribin, formycin, guanosine and inosine and others, Prof. Dr. Rosemeyer et al. designed and synthesized a various number of novel nucleolipids (Malecki & Rosemeyer, 2010; Rosemeyer et al., 2012; Rosemeyer & Malecki, 2012; Köstler et al., 2013; Malecki E. 2013; Malecki et al., 2013; Malecki, Viere & Rosemeyer, 2013; Malecki et al., 2014; Werz et al. 2013; Farhat et al., 2014; Knies et al., 2015a; Knies et al., 2015b; Farhat, 2016; Knies et al., 2016; Hammerbacher et al., 2018; Knies et al., 2018; Rosemeyer et al., 2019; Reuter et al., 2019). These novel nu-

cleolipids have been modified at several positions and bear different side chains, which influence the lipophilic and hydrophilic properties of the molecules. Thus, these modifications alter the polarity and hopefully lead to a higher access into the cells and an improved penetrability through the blood-brain-barrier.

Over the last six years, we investigated the effects of more than 120 of these novel synthesized nucleolipids on the viability of rat BT4Ca glioma cells, human GOS3 glioma cells and human THP1 immune cells (PMA-differentiated macrophages) (Farhat et al., 2014; Knies et al., 2015a; Knies et al., 2015b; Knies et al., 2016; Hammerbacher et al., 2018; Knies et al., 2018; Rosemeyer et al., 2019; Reuter et al., 2019). The PMA-differentiated human THP1 macrophages represent effector cells of the innate immune system and give first hints of possible side effects. The BT4Ca cells enable an insight on the effects towards rat glioma cells, to eventually use in a rat animal model, whereas the human GOS3 cells show the impact on human glioma cells. Subsequently, we selected derivatives, which had to fulfill two selection criteria:

1. Efficiency comparable or stronger than 5-FUrd in inhibiting the viability or inducing cytotoxicity on the above mentioned rat BT4Ca and human GOS3 glioma cell lines
2. Minimally destructive towards the THP1 immune cells, indicating presumably low side effects

Five derivatives (S. 18, 19, 38, 98 and 101) were selected to be further examined. In this study we compare the effects of these derivatives with the effects of 5-FUrd. Although 5-FUrd (accordingly 5-FU) is used as a therapeutic agent against brain tumors (Lakkadwala & Singh, 2018; Roullin et al., 2004; Larner et al., 1991), it is not the common therapy of choice for gliomas. Temozolomide (TMZ) is currently considered to be the standard chemotherapeutic agent for the treatment of brain tumors (Fernandes et al., 2017; Portnow et al., 2009; NIH, National Cancer Institute, 2016). Despite, we used 5-FUrd as the substance to compare, because it has a high structural similarity with our derivatives and thus presumably has a comparable mechanism of action (Weiss et al., 2014).

Cell membranes are described as complex and highly dynamic systems, which mainly consist out of several types of phospholipids and proteins (Cooper, 2000). It is known

that the morphological tumoral transformation goes along with changes in the lipid composition of the plasma membrane. Thus, this transformation might be also related to the malignancy of the tumor (Azordegan et al., 2013). In this study, rat BT4Ca glioma cells are used as a model of grade IV astrocytoma with high metastatic aggressiveness. Moreover, the cell lines used as model for human gliomas are represented by GOS3 glioma cells, a mixed grade II/III astro-oligodendroglioma as well as G28 glioma cells from a gliosarcoma still expressing the glial fibrillary acidic protein (GFAP), a marker of astrocytic differentiation and expressed in astroglial tumors as well (Westphal et al., 1988; Westphal et al., 1994). G112 glioma cells, also with intact GFAP expression, are classified as glioblastoma grade IV (Westphal et al., 1994). The U251 glioma cells, with morphological irregular cell shapes and long protrusions (Diao et al., 2019; Torsvik et al., 2014) as well as the U87 glioma cells, which move very fast and tend to aggregate as clusters, are classified as grade IV astrocytoma (Clark et al., 2010; Diao et al., 2019). Accordingly, the composition of the membrane lipids and the penetrability properties of derivatives across the plasma membrane may be different for these cell lines. Hence, the access of the derivatives across the cell membrane is suggested to depend on the size, symmetry and position of the modified side chains (especially the farnesyl chain) as well as the lipophilic and hydrophilic properties of the test derivatives, as observed in this study. But obviously it also depends on the metabolic characteristics of the cancer cell type.

Regarding the amount of different derivatives (over 120) which include also purines, it is noticeable that the five selected derivatives, which are demonstrated to be more effective, belong to the group of pyrimidines. Furthermore, comparing the chemical structure of the derivatives in detail, it seems that there is no huge difference between the effects of derivatives derived from adenosine, inosine or formycin. Also the different side chains, added to the ribose, do not seem to lead to a big difference in the effectiveness of the derivatives. Only the positions of the attached farnesyl chain at position 9 (S.98) seems to trigger a high effectiveness against the rat as well as the human glioma cells.

We were able to show, that 5-FUrd exhibits a cytostatic effect on the viability of the rat BT4Ca and human GOS3 glioma cells after 48 h (Figs. 12 and 13), whereas it shows different patterns of cytotoxicity depending on the tested human glioma cell lines (G28,

G112, U251, U87) at higher concentrations (12.5-50 µM) (Figs.14-17). The five selected derivatives (S. 18, 19, 38, 98 and 101) reveal cytotoxic effects on the viability of all six tested glioma cell lines (Fig. 14-17). The effects of the derivatives might be similar by trend throughout the cell lines, but seem to differ in intensity depending on the proliferation rate. It looks like the faster the cells proliferate, the stronger are the effects on the viability. Nevertheless, the incubation with every selected derivative shows, at least at one concentration, a potent inhibition of the viability after 48 h, which is comparable or even stronger than the inhibition by 5-FUrd. However, the treatment with derivative S.19 and S.98 reveal the highest inhibitory effects on the cell viability, whereat S.98 is highly effective even at lower concentrations (1.56-6.25 µM).

These results are in agreement with the observed cytotoxicity (Figs. 18-23), which rises along with the higher concentrations of the derivatives. Thus, we were able to show, that 5-FUrd and the five selected derivatives not only diminish the metabolic activity of the cells but also trigger some kind of cell death.

Additionally, after treatment (48 h) of the rat BT4Ca glioma cells with the five selected derivatives (S. 18, 19, 38, 98 and 101) the cell amount, measured by the Hoechst staining (Merck, Sigma-Aldrich, 2019), also indicates a significant loss of cells depending on the concentration (12.5-50 µM) of the derivatives (Figs. 27, 30, 33, 36 and 39), whereas the treatment with 5-FUrd shows a consistent loss of cells at each concentration tested (Fig. 24). Hence, we analyzed several molecular mechanisms by **exemplarily using rat BT4Ca glioma** cells, to identify potential signaling effects of 5-FUrd and the five selected derivatives.

During cancer genesis, altered cells acquire and develop different mechanisms to evade cell death, which is described as one of the six hallmarks of cancer (Hanahan & Weinberg, 2011).

Thus, malignantly transformed cells are able to encounter apoptosis, the programmed cell death. Physiologically apoptosis is necessary to eliminate damaged or abnormal cells (Fernald & Kurokawa, 2013). Defects of this ubiquitous cellular process can not only lead to the formation of cancer but also contribute to tumor metastasis and drug resistance (Wong, 2001). Hence the capacity of inducing apoptosis can be one beneficial attribute of chemotherapeutic agents. In this context, we analyzed the induction of apoptosis through the treatment of the rat BT4Ca glioma cells with 5-FUrd or the five

selected derivatives (S. 18, 19, 38, 98 and 101). For the differentiation between the induction of apoptosis and necrosis we used a triple staining with YO-PRO®-1, propidium iodine and Hoechst 33342. YO-PRO®-1 is a non-permeant fluorescent for intact cells. Due to apoptosis, the membrane becomes permeant and YO-PRO®-1 can enter the cells. Thus, YO-PRO®-1 marks late apoptosis. Whereas propidium iodine (PI) remains impermeable to apoptotic and living cells but permeable for injured cells. Thus, PI serves as necrosis marker. Counterstaining with Hoechst 33342 allows the visualization of cell nuclei. Hence, by measuring the fluorescence intensity of these three dyes allows to differentiate between the apoptotic cell rate and the rate of necrotic cells. According to this we showed, that incubation (48 h) with the five derivatives increase the amount of apoptotic rat BT4Ca glioma cells throughout ascending concentrations (Fig. 28, 31, 34, 37 and 40). The treatment with 5-FUrd shows a constant high level of apoptotic rat BT4Ca glioma cells at concentrations 12.5-50 µM (Fig. 25). This observation is in agreement with earlier results, showing that 5-FU induces cell death via apoptosis in several cell lines like colorectal cancer or oral epithelial cells (Mhaidat et al., 2014; Tong et al., 2000, Voboril et al., 2004).

Staining with PI also reveales an increase of the percentage of necrotic rat BT4Ca glioma cells (Fig. 26, 29, 32, 35, 38 and 41). This increase of necrotic rat BT4Ca glioma cells could be due to the so-called secondary necrosis: At some point during apoptosis, the cell membrane breaks down and becomes permeable to propidium iodine, too. Therefore, after 48 h of incubation with 5-FUrd or the selected derivatives the measurement might include some YO-PRO®-1/ propidium iodine double stained dead cells (Invitrogen™, 2010) explaining the observed higher amount of necrotic rat BT4Ca glioma cells.

Thus, we decided to use another method to measure apoptotic cells, i.e. the detection of the activation of specific caspases. Caspase 3 is known as a key enzyme in the process of apoptosis. It plays an important role for the apoptotic chromatin condensation and DNA fragmentation as well as the dismantling of the cell and the formation of apoptotic bodies (Porter & Jänicke, 1999). Hence, the activity of caspase 3 is crucial evidence for the induction of apoptosis. In our study we could show, that incubation with 5-FUrd or the five selected derivatives (S.18, 19, 38, 98 and 101; 12.5-50 µM) induce a high activity of caspase 3 in rat BT4Ca glioma cells (Fig. 42-47). These results confirm our previous observations of the induction of apoptosis and indicate an apop-

tosis mediated cell death of the rat BT4Ca glioma cells triggered by the treatment (48 h) with 5-FUrd or the selected derivatives.

Another hallmark of cancer, pivotal for the transformation of healthy cells into tumors cells and acquired during the multistep development of human tumors, is the capability to sustain proliferative signaling (Hanahan & Weinberg, 2011). Thus, the capacity of inhibiting or preventing cell proliferation would be beneficial for anticancer drugs. The proliferating cell nuclear antigen (PCNA) is known to interact with several proteins involved in cell-cycle progression. It also plays a crucial role for DNA synthesis during replication and is important for chromatin remodelling, DNA repair as well as sister-chromatid cohesion (Kelman, 1997; Kubben et al., 1994; Boehm, Gildenberg & Wahington, 2017). Therefore, PCNA is essential for cell proliferation and thus often used as a marker.

Hence, we analyzed the level of PCNA in the rat BT4Ca glioma cells after treatment (24 h) with 5-FUrd or the five selected derivatives S. 18, 19, 38, 98 and 101. Interestingly, after 24 h of treatment all five selected derivatives under test (12.5 and 25 µM), inhibit the proliferation of rat BT4Ca glioma cells, indicated by a reduced amount of PCNA (Fig. 48). In contrast, the treatment (24 h) of the rat BT4Ca glioma cells with 5-FUrd (12.5 and 25 µM) does not reveal a decline of PCNA quantity (Fig. 48). Thus, at our experimental conditions 5-FUrd does not affect the proliferation rate of the rat BT4Ca glioma cells measured by PCNA. These results might explain the previous examined cytostatic effect of 5-FUrd on the viability of these glioma cells, described above. In this regard our results for 5-FUrd are in opposition to the documented inhibitory effect of 5-FU on the proliferation, which however were performed by using neuroblasts of the retinal margin (Negishi, 1994). Noticeable, our selected derivatives not only lead to a reduction of the cell amount by inducing apoptosis, but furthermore diminish the cell mass, because of an additional inhibition of the cell proliferation.

Due to the high metabolic activity of cancer cells the cellular appearance of reactive oxygen species (ROS) is naturally elevated. It is further described that ROS is crucial for every stage of cancer development, including initiation, promotion, and progression (Kumari et al., 2018). On the other side, oxidative stress, induced by an excess of ROS, is described to play an essential role in apoptosis signaling (Kannan & Jain, 2000).

Thus, we examined the occurrence of oxidative stress in rat BT4Ca glioma cells upon treatment (48 h) with 5-FUrd and the selected derivatives S. 18, 19, 38, 98 and 101 at a concentration of 50 µM. In rat BT4Ca glioma cells the treatment with the five selected derivatives caused a tremendous increase of ROS per cell (Fig. 50). Especially the treatment with derivatives S.18, 19 and 98 (50 µM) induces an elevated production of ROS and consequently an induction of oxidative stress in this glioma cell line. The incubation with 5-FUrd also elevates the level of ROS in the rat BT4Ca glioma cells, however not in the same extent as the derivatives (Fig. 50). These data indicate that 5-FUrd and especially the derivatives trigger the production of ROS in the rat BT4Ca glioma cells. Hence, the appearance of oxidative stress in rat BT4Ca glioma cells is increased through the treatment with the derivatives or 5-FUrd (50 µM). These observations go hand in hand with the former results, describing a raised level of intracellular oxidative stress induced by treatment with 5-FU in the salivary glands (Bomfin et al., 2017) and in the blood of patients with colorectal cancer (Koçer & Nazıroğlu, 2013) and associated with cell death induction.

Additionally, it has been shown, that antioxidants can inhibit 5-FU –induced apoptosis (Fu et al., 2014). To maintain the balance of the cellular redox status, cancer cells establish a huge antioxidant system, including glutathione. Under physiological conditions 98 % of the cellular glutathione (GSH) is in a reduced status. Due to oxidative stress, ROS can occur in large quantities. Thus the GSH acts as a scavenger, removing the free radicals and is thereby oxidized. Hence the ratio of reduced glutathione (rGSH) to oxidized glutathione (GSSG) is an important index for oxidative stress within a cell. It is generally accepted that the rGSH/GSSG ratio is a useful indicator of oxidative stress in cells and tissues (Owen & Butterfield, 2010). In this context, we additionally analyzed the intracellular glutathione redox status by determination of the rGSH/GSSG ratio in rat BT4Ca glioma cells after treatment (24 h) with 5-FUrd or the selected derivatives S. 18, 19, 38, 98 and 101 (6.25 and 12.5 µM). Under physiological conditions the rGSH/GSSG ratio exceeds 100:1 in resting cells. With increased levels of oxidative stress, intracellular GSSG will accumulate, by the oxidation of two rGSH molecules to one GSSG and the rGSH/GSSG ratio will decrease (Forman et al., 2009). Thus, a low rGSH/GSSG ratio indicates a high occurrence of ROS and displays oxidative stress (Zitka et al., 2012). Due to the high cytotoxicity of 5-FUrd and the derivatives at the concen-

trations of 25 and 50 µM, we were forced to treat the rat BT4Ca glioma cells with lower concentrations enabling us to collect enough material, particularly cells and proteins. Therefore, we performed the rGSH/GSSG assay with lower concentrations (6.25 and 12.5µM) to determine the data of interest. Interestingly, the treatment with derivative S. 18, 19 and 38 does not reveal any effect on the rGSH/GSSG ratio in the rat BT4Ca glioma cells (Fig. 51), although the treatment elevates the ROS level per cell. This unaffected ratio of rGSH/GSSG could be explained by the lower concentrations (6.25 and 12.5µM) of the derivatives (S. 18, 19 and 38) used to assay the ratio of rGSH/GSSG in the rat BT4Ca glioma cells. These lower concentrations (6.25 and 12.5µM) presumably are not high enough to affect the intracellular GSH redox status. In contrast, treatment with 5-FUrd as well as the derivatives S. 98 and S.101 lead to a decrease of the ratio of rGSH/GSSG in the rat BT4Ca glioma cells (Fig. 51) accompanied by the elevated production of ROS as described. Moreover, incubation with S.98 clearly excels the effect of 5-FUrd and causes an even higher level of oxidative stress for the rat BT4Ca glioma cells, with characteristic ROS increment. Thus, the treatment with S.98 leads to the consumption of almost every rGSH in the rat BT4Ca glioma cells. The low level of remaining antioxidants in the rat BT4Ca glioma cells presumably can't balance the cellular redox status anymore; thereby the not bound ROS can contribute to the induction of apoptosis.

Abnormalities in cellular signaling pathways can lead to the formation of tumors and thus, are critical for the transformation of healthy cells into malignantly growing and uncontrollable proliferating cancer cells. The nuclear factor kappa-light-chain-enhancer of activated B cells, i.e. NFκB, is an important redox regulated transcription factor and plays a central role for the intracellular signaling transduction. This huge protein complex consists of several subunits including p65 and is present in almost every cell type. Upon different stimuli the subunit p65 translocates from the cytosol to the nucleus, where it leads to the transcription of e.g. cytokines, chemokines and adhesion molecules (Perkins, 2007; Liu et al., 2017). Thus, by controlling the expression of different target genes, NFκB is involved in the pro- and anti-inflammatory cell response as well as proliferation, survival, and angiogenesis. For several tumor tissues an excessive activation of the NFκB-signaling pathway has been described, therefore linking NFκB activation to tumor pathogenesis (Xia et al., 2018). However, Lui et al. (2012) indicated a

suppressive role of NFκB in certain cancer types (Liu et al., 2012). Regarding this controversy and to address the question, whether the induction of apoptosis and the elevated production of ROS caused by our derivatives (described above) is mediated by NFκB, we analyzed the influence of our five selected derivatives on the activation of NFκB. Therefore, we determined the location of p65 within the rat BT4Ca glioma cells after the treatment (24 h) with 5-FUrd or the derivatives S. 18, 19, 38, 98 and 101 (12.5 and 25 µM). We could observe that the rat BT4Ca glioma cells do not show any activation of NFκB by translocation of p65 after the treatment (24 h) with neither 5-FUrd nor one of our derivatives of interest (Fig. 52 and supplements page 168-173, Fig. 46-51). We also tried to examine the activation of NFκB after the incubation of rat BT4Ca glioma cells for 48 h, but due to the cytotoxic effects of the derivatives, a qualitative analysis of the cells was rather impossible. In addition to our results, it is described, that 5-FU can even suppress NFκB in salivary gland cancer cells, leading to the induction of apoptosis (Azuma et al., 2001). Moreover, Voboril et al. (2004) indicated an increased sensitivity of colon cancer cells to 5-FU, due to the inhibition of NFκB.

Another hallmark of cancer is the activation of tissue invasion and metastasis (Hanahan & Weinberg, 2000 and 2011). The invasive migration ability of tumor cells is a basic requirement for metastasis and a characteristic of high tumor malignancy. Therefore, an inhibitory effect towards the migration capacity of cancers cells is a beneficial feature for antitumor drugs. In this context, we examined the capacity for migration of rat BT4Ca glioma cells after treatment (6 h) with 5-FUrd or the five selected derivatives via a wound healing assay. Interestingly, the treatment with the derivatives S.18, 19, 38 and 101 (12.5 and 25 µM) tend to result in an inhibition of the migration ability of the rat BT4Ca glioma cells, whereas 5-FUrd and the derivative S.98 do not (Fig. 54). Additionally, 5-FUrd and the derivatives induce apoptotic cell death. Apoptosis induces loss of cell adhesion, whereas necrosis does not affect cell adhesion (Kwon et al., 2015). After apoptosis the adherent rat BT4Ca glioma cells detach from the ground with consequent loss of adhesion. Moreover, every time the culturing medium was moved by transport, it led to a further detachment of more cells. Hence, the non-adherent cells could have influenced accurate measurement of migration. Due to these reasons, it is necessary to use an additional method for the examination of the migratory capability. For an accurate analysis, a new live-cell imaging assay is available,

as described by Restall et al. (2018). In the future this method would be suitable to measure the migration and invasion properties of the rat BT4Ca glioma cells during the treatment with 5-FUrd or the derivatives S. 18, 19, 38, 98 and 101.

To investigate possible side effects, we also examined the impact of the derivatives on the viability of human, PMA differentiated macrophages (THP1). These cells are derived out of monocytes from a patient with acute monocytic leukemia (DSMZ, 2019c). As a part of the cellular immune system, they are eligible to give a first impression of unwished secondary effects of the derivatives. We observed that the treatment with all five selected derivatives also have inhibitory effects on the viability of the THP1 cells at 12.5-50 µM, the highest concentrations tested (see supplements page 147, Fig. 22). How severe these side effects are for our immune system has to be examined in further experiments.

Beside the studies on different glioma cell lines, we also investigated the effects of the five selected derivatives on other tumor entities. Interestingly, the incubation with the derivatives S.18, 19, 38, 98 and 101 show also inhibitive effects on the viability of human colorectal carcinoma (HT29), human hepatocellular carcinoma (HepG2), human pancreas carcinoma (Panc-1) and murine renal carcinoma (RenCa) cells (see supplements page 147-149, Fig. 23-26). Hence, the treatment with theses novelly synthesized derivatives reveal a wide range of anticancer effects.

In this study we show for the first time that chemically modified derivatives, derived from nucleosides such as adenosine, formycin and inosine are able to keep up with or even overcome the cytostatic/cytotoxic effects of the well-known chemotherapeutic agent 5-FU. We suggest that the five selected derivatives S. 18, 19, 38, 98 and 101 are eligible for the treatment of different human glioma cell lines like GOS3, G28, G112, U251 and U87. Moreover, we demonstrate a broad range of the cytotoxcitiy of these derivatives on further carcinoma cell lines like HT29, HepG2, Panc-1 and RenCa. By **exemplarily using the rat BT4Ca glioma** cells we examine the cytotoxic effects of these derivatives in more detail. Therefore, we propose that these effects may be due to an increased level of intracellular oxidative stress that activates apoptotic signaling pathways mediating cell death. Remarkably, the intracellular proliferation signaling is additionally inhibited by the derivatives. Thus, these derivatives carry along some fundamental anti-cancer properties, which make them highly interesting as prospects for the

use as possible novel chemotherapeutic agents. Potentially, they could be used for the treatment of several different tumor entities, including highly aggressive tumors like glioma, pancreatic or other cancer types with bad prognosis.

Further *in vitro* experiments have to be performed to proof our results and to provide a more detailed view on the mechanisms of action of these derivatives. It will be essential to look at the protein expression of treated cells. Especially the expression pattern of proteins, which are part of the signaling cascade of apoptosis e.g. different caspases or key proteins like p62 and Bax (Papaliagkas et al., 2007), or proteins involved in the transmission of oxidative stress signaling like different MAP kinases, ERK or p38 and p53 would be of major interest (Martindale & Holbrook, 2002; Camhi et al., 1995). Certainly, a detailed analysis of the expression of proteins, which regulate cell proliferation e.g. different cyclins or growth factors should also be examined (Duronio & Xiong, 2013). Additionally, it would be of great interest to study the long-term effects (above 48 h) of the derivatives and to look for possible induction/inhibition of drug resistance and cell recovery. For such investigations primary glioma cells obtained from patients after tumor resection should be considered. Furthermore, possible side effects of the derivatives towards healthy cells responsible for the detoxification like renal or liver cells should be investigated. In addition, the effects towards healthy neurons or glia cells like astrocytes should also be analyzed. Following *in vivo* experiments, as well as clinical studies, respectively, have to be performed to clarify the potential of these novelly synthetized derivatives as chemotherapeutic drugs in detail.

6. Summary

Today cancer is the second leading cause of death around the world. The World Health Organization predicts an increase from 9.6 million in 2018 up to 16.4 million cancer deaths in 2040. Although tumors of the brain and the nervous system are rather unusual among adults (2 %), they are the second most common diagnosed types of cancer in childhood.

Gliomas and meningiomas are the most frequent types of brain tumors and account for 30 % of all tumors in the brain and central nervous system as well as for 80 % of all malignant intracranial tumors. Usually surgical excision is the first step in the treatment of cancer followed by radio- and chemotherapy. Due to the mainly intracranial location of gliomas, surgical interventions are extremely risky. Therefore, the use of radiation and chemotherapeutic agents become more important.

5-Fluorouracil (5-FU) is a well-known drug, usually used as chemotherapeutic agent in the standard treatment of fast proliferating cancer cells. Unfortunately, it carries along a wide range of unpleasant side effects in multiple organ systems. To improve the passage through the blood-brain-barrier and the cell membrane penetration thereby gaining a higher efficiency, our cooperation partners Prof. Dr. Rosemeyer and his colleagues from the Institute of Chemistry and Materials of the University of Osnabrück synthesized more than 120 novel nucleolipids. These molecules have been designed based on the 5-FU derivative 5-Fluorouridine (5-FUrd) or the nucleosides adenosine, cladribin, formycin, guanosine, inosine and others. The derivatives are modified at several positions and have different additional chemical side groups to mainly influence the hydrophilicity and lipophilicity and thus, to consequently improve the permeability across the blood-brain-barrier as well as the uptake into the cells.

At first we screened the impact of 5-FUrd and the 120 novelly synthesized derivatives on the viability of rat BT4Ca and human GOS3 glioma cells as well as differentiated human macrophages (THP1). Five derivatives (S.18, 19, 38, 98 and 101), which show low cytotoxic effects on the macrophages and are effective against both, the rat BT4Ca and the human GOS3 glioma cells, were selected to be further analyzed. Although we screened 120 derivatives consisting of purines and pyrimidines, it is remarkable that all five selected, most effective derivatives (S.18, 19, 38, 98 and 101) belong to the group of pyrimidines. Comparing the chemical structure of the selected derivatives, the position of the attached farnesyl chain seems to be of high importance for the effectiveness of the most efficient derivative (S.98) against rat as well as human glioma cell lines.

We were able to show that the selected derivatives, derived out of the nucleosides adenosine (S.38), formycin (S.98) and inosine (S.18, 19 and 101) are able to keep up with or even over-

come the cytostatic/cytotoxic effects of the well-known chemotherapeutic agent 5-FU on further human glioma cell lines (G28, G112, U251 and U87) and several other tumor entities (HT29, HepG2, Panc-1 and RenCa). Certainly, these effects depend on the applied derivative as well as its concentration and vary among the specific cell type analyzed. Furthermore, using the rat BT4Ca glioma cells as a model of fast proliferating glioblastomas, we studied several intracellular mechanisms, possibly responsible for the examined cytotoxic effects of the selected derivatives (S.18, 19, 38, 98 and 101).

Our results indicate that the treatment of the rat BT4Ca glioma cells with each derivative lead to a concentration-dependent increase of the apoptotic cell rate. At concentrations 25 and 50 µM each of the selected derivatives led to a distinct activation of the caspase 3, confirming the induction of apoptosis. We also observed an increase of the necrotic cell rate with ascending concentration (12.5, 25 and 50 µM) of each derivative presumably due to secondary necrosis. Beside the loss of cell mass due to apoptosis, we detected lower levels of PCNA after the treatment with any selected derivative (12.5 and 25 µM) indicating a reduced cell proliferation of the rat BT4Ca glioma cells. In contrast, the treatment of the rat BT4Ca glioma cells with 5-FUrd did not affect the amount of PCNA. Thus, at our experimental conditions 5-FUrd showed no impact on the proliferation rate consistent with its cytostatic effects. Moreover, we determined a tremendous accumulation of ROS per cell after the treatment with each derivative (50 µM). Especially the treatment with the derivatives S.18, 38 and 98 caused high oxidative stress in the rat BT4Ca glioma cells. But regarding the ratio of rGSH/GSSG only the derivative S.98 showed an explicit effect on the glutathione antioxidant system by lowering the rGSH/GSSG ratio.

Nevertheless, the activation of NFκB, through the translocation of the subunit p65 from the cytoplasm to the nucleus, was not triggered by the treatment with any selected derivative or 5-FUrd. For a validation of the effects of the derivatives on the migratory capacity of the rat BT4Ca glioma cells during the treatment, further experiments need to be done with a more accurate method.

The results indicate that our five selected derivatives S.18, 19, 38, 98 and 101 bear fundamental attributes, which are beneficial for the treatment of malignant cancer cells. These properties and the broad range of cytotoxicity as well as the inhibition of the cell proliferation make the five derivatives, especially S.19 and S.98, highly interesting as prospects against several tumor entities for the use as possible novel drugs with a high potential as chemotherapeutic agent.

6.1. Zusammenfassung

Aktuell gehört Krebs zu den häufigsten Todesursachen weltweit. Die Welt-Gesundheits-Organisation prognostiziert einen Anstieg von 9,5 Millionen Krebs assoziierten Todesfällen im Jahre 2018 auf 16,4 Millionen im Jahre 2040. Obwohl Tumore des Gehirns und des zentralen Nervensystems bei Erwachsenen eher selten vorkommen (2 %), sind sie bei Kindern die am zweithäufigsten diagnostizierte Krebsart. Gliome und Meningiome stellen 30 % aller Tumore des Gehirns und Zentralen Nervensystems sowie 80 % aller bösartigen intrakranialen Tumore. Die Standardtherapie beginnt im Regelfall mit der operativen Entfernung, gefolgt von Radio- und Chemotherapie. Auf Grund der intrakranialen Lokalisation von Gliomen sind chirurgische Maßnahmen jedoch sehr riskant, wodurch Bestrahlungen und chemotherapeutische Behandlungen an Bedeutung gewinnen.

5-Fluorouracil (5-FU) ist ein seit vielen Jahren genutzter Wirkstoff, das als Chemotherapeutikum gegen schnell wachsende Krebszellen eingesetzt wird. Bedauerlicherweise bringt er auch ein breites Spektrum an unerwünschten Nebeneffekten für einige Organsysteme mit sich. Um die Passage durch die Blut-Hirn-Schranke und die Aufnahme in die Zelle und damit die Effektivität solcher Substanzen zu verbessern, entwickelten und synthetisierten unsere Kooperationspartner Prof. Dr. Rosemeyer und seine Kollegen am Institut für Chemie und Materialien der Universität Osnabrück über 120 neue Nukleolipidderivate. Die Struktur dieser Nukleolipide beruht auf dem 5-FU Derivat 5-Fluorouridine (5-FUrd) oder den Nukleosiden Adenosin, Cladribin, Formycin, Guanosin, Inosin und weiteren. Die Derivate dieser Grundsubstanzen sind an mehreren Positionen verändert und tragen zusätzlich verschiedene chemische Seitenketten um ihre Wasser- und Fettlöslichkeit zu beeinflussen. Durch diese Modifikationen soll der Übergang durch die Blut-Hirn-Schranke sowie die Aufnahme in die Zelle erleichtert werden.

Zu Beginn der Studie untersuchten wir den Einfluss von 5-FUrd und den 120 neu synthetisierten Derivaten auf die Viabilität der aus Ratten stammenden BT4Ca und humanen GOS3 Gliom Zellen sowie differenzierten humanen Makrophagen (THP1). Fünf Derivate (S.18, 19, 38, 98 und 101), die keine oder nur eine geringe schädliche Wirkung für die Makrophagen zeigten, gleichzeitig jedoch effektiv gegen beide Gliom Zelllinien (BT4Ca und GOS3) wirkten, wurden ausgewählt und weiter analysiert. Bemerkenswert ist, dass trotz der Anzahl von 120 getesteten Substanzen, die sowohl Purine als auch Pyrimidine einschlossen, alle fünf ausgewählten Derivate zur Gruppe der Pyrimidine gehören. Vergleicht man die chemische Struktur der ausgewählten Derivate, spielt die Position der angehängten Farnesylkette offenbar eine wichtige Rolle für die Effektivität (S.98 versus S.18, 38 und 101).

Wir zeigen, dass die ausgewählten Derivate, deren Grundlage Adenosin (S.38), Formycin (S.98) und Inosin (S.18, 19, 101) bilden, einen vergleichbaren oder sogar stärkeren zytostatischen/zytotoxischen Effekt wie das bekannte chemotherapeutische Mittel 5-FU haben. Auch bei weiteren untersuchten humanen Gliom Zellen (G28, G112, U251 und U87) und anderen Tumorenti-

täten (HT29, HepG2, Panc-1 und RenCa) können wir diese Effekte beobachten. Diese sind abhängig vom eingesetzten Derivat sowie dessen Konzentration und des verwendeten, spezifischen Zelltyps. Für weiterführende Versuche wurden die Ratten BT4Ca Gliom Zellen exemplarisch als Model für schnellwachsende Glioblastomzellen verwendet. Wir analysierten unterschiedliche intrazelluläre Mechanismen, die möglicherweise an den bereits beobachteten zytotoxischen Wirkungen der fünf ausgewählten Derivate (S.18, 19, 38, 98 und 101) beteiligt sind.

Unsere Versuchsergebnisse dokumentieren, dass die Behandlung der Ratten BT4Ca Gliom Zellen mit einem dieser fünf Derivate zu einem konzentrationsabhängigen Anstieg der apoptotischen Zellzahl führt. In den Konzentrationen 25 und 50 µM löst jedes der ausgewählten Derivate eine deutliche Steigerung der Capspase 3 Aktivität aus, wodurch die beobachtete Induktion der Apoptose bestätigt wird. Mit steigenden Konzentrationen (12.5, 25 und 50 µM) sehen wir allerdings auch einen erhöhten Anteil an nekrotischen Zellen. Dieser Anstieg ist vermutlich auf den Prozess der sekundär-Nekrose zurückzuführen. Neben dem Zelltod durch Apoptose, detektieren wir nach der Behandlung mit den jeweiligen Derivaten auch ein verringertes Level des Proteins PCNA, wodurch die Zellteilung der Ratten BT4Ca Zellen zusätzlich vermindert wird. Im Gegensatz zu den Derivaten hat die Behandlung mit 5-FUrd keinen Einfluss auf die gemessene Menge von PCNA. Demnach hat 5-FUrd unter unseren experimentellen Bedingungen keinen Einfluss auf die Zellteilungsrate der Ratten BT4Ca Zellen, was den beobachteten zytostatischen Effekt von 5-FUrd erklärt. Darüber hinaus beobachten wir nach der Behandlung der Ratten BT4Ca Zellen mit den Derivaten (50 µM) eine enorme Anhäufung von Sauerstoff Radikalen (ROS) pro Zelle. Besonders der Einsatz der Derivate S.18, 38 und 98 verursacht hohen oxidativen Stress für die Ratten BT4Ca Zellen. Allerdings führt nur die Behandlung mit Derivat S.98 zu einer eindeutigen Verringerung des rGSH/GSSG Verhältnisses und beeinflusst damit die physiologisch zur Verfügung stehende Menge des Antioxidans Glutathion. Keines der fünf ausgewählten Derivate führt zur Translokation der NFκB-Untereinheit p65 vom Zytoplasma in den Zellkern und damit zur Aktivierung von NFκB in den Ratten BT4Ca Zellen. Der Einfluss der Derivate auf die Migration der Ratten BT4Ca Zellen muss durch weitere Untersuchungen validiert werden. Die bisherigen Analysen zeigen, dass die Derivate S.18, 19, 38, 98 und 101 grundlegende Eigenschaften aufweisen, wodurch sie für die Behandlung von diversen bösartigen Krebszellen geeignet sind. Die fünf ausgewählten Derivate, besonders, S.19 und S.98, tragen durch ihr breites zytotoxisches Wirkungsspektrum und die Hemmung der Zellteilungsrate ein hohes Potential gegen mehrere, unterschiedliche Tumorentitäten als neue Wirkstoffe im Bereich der Chemotherapie Verwendung zu finden.

7. References

This bibliography was generated by the use of the APA generator Scribbr.
https://www.scribbr.de/plagiatspruefung/apa-generator/#/

Abcam. (2019a, März 27). DCFDA / H2DCFDA – Cellular Reactive Oxygen Species Detection Assay Kit. Abgerufen 28. März 2019, von https://www.abcam.com/dcfda--h2dcfda-cellular-ros-assay-kit-ab113851.html

Abcam. (2019b, April 16). NF-kB signaling | Abcam. Abgerufen 16. April 2019, von https://www.abcam.com/research-areas/overview-of-nf-kb-signaling

Aherne, G. W., Hardcastle, A., Raynaud, F., & Jackman, A. L. (1996, Mai). „Immunoreactive dUMP and TTP pools as an index of thymidylate synthase inhibition; effect of tomudex (ZD1694) and a nonpolyglutamated quinazoline an... “. Biochemical Pharmacology, Volume 51, Issue 10, 17 May 1996, Pages 1293-1301 - PubMed - NCBI. Abgerufen 26. März 2019, von https://www.ncbi.nlm.nih.gov/pubmed/8787544

ATCC. (2019a). Hep G2 [HEPG2] ATCC® HB-8065TM. Abgerufen 16. April 2019, von http://www.lgcstandards-atcc.org/products/all/HB-8065.aspx?geo_country=de

ATCC. (2019b). HT-29 ATCC ® HTB-38TM Homo sapiens colon colorectal adenocar. Abgerufen 16. April 2019, von http://www.lgcstandards-atcc.org/Products/All/HTB-38.aspx?geo_country=de

ATCC. (2019c). Renca ATCC ® CRL-2947TM Mus musculus kidney renal adenocarcin. Abgerufen 16. April 2019, von http://www.lgcstandards-atcc.org/products/all/CRL-2947.aspx?geo_country=de

ATCC. (2019d). U-87 MG ATCC ® HTB-14TM Homo sapiens brain Likely glioblastom. Abgerufen 28. März 2019, von http://www.lgcstandards-atcc.org/Products/All/HTB-14.aspx?geo_country=nl

ATCC. (2019e). U-87 MG ATCC ® HTB-14TM Homo sapiens brain Likely glioblastom. Abgerufen 16. April 2019, von http://www.lgcstandards-atcc.org/Products/All/HTB-14.aspx?geo_country=de

Azordegan, N., Fraser, V., Le, K., Hillyer, L., Ma, D., Fischer, G., & Moghadasian, M. (2013, Februar). „Carcinogenesis alters fatty acid profile in breast tissue”. Mol Molecular and Cellular Biochemistry, February 2013, Volume 374, Issue 1–2, pp 223–232. - PubMed - NCBI. Abgerufen 6. September 2019, von https://www.ncbi.nlm.nih.gov/pubmed/23180247

Azuma, M., Yamashita, T., Aota, K., Tamatani, T., & Sato, M. (2001, März). “5-Fluorouracil suppression of NF-KappaB is mediated by the inhibition of IKappab kinase activity in human salivary gland cancer cells.” Biochem. Biophys. Res. Commun. 2001 Mar 23;282(1):292-6.- PubMed - NCBI. Abgerufen 13. Oktober 2019, von https://www.ncbi.nlm.nih.gov/pubmed/11264006

Beck W.R., Wright G.E., Nusbaum N.J., Chang J.D., Isselbacher E.M. (1986) “Enhancement of Methotrexate Cytotoxicity by Uracil Analogues that Inhibit Deoxyuridine Triphosphate Nucleotidohydrolase (dUTPase) Activity.” In: Nyhan W.L., Thompson L.F., Watts R.W.E. (eds) Purine and Pyrimidine Metabolism in Man V. Advances in Experimental Medicine and Biology, vol 195B. Springer, New York, NY [Book]. Abgerufen 26. März 2019, von https://doi.org/10.1007/978-1-4684-1248-2_16

BioLegend, Inc. (2019). Propidium Iodide Solution. Abgerufen 28. März 2019, von https://www.biolegend.com/en-us/products/propidium-iodide-solution-2651

Bodner-Adler, B., Bodner, K., & Zeisler, H. (2007, Mai). „Breast cancer diagnosed during pregnancy.” Anticancer Res. 2007 May-Jun;27(3B):1705-7. - PubMed - NCBI. Abgerufen 26. März 2019, von https://www.ncbi.nlm.nih.gov/pubmed/17595801

Boehm, E. M., Gildenberg, M. S., & Wahington, M. T. (2017, April 19). “The many roles of PCNA in eukaryotic DNA replication.” The Enzymes, Volume 39, 2016, Pages 231-254 Abgerufen 19. Juni 2019, von https://www.ncbi.nlm.nih.gov/pmc/articles/PMC4890617/

Bomfin, L. E., Braga, C. M., Oliveira, T. A., Martins, C. S., Foschetti, D. A., Santos, A. A. Q. A., … Brito, G. A. C. (2017, Dezember). “5-Fluorouracil induces inflammation and oxidative stress in the major salivary glands affecting salivary flow and saliva composition.” Biochem. Pharmacol. 2017 Dec 1;145:34-45. doi: 10.1016/j.bcp.2017.08.024. Epub 2017 Sep 1.- PubMed - NCBI. Abgerufen 6. August 2019, von https://www.ncbi.nlm.nih.gov/pubmed/28867645

Bosch, L., Harbers, E., & Heidelberger, C. (1958). „Studies on fluorinated pyrimidines. V. Effects on nucleic acid metabolism in vitro.” Cancer Res. 1958 Apr;18(3):335-43. - PubMed - NCBI. Abgerufen 26. März 2019, von https://www.ncbi.nlm.nih.gov/pubmed/13523600

Bray, F., Ferlay, J., Soerjomataram, I., Siegel, R. L., Torre, L. A., & Jemal, A. (2018, September 12). “Global cancer statistics 2018: GLOBOCAN estimates of incidence and mortality worldwide for 36 cancers in 185 countries.” CA Cancer J Clin. 2018 Nov;68(6):394-424. doi: 10.3322/caac.21492. Epub 2018 Sep 12. Abgerufen 25. März 2019, von https://www.ncbi.nlm.nih.gov/pubmed/30207593

Butt, A. M., Jones, H. C., & Abbott, N. J. (1990). “Electrical resistance across the blood-brain barrier in anaesthetized rats: a developmental study.” J Physiol. 1990 Oct; 429: 47–62. Abgerufen 26. März 2019, von https://www.ncbi.nlm.nih.gov/pmc/articles/PMC1181686/

Camhi, S., Lee, P., & Choi , A. (1995, Mai). “The oxidative stress response.” New Horiz. 1995 May;3(2):170-82.- PubMed - NCBI. Abgerufen 10. September 2019, von https://www.ncbi.nlm.nih.gov/pubmed/7583159

Carrato, A., Köhne, C., Bedenne, L., Popov, I., Bouche, O., Gaspar, E., … Becker, H. (2006). „Folinic acid modulated bolus 5-FU or infusional 5-FU for adjuvant treatment of patients of UICC stage III colon cancer: Preliminary analysis of the PETACC-2-study.” Journal of Clinical Oncology 24, no. 18_suppl (June 20, 2006) 3563-3563. Abgerufen 26. März 2019, von https://ascopubs.org/doi/abs/10.1200/jco.2006.24.18_suppl.3563

Cell Biolabs, Inc. (2019). PCNA ELISA Kit | Cell Biolabs, Inc. Abgerufen 16. April 2019, von https://www.cellbiolabs.com/pcna-elisa-kit?gclid=Cj0KCQjw-tXlBRDWARIsAGYQAmfyj4cKXIV6uNo6nLmnEI-pgzgDJ1zH7u4BiebynjruqD9ZEIlW0VsaAnoaEALw_wcB

Chaudhuri, N. K., Montag, B. J., & Heidelberger, C. (1958). „Studies on fluorinated pyrimidines. III. The metabolism of 5-fluorouracil-2-C14 and 5-fluoroorotic-2-C14 acid in vivo.” Cancer Res. 1958 Apr;18(3):318-28. - PubMed - NCBI. Abgerufen 26. März 2019, von https://www.ncbi.nlm.nih.gov/pubmed/13523598

Cheng, M., Bing He, B., Tao Wan, T., Zhu, W., Han, J., Zha, B., … Ye, T. (2012 1). “5-Fluorouracil Nanoparticles Inhibit Hepatocellular Carcinoma via Activation of the p53 Pathway in the Orthotopic Transplant Mouse Model.” PLoS One. 2012; 7(10): e47115. Abgerufen 26. März 2019, von https://www.ncbi.nlm.nih.gov/pmc/articles/PMC3471936/

Clark, M., Homer, N., O’Connor, B., Chen, Z., Eskin, A., Lee, H., … Nelson, S. (2010, Januar). “U87MG Decoded: The Genomic Sequence of a Cytogenetically Aberrant Human Cancer Cell Line.” PLoS Genet. 2010 Jan; 6(1): e1000832. Abgerufen 6. September 2019, von https://www.ncbi.nlm.nih.gov/pmc/articles/PMC2813426/

CLS, cell lines service. (2019). CLS Product Information: U251 MG. Abgerufen 28. März 2019, von http://www.clsgmbh.de/pdf/u251-mg.pdf

Cooper, G. (2000). “Structure of the Plasma Membrane.” The Cell: A Molecular Approach. 2nd edition. - NCBI Bookshelf. Abgerufen 6. September 2019, von https://www.ncbi.nlm.nih.gov/books/NBK9898/

Danneberg, P. B., Montag, B. J., & Heidelberger, C. (1958). „Studies on fluorinated pyrimidines. IV. Effects on nucleic acid metabolism in vivo." Cancer Res. 1958 Apr;18(3):329-34.- PubMed - NCBI. Abgerufen 26. März 2019, von https://www.ncbi.nlm.nih.gov/pubmed/13523599

Diao, W., Tong, X., Yang, C., Zhang, F., Bao, C., Chen, H., … Ou-Yang , Z. (2019, Januar). "Behaviors of Glioblastoma Cells in in Vitro Microenvironments." Sci Rep. 2019; 9: 85. Abgerufen 6. September 2019, von https://www.ncbi.nlm.nih.gov/pmc/articles/PMC6331579/

Diasio, R. B., & Harris, B. E. (1989, April). "Clinical pharmacology of 5-fluorouracil." Clin Pharmacokinet. 1989 Apr;16(4):215-37. - PubMed - NCBI. Abgerufen 26. März 2019, von https://www.ncbi.nlm.nih.gov/pubmed/2656050

Doong, S. L., & Dolnick, B. J. (1988, März). "5-Fluorouracil substitution alters pre-mRNA splicing in vitro." J Biol Chem. 1988 Mar 25;263(9):4467-73. - PubMed - NCBI. Abgerufen 26. März 2019, von https://www.ncbi.nlm.nih.gov/pubmed/3346255

DSMZ, Leibniz Insitute DSMZ-German Collection of Microorganisms and Cell Cultures. (2019a). Catalogue: ACC-16. Abgerufen 16. April 2019, von https://www.dsmz.de/de/kataloge/catalogue/culture/ACC-16.html

DSMZ, Leibniz Insitute DSMZ-German Collection of Microorganisms and Cell Cultures. (2019b). Catalogue: ACC-408. Abgerufen 16. April 2019, von https://www.dsmz.de/de/kataloge/catalogue/culture/ACC-408.html

DSMZ, Leibniz Insitute DSMZ-German Collection of Microorganisms and Cell Cultures. (2019c). Details: ACC-783. Abgerufen 16. April 2019, von https://www.dsmz.de/catalogues/details/culture/ACC-783.html

Duronio, R., & Xiong, Y. (2013, März 1). „Signaling Pathways that Control Cell Proliferation." Cold Spring Harb Perspect Biol. 2013 Mar; 5(3): a008904. Abgerufen 10. September 2019, von https://www.ncbi.nlm.nih.gov/pmc/articles/PMC3578363/

ExPASy. (2019a). Cellosaurus cell line NCE-G 28 (CVCL_N724). Abgerufen 16. April 2019, von https://web.expasy.org/cellosaurus/CVCL_N724

ExPASy. (2019b). Cellosaurus cell line NCE-G 112 (CVCL_N740). Abgerufen 16. April 2019, von https://web.expasy.org/cellosaurus/CVCL_N740

Farhat, A. (2016). „Überprüfung des Drug Delivery Konzepts von „Lipid-Nucleosid-und Polysaccharid-Konjugaten von 5-Fluorouracil“ [Dissertation]. Abgerufen 5. August 2019, von http://archiv.ub.uni-marburg.de/diss/z2016/0544/pdf/daf.pdf

Farhat, A., Malecki, E., Bonaterra, G. A., Röthlein, D., Wolf, M., Schmitt, J., … Kinscherf, R. (2014, März). “Cytostatic/cytotoxic effects of 5-fluorouridine nucleolipids on colon, hepatocellular, and renal carcinoma cells: in vitro identification of a po-te...” Chem Biodivers. 2014 Mar;11(3):469-82. doi: 10.1002/cbdv.201300347. - PubMed - NCBI. Abgerufen 5. August 2019, von https://www.ncbi.nlm.nih.gov/pubmed/24634076

Fernald, K., & Kurokaw acorresponding author, M. (2013, Dezember). “Evading apoptosis in cancer.” Trends Cell Biol. 2013 Dec; 23(12): 620–633. Abgerufen 13. Oktober 2019, von https://www.ncbi.nlm.nih.gov/pmc/articles/PMC4091735/

Fernandes, C., Costa, A., Osório, L., Costa Lago, R., Linhares, P., Carvalho, B., & Caeiro, C. (2017, September). “Glioblastoma, Chapter 11 - Current Standards of Care in Glioblastoma Therapy”. Brisbane (AU): Codon Publications; 2017 Sep 27. ISBN-13: 978-0-9944381-2-6 Abgerufen 27. August 2019, von https://www.ncbi.nlm.nih.gov/books/NBK469987/

Figueroa, D., Asaduzzaman, M., & Young, F. (2018, April). “Real time monitoring and quantification of reactive oxygen species in breast cancer cell line MCF-7 by 2',7'-dichlorofluorescin diacetate (DCFDA) a...” J Pharmacol Toxicol Methods. 2018 Nov - Dec;94(Pt 1):26-33. doi: 10.1016/j.vascn.2018.03.007. Epub 2018 Apr 7. - PubMed - NCBI. Abgerufen 6. Juli 2019, von https://www.ncbi.nlm.nih.gov/pubmed/29630935

Focaccetti, C., Bruno, A., Magnani, E., Bartolini, D., Principi, E., Dallaglio, K., … Albini, A. (2015, Februar). “Effects of 5-fluorouracil on morphology, cell cycle, proliferation, apoptosis, autophagy and ROS production in endothelial cells and cardiomyocytes.” PLoS One. 2015 Feb 11;10(2):e0115686. doi: 10.1371/journal.pone.0115686. eCollection 2015. - PubMed - NCBI. Abgerufen 9. August 2019, von https://www.ncbi.nlm.nih.gov/pubmed/25671635

Forman, H. J., Zhang, H., & Rinna, A. (2009). “Glutathione: Overview of its protective roles, measurement, and biosynthesis.” Mol Aspects Med. 2009; 30(1-2): 1–12. Abgerufen 9. August 2019, von https://www.ncbi.nlm.nih.gov/pmc/articles/PMC2696075/

Fu, Y., Yang, G., Zhu, F., Peng, C., Li, W., Li, H., … Dong, Z. (2014, Januar). Antioxidants decrease the apoptotic effect of 5-Fu incolon cancer by regulating Src-dependent caspase-7phosphorylation. Abgerufen 6. August 2019, von Cell Death and Disease (2014) 5, e983; doi:10.1038/cddis.2013.509

Fujisawa, S., Romin, Y., Barlas, A., Petrovic, L. M., Turkekul, M., Fan, N., … Sofocleous, C. T. (2014, März 1). “Evaluation of YO-PRO-1 as an early marker of apoptosis following radiofrequency ablation of colon cancer liver metastases.” Cytotechnology. 2014 Mar; 66(2): 259–273. Abgerufen 28. März 2019, von https://www.ncbi.nlm.nih.gov/pmc/articles/PMC3918265/

Gawlitta, D., Oomens, C. W., Baaijens, F. P., & Bouten, C. V. (2005, November 30). “Evaluation of a continuous quantification method of apoptosis and necrosis in tissue cultures.” Cytotechnology. 2004 Oct;46(2-3):139-50. doi: 10.1007/s10616-005-2551-7. Epub 2005 Nov 30. - PubMed - NCBI. Abgerufen 19. Juni 2019, von https://www.ncbi.nlm.nih.gov/pubmed/19003268

GLOBOCAN 2018; Graph production: (2018). Global Cancer Observatory. Abgerufen 25. März 2019, von http://gco.iarc.fr/

Goodenberger, M. L., & Jenkins RB, R. B. (2012, Dezember). „Genetics of adult glioma.” Cancer Genet. 2012 Dec;205(12):613-21. doi: 10.1016/j.cancergen.2012.10.009. Epub 2012 Dec 11. - PubMed - NCBI. Abgerufen 25. März 2019, von https://www.ncbi.nlm.nih.gov/pubmed/23238284

Grogan, B. C., Parker, J. B., Guminski, A. F., & Stivers, J. T. (2011, Februar). “Effect of the thymidylate synthase inhibitors on dUTP and TTP pool levels and the activities of DNA repair glycosylases on uracil and 5-fluorouraci...” Biochemistry. 2011 Feb 8;50(5):618-27. doi: 10.1021/bi102046h. Epub 2011 Jan 11. - PubMed - NCBI. Abgerufen 26. März 2019, von https://www.ncbi.nlm.nih.gov/pubmed/21222484

Hammerbacher, K., Görtemaker, K., Knies, C., Bender, E., Bonaterra, G. A., Rosemeyer, H., & Kinscherf, R. (2018, September). „Combinatorial Synthesis of New Pyrimidine- and Purine-β-d-Ribonucleoside Nucleolipids: Their Distribution Between Aqueous and Organic Phases and Th...” Chem Biodivers. 2018 Sep;15(9):e1800173. doi: 10.1002/cbdv.201800173. Epub 2018 Aug 20. - PubMed - NCBI. Abgerufen 26. März 2019, von https://www.ncbi.nlm.nih.gov/pubmed/29928783

Han, R., Yang, Y. M., Dietrich, J., Luebke, A., Mayer-Pröschel, M., & Noble, M. (2008, April 22). “Systemic 5-fluorouracil treatment causes a syndrome of delayed myelin destruction in the central nervous system.” J Biol. 2008;7(4):12. doi: 10.1186/jbiol69. Epub 2008 Apr 22. - PubMed - NCBI. Abgerufen 19. Juni 2019, von https://www.ncbi.nlm.nih.gov/pubmed/18430259

Hanahan, D., & Weinberg, R. (2000, Januar). „The hallmarks of cancer.” Cell. 2000 Jan 7;100(1):57-70. - PubMed - NCBI. Abgerufen 11. September 2019, von https://www.ncbi.nlm.nih.gov/pubmed/10647931

Hanahan, D., & Weinberg, R. A. (2011, März). „Hallmarks of cancer: the next generation." Cell. 2011 Mar 4;144(5):646-74. doi: 10.1016/j.cell.2011.02.013. - PubMed - NCBI. Abgerufen 9. August 2019, von https://www.ncbi.nlm.nih.gov/pubmed/21376230

Heidelberger, C., Chaudhuri, N. K., Dannberg, P., Mooren, D., Griesbach, L., Duschinsky, R., … Scheiner, J. (1957). "Fluorinated pyrimidines, a new class of tumour-inhibitory compounds." Nature. 1957 Mar 30;179(4561):663-6. - PubMed - NCBI. Abgerufen 26. März 2019, von https://www.ncbi.nlm.nih.gov/pubmed/13418758

InvitrogenTM. (2010, Februar). MAN0002110Revised: 17–February–2010 | MP 13243Membrane Permeability/Dead Cell Apoptosis Kit with YO-PRO®-1 and PI for Flow Cytometry. Abgerufen 7. August 2019, von http://tools.thermofisher.com/content/sfs/manuals/mp13243.pdf

Jackson A., & Grindley R. C., (1984). The biochemical basis for methotrexate cytotoxicity, in: "Folate Antagonists as Therapeutic Agents, Vol. 1. Biochemistry, Molecular Actions, and Synthetic Design,"F.M. Sirotnak, J.J. Burchall, W.B. Ensminger, and J.A. Montgomery, eds., Academic Press, Orlando (1984) [Book]. Abgerufen 26. März 2019, von https://link.springer.com/chapter/10.1007/978-1-4684-1248-2_16

Jahangirian, H., Kalantari, K., Izadiyan, Z., Rafiee-Moghaddam, R., Shameli, K., & Webster, T. J. (2019, März). „A review of small molecules and drug delivery applications using gold and iron nanoparticles." Int J Nanomedicine. 2019; 14: 1633–1657. Abgerufen 5. August 2019, von https://www.ncbi.nlm.nih.gov/pmc/articles/PMC6417854/

Johansen, A., Hansen, H. D., Svarer, C., Lehel, S., Leth-Petersen, S., Kristensen, J. L., … Knudsen, G. M. (2017, Dezember 7). "The importance of small polar radiometabolites in molecular neuroimaging: A PET study with [11C]Cimbi-36 labeled in two positions." J Cereb Blood Flow Metab. 2018 Apr;38(4):659-668. doi: 10.1177/0271678X17746179. Epub 2017 Dec 7. - PubMed - NCBI. Abgerufen 19. Juni 2019, von https://www.ncbi.nlm.nih.gov/pubmed/29215308

Kannan, K., & Jain, S. K. (2000, September). "Oxidative stress and apoptosis." Pathophysiology. 2000 Sep;7(3):153-163. - PubMed - NCBI. Abgerufen 13. Oktober 2019, von https://www.ncbi.nlm.nih.gov/pubmed/10996508

Kelman, Z. (1997, Februar). "PCNA: structure, functions and interactions." Oncogene. 1997 Feb 13;14(6):629-40. - PubMed - NCBI. Abgerufen 9. August 2019, von https://www.ncbi.nlm.nih.gov/pubmed/9038370

Khosravi Shahi, P., Díaz Muñoz de la Espada, V. M., García Alfonso, P., Encina García, S., Izarzugaza Perón, Y., Arranz Cozar, J. L., … Pérez Manga, G. (2007, Juli). „Management of gastric adenocarcinoma.“ Clin Transl Oncol. 2007 Jul;9(7):438-42. - PubMed - NCBI. Abgerufen 26. März 2019, von https://www.ncbi.nlm.nih.gov/pubmed/17652057

Knies, C., Bonaterra, G., Hammerbacher, K., Cordes, A., Kinscherf , R., & Rosemeyer, H. (2015a, Dezember). “Ameliorated or Acquired Cytostatic/Cytotoxic Properties of Nucleosides by Lipophilization.” Chem Biodivers. 2015 Dec;12(12):1902-44. doi: 10.1002/cbdv.201500096. - PubMed - NCBI. Abgerufen 12. September 2019, von https://www.ncbi.nlm.nih.gov/pubmed/26663843

Knies, C., Hammerbacher, K., Bonaterra, G. A., Kinscherf, R., & Rosemeyer, H. (2015b, Dezember). „Nucleolipids of Canonical Purine ß-d-Ribo-Nucleosides: Synthesis and Cytostatic/Cytotoxic Activities Toward Human and Rat Glioblastoma Cells.” ChemistryOpen. 2016 Apr; 5(2): 129–141. Abgerufen 26. März 2019, von https://www.ncbi.nlm.nih.gov/pmc/articles/PMC4906469/

Knies, C., Hammerbacher, K., Bonaterra, G. A., Kinscherf, R., & Rosemeyer, H. (2016, Februar). „Novel Nucleolipids of Pyrimidine β-D-Ribonucleosides: Combinatorial Synthesis, Spectroscopic Characterization, and Cytostatic/Cytotoxic Activities.” Chem Biodivers. 2016 Feb;13(2):160-80. doi: 10.1002/cbdv.201500158.- PubMed - NCBI. Abgerufen 26. März 2019, von https://www.ncbi.nlm.nih.gov/pubmed/26880429

Knies, C., Reuter, H., Hammerbacher, K., Bender , E., Bonaterra, G. A., Kinscherf , R., & Rosemeyer, H. (2019, März). „Synthesis of New Potential Lipophilic Co-Drugs of 2-Chloro-2’-deoxyadenosine (Cladribine, 2-CdA, Mavenclad®, Leustatin®) and 6-Azauridine (z6 U) wi...” Chem Biodivers. 2019 Mar;16(3):e1800497. doi: 10.1002/cbdv.201800497. Epub 2019 Feb 25. - PubMed - NCBI. Abgerufen 12. September 2019, von https://www.ncbi.nlm.nih.gov/pubmed/30614625

Knies, C., & Rosemeyer, H. (2015, Januar). logPOW-Values of Nucleosides and Nucleolipids. Abgerufen 19. Juni 2019, von https://www.researchgate.net/publication/270450178_logP-Values_of_Nucleosides_and_Nucleolipids

Koçer, M., & Nazıroğlu, M. (2013, Dezember). „Effects of 5-Fluorouracil on Oxidative Stress and Calcium Levels in the Blood of Patients with Newly Diagnosed Colorectal Cancer.” Biological Trace Element Research

December 2013, Volume 155, Issue 3, pp 327–332 Abgerufen 6. August 2019, von https://doi.org/10.1007/s12011-013-9795-4

Köstler, K., Werz, E., Malecki, E., Montilla-Martinez, M., & Rosemeyer, H. (2013, Januar). “Nucleoterpenes of thymidine and 2’-deoxyinosine: synthons for a biomimetic lipophilization of oligonucleotides”. Chem Biodivers. 2013 Jan;10(1):39-61. doi: 10.1002/cbdv.201100338. - PubMed - NCBI. Abgerufen 5. August 2019, von https://www.ncbi.nlm.nih.gov/pubmed/23341207

Krebsgesellschaft. (2019, März 25). Die Molekularbiologische Therapie bei Krebs. Abgerufen 25. März 2019, von https://www.krebsgesellschaft.de/onko-internetportal/basis-informationen-krebs/therapieformen/molekularbiologische-therapie.html

Kubben, F. J., Peeters-Haesevoets, A., Engels, L. G., Baeten, C. G., Schutte, B., Arends, J. W., … Blijham, G. H. (1994, April). “Proliferating cell nuclear antigen (PCNA): a new marker to study human colonic cell proliferation.” Gut. 1994 Apr; 35(4): 530–535. Abgerufen 9. August 2019, von https://www.ncbi.nlm.nih.gov/pmc/articles/PMC1374804/

Kufe, D. W., Major, P. P., Egan, E. M., & Loh, E. (1981, September). “5-Fluoro-2’-deoxyuridine incorporation in L1210 DNA.” J Biol Chem. 1981 Sep 10;256(17):8885-8. - PubMed - NCBI. Abgerufen 26. März 2019, von https://www.ncbi.nlm.nih.gov/pubmed/6455432

Kumari, S., Badana, A. K., G, M. M., G, S., & Malla, R. R. (2018, Februar). „Reactive Oxygen Species: A Key Constituent in Cancer Survival.” Biomark Insights. 2018; 13: 1177271918755391. Abgerufen 13. Oktober 2019, von https://www.ncbi.nlm.nih.gov/pmc/articles/PMC5808965/

Kwon, H., Lee, J., Shin, H., Kim, J., & Choi, S. (2015, Oktober). “Structural and functional analysis of cell adhesion and nuclear envelope nano-topography in cell death.” Sci Rep. 2015 Oct 22;5:15623. doi: 10.1038/srep15623.- PubMed - NCBI. Abgerufen 11. September 2019, von https://www.ncbi.nlm.nih.gov/pubmed/26490051

Laerum, O. D., Rajewsky, M. F., Schachner, M., Stavrou, D., Haglid, K. G., & Haugen, Å. (1977). „Phenotypic properties of neoplastic cell lines developed from fetal ra." Zeitschrift für Krebsforschung und Klinische Onkologie January 1977, Volume 89, Issue 3, pp 273–295 Abgerufen 28. August 2019, von https://link.springer.com/article/10.1007%2FBF00283783

Lakkadwala, S., & Singh, J. (2018, November). "Dual Functionalized 5-Fluorouracil Liposomes as Highly Efficient Nanomedicine for Glioblastoma Treatment as Assessed in an In Vitro Brain Tumor Model." J Pharm Sci. 2018 Nov;107(11):2902-2913. doi: 10.1016/j.xphs.2018.07.020. Epub 2018 Jul 25. - PubMed - NCBI. Abgerufen 27. August 2019, von https://www.ncbi.nlm.nih.gov/pubmed/30055226

Larner, J. M., Kersh, C. R., Constable, W. C., Kline, P., Ferguson, R., Short, R., & Jane, J. A. (1991). "Phase I/II trial of superselective arterial 5-FU infusion with concomitant external beam radiation for patients with either anaplastic astrocytoma or glioblastoma multiforme." Am J Clin Oncol. 1991 Dec;14(6):514-8. Abgerufen 27. August 2019, von https://www.ncbi.nlm.nih.gov/pubmed/1659783

Lévi, F., Zidani, R., Brienza, S., Dogliotti, L., Perpoint, B., Rotarski, M., … Focan, C. (1999, Juni). "A multicenter evaluation of intensified, ambulatory, chronomodulated chemotherapy with oxaliplatin, 5-fluorouracil, and leucovorin as initial treat..." Cancer. 1999 Jun 15;85(12):2532-40. - PubMed - NCBI. Abgerufen 26. März 2019, von https://www.ncbi.nlm.nih.gov/pubmed/10375099

Lindahl, T. (1974, September). "An N-glycosidase from Escherichia coli that releases free uracil from DNA containing deaminated cytosine residues." Proc Natl Acad Sci U S A. 1974 Sep;71(9):3649-53 - PubMed - NCBI. Abgerufen 26. März 2019, von https://www.ncbi.nlm.nih.gov/pubmed/4610583

Lipinski, C. A., Lombardo, F., Dominy, B. W., & Feeney, P. J. (2001, März). "Experimental and computational approaches to estimate solubility and permeability in drug discovery and development settings." Adv Drug Deliv Rev. 2001 Mar 1;46(1-3):3-26. - PubMed - NCBI. Abgerufen 5. August 2019, von https://www.ncbi.nlm.nih.gov/pubmed/11259830

Liu, F., Bardhan, K., Yang, D., Thangaraju, M., Ganapathy , V., Waller, J. L., … Liu, K. (2012, Juli). "NF-κB directly regulates Fas transcription to modulate Fas-mediated apoptosis and tumor suppression." J Biol Chem. 2012 Jul 20;287(30):25530-40. doi: 10.1074/jbc.M112.356279. Epub 2012 Jun 5. - PubMed - NCBI. Abgerufen 13. Oktober 2019, von https://www.ncbi.nlm.nih.gov/pubmed/22669972

Liu, T., Zhang, L., Joo, D., & Sun, S. C. (2017, Juli). „NF-κB signaling in inflammation.“ Signal Transduct Target Ther. 2017; 2: 17023. Abgerufen 9. August 2019, von https://www.ncbi.nlm.nih.gov/pmc/articles/PMC5661633/

Longley, D. B., Harkin, D. P., & Johnston, P. G. (2003a, Mai).” 5-fluorouracil: mechanisms of action and clinical strategies.” Nat Rev Cancer. 2003 May;3(5):330-8 - PubMed - NCBI. Abgerufen 26. März 2019, von https://www.ncbi.nlm.nih.gov/pubmed/12724731

Malecki, E. (2013). Nucleolipids and Lipo-Oligonucleotides of 5-Fluorouridine: Synthesis, Biological Applications and Immobilization [Dissertation]. Abgerufen 5. August 2019, von https://repositorium.ub.uni-osnabrueck.de/bitstream/urn:nbn:de:gbv:700-2014040412368/1/thesis_malecki.pdf

Malecki, E., Farhat, A., Bonaterra, G. A., Röthlein, D., Wolf, M., Schmitt, J., … Rosemeyer, H. (2013, Dezember). “Synthesis of 5-fluorouridine nucleolipid derivatives and their cytostatic/cytotoxic activities on human HT-29 colon carcinoma cells.” Chem Biodivers. 2013 Dec;10(12):2235-46. doi: 10.1002/cbdv.201300219.- PubMed - NCBI. Abgerufen 5. August 2019, von https://www.ncbi.nlm.nih.gov/pubmed/24327444

Malecki, E., Ottenhaus, V., Werz, E., Knies, C., Montilla Martinez, M., & Rosemeyer, H. (2014, Februar). “Nucleolipids of the cancerostatic 5-fluorouridine: synthesis, adherence to oligonucleotides, and incorporation in artificial lipid bilayers.” Chem Biodivers. 2014 Feb;11(2):217-32. doi: 10.1002/cbdv.201300127. - PubMed - NCBI. Abgerufen 5. August 2019, von https://www.ncbi.nlm.nih.gov/pubmed/24591313

Malecki, E., & Rosemeyer, H. (2010). “O-2’,3’-Ketal-Nucleolipids of the Cytostatic 5-Fluorouridine: Synthesis, Lipophilicity, and Acidic Stability.” Chem Biodivers. 2014 Feb;11(2):217-32. doi: 10.1002/cbdv.201300127. Abgerufen 5. August 2019, von https://www.academia.edu/18486786/O-2_3_-Ketal-Nucleolipids_of_the_Cytostatic_5-Fluorouridine_Synthesis_Lipophilicity_and_Acidic_Stability

Malecki, E., Viere, R., & Rosemeyer, H. (2013, Oktober). „Immobilization of 5-fluorouridine on chitosan.” Chem Biodivers. 2013 Oct;10(10):1828-41. doi: 10.1002/cbdv.201300025. - PubMed - NCBI. Abgerufen 12. September 2019, von https://www.ncbi.nlm.nih.gov/pubmed/24130026

Marin-Vicente, C., Lyutvinskiy, Y., Romans Fuertes, P., Zubarev, R. A., & Visa, N. (2013, April). “The effects of 5-fluorouracil on the proteome of colon cancer cells.” J Proteome Res. 2013 Apr 5;12(4):1969-79. doi: 10.1021/pr400052p. Epub 2013 Mar 21. - PubMed - NCBI. Abgerufen 26. März 2019, von https://www.ncbi.nlm.nih.gov/pubmed/23477467

Martindale, J., & Holbrook, N. (2002, Juli). “Cellular response to oxidative stress: signaling for suicide and survival.” J Cell Physiol. 2002 Jul;192(1):1-15. - PubMed - NCBI. Abgerufen 10. September 2019, von https://www.ncbi.nlm.nih.gov/pubmed/12115731

Merck, Sigma-Aldrich. (2019). bisBenzimide H 33342 trihydrochloride. Abgerufen 28. März 2019, von https://www.sigmaaldrich.com/catalog/product/sigma/14533?lang=en®ion=US&gclid=EAIaIQobChMIk4Hv3aPn3QIVz6iaCh336w8WEAAYASAAEgJfavD_BwE

Mhaidat, N. M., Bouklihacene, M., & Thorne, R. F. (2014, August). “5-Fluorouracil-induced apoptosis in colorectal cancer cells is caspase-9-dependent and mediated by activation of protein kinase C-δ.” Oncol Lett. 2014 Aug; 8(2): 699–704. Abgerufen 7. August 2019, von https://www.ncbi.nlm.nih.gov/pmc/articles/PMC4081407/

Moynagh, P. N. (2015, Oktober 15). “The NF-kappaB pathway.” J Cell Sci. 2005 Oct 15;118(Pt 20):4589-92. - PubMed - NCBI. Abgerufen 16. April 2019, von https://www.ncbi.nlm.nih.gov/pubmed/16219681

Nature. (2019). Small moclecules. Abgerufen 5. August 2019, von https://www.nature.com/subjects/small-molecules

Negishi, K. (1994, Februar). “5-Fluorouracil reduces proliferating cell nuclear antigen immunoreactive cells in goldfish retina.” Neurosci Res. 1994 Feb;19(1):21-9. - PubMed - NCBI. Abgerufen 9. August 2019, von https://www.ncbi.nlm.nih.gov/pubmed/7911984

Newsholme, P., Cruzat, V. F., Keane, K. N., Carlessi, R., & Bittencourt, P. I. (2016, Dezember). “Molecular mechanisms of ROS production and oxidative stress in diabetes.” Biochem J. 2016 Dec 15;473(24):4527-4550. - PubMed - NCBI. Abgerufen 28. März 2019, von https://www.ncbi.nlm.nih.gov/pubmed/27941030

NIH, National Cancer Institute. (2016, Juni). Temozolomide for brain cancer. Abgerufen 27. August 2019, von https://www.cancer.gov/news-events/cancer-currents-blog/2016/asco-temozolomide-brain

NIH, National Cancer Institute. (2019). NCI Dictionary of Cancer Terms. Abgerufen 5. August 2019, von https://www.cancer.gov/publications/dictionaries/cancer-terms/def/small-molecule-drug

Orellana, E. A., & Kasinski, A. L. (2016, November 5). “Sulforhodamine B (SRB) Assay in Cell Culture to Investigate Cell Proliferation.” Bio Protoc. 2016 Nov 5; 6(21): e1984. Abgerufen 28. März 2019, von https://www.ncbi.nlm.nih.gov/pmc/articles/PMC5448418/

Owen, J. B., & Butterfield, D. A. (2010). “Measurement of oxidized/reduced glutathione ratio.” Methods Mol Biol. 2010;648:269-77. doi: 10.1007/978-1-60761-756-3_18. - PubMed - NCBI. Abgerufen 1. Juli 2019, von https://www.ncbi.nlm.nih.gov/pubmed/20700719

Papaliagkas, V., Anogianaki, A., Anogianakis, G., & Ilonidis, G. (2007, September). “The proteins and the mechanisms of apoptosis: A mini-review of the fundamentals.” Hippokratia. 2007 Jul-Sep; 11(3): 108–113. Abgerufen 10. September 2019, von https://www.ncbi.nlm.nih.gov/pmc/articles/PMC2658792/

Patton, J. R. (1993, März). “Multiple pseudouridine synthase activities for small nuclear RNAs.” Biochem J. 1993 Mar 1;290 (Pt 2):595-600. - PubMed - NCBI. Abgerufen 26. März 2019, von https://www.ncbi.nlm.nih.gov/pubmed/8452551

Paulus of Aeginata. (o. J.). The Seven Books of Paulus Aegineta. Abgerufen 25. März 2019, von https://books.google.de/books?id=-g1kAAAAcAAJ

Perkins, N. D. (2007, Januar). “Integrating cell-signalling pathways with NF-κB and IKK function.” Nature Reviews Molecular Cell Biology volume 8, pages49–62(2007 - PubMed - NCBI. Abgerufen 9. August 2019, von https://www.nature.com/articles/nrm2083

Pettersen, H. S., Visnes, T., Broberg Vågbø, C., Svaasand, E. K., Doseth, B., Slupphaug, G., … Krokan, H. E. (2011, Oktober 1). “UNG-initiated base excision repair is the major repair route for 5-fluorouracil in DNA, but 5-fluorouracil cytotoxicity depends mainly on RNA incorporation.” Nucleic Acids Res. 2011 Oct; 39(19): 8430–8444. Abgerufen 26. März 2019, von https://www.ncbi.nlm.nih.gov/pmc/articles/PMC3201877/

Porter, A. G., & Jänicke, R. U. (1999, Februar). „Emerging roles of caspase-3 in apoptosis.” Cell Death Differ. 1999 Feb;6(2):99-104. - PubMed - NCBI. Abgerufen 6. August 2019, von https://www.ncbi.nlm.nih.gov/pubmed/10200555

Portnow, J., Badie, B., Chen, M., Liu, A., Blanchard, S., & Synold, T. W. (2009, Oktober). "THE NEUROPHARMACOKINETICS OF TEMOZOLOMIDE IN PATIENTS WITH RESECTABLE BRAIN TUMORS: POTENTIAL IMPLICATIONS FOR THE CURRENT APPROACH TO CHEMORADIATION." Clin Cancer Res. 2009 Nov 15; 15(22): 7092–7098. Abgerufen 27. August 2019, von https://www.ncbi.nlm.nih.gov/pmc/articles/PMC2908372/

Rahal, A., Kumar, A., Singh, V., Yadav, B., Tiwari, R., Chakraborty, S., & Dhama, K. (2014). „Oxidative stress, prooxidants, and antioxidants: the interplay." Biomed Res Int. 2014;2014:761264. doi: 10.1155/2014/761264. Epub 2014 Jan 23. - PubMed - NCBI. Abgerufen 28. August 2019, von https://www.ncbi.nlm.nih.gov/pubmed/24587990

Rahman, I., Kode, A., & Biswas, S. K. (2006). „Assay for quantitative determination of glutathione and glutathione disulfide levels using enzymatic recycling method." Nat Protoc. 2006;1(6):3159-65. - PubMed - NCBI. Abgerufen 1. Juli 2019, von https://www.ncbi.nlm.nih.gov/pubmed/17406579

Ray, P. D., Huang, B. W., & Tsuji, Y. (2012, Mai). „Reactive oxygen species (ROS) homeostasis and redox regulation in cellular signaling." Cell Signal. 2012 May;24(5):981-90. doi: 10.1016/j.cellsig.2012.01.008. Epub 2012 Jan 20. - PubMed - NCBI. Abgerufen 6. Juli 2019, von https://www.ncbi.nlm.nih.gov/pubmed/22286106

Restall, I., Bozek, D. A., Chesnelong, C., Weiss, S., & Luchman, H. A. (2018, August). Live-Cell Imaging Assays to Study Glioblastoma Brain Tumor Stem Cell Migration and Invasion | Protocol. Abgerufen 9. August 2019, von https://www.jove.com/video/58152/live-cell-imaging-assays-to-study-glioblastoma-brain-tumor-stem-cell

Reuter, H., Van Bodegraven, A.M., Bender, E., Knies, C., Diek, N., Beginn, U., Hammerba-cher, K., Schneider, V., Kinscherf, R., Bonaterra, G. A., Svajda, R., Rosemeyer, H. (2019). Guanosine Nucle-olipids: Synthesis, Characterization, Aggregation and X-Ray Crystallographic Identification of Electricity-Conducting G-ribbons. Chem Biodivers. 2019 Feb. 22. doi: https://doi.org/10.1002/cbdv.201900024; PMID: 30793846

Ritu, L. (2014, Mai 1). "A Brief History of Breast Cancer: Part I: Surgical domination reinvented." Sultan Qaboos Univ Med J. 2014 May; 14(2): e166–e169. Abgerufen 25. März 2019, von https://www.ncbi.nlm.nih.gov/pmc/articles/PMC3997531/

Rosemeyer H, Knies C, Hammerbacher K, Bender E, Bonaterra GA, Hannen R, Bartsch JW, Nimsky C, Kinscherf R. (2019). „Nucleolipids of the Nucleoside Antibiotics Formycin A and B: Synthesis and Biomedical Characterization particularly using Glioblastoma Cells." Chemistry&Biodiversity Volume16, Issue4, April 2019. Abgerufen 12. September 2019, von https://doi.org/10.1002/cbdv.201900012; PMID: 30773842

Rosemeyer H, Malecki E., Eur. Pat. Appl. EP 12 186 564.6, 2012

Rosemeyer, H., Malecki, E., Werz, E., Korneev, S., Gall, K., Eur. Pat. Appl. EP 12 186 576.0, 2012

Roullin, V. G., Mege, M., Lemaire, L., Cueyssac, J. P., Venier-Julienne, M. C., Menei, P., … Benoit, J. P. (2004, September). "Influence of 5-Fluorouracil-Loaded Microsphere Formulation on Efficien." Pharmaceutical Research September 2004, Volume 21, Issue 9, pp 1558–1563 Abgerufen 27. August 2019, von https://link.springer.com/article/10.1023/B:PHAM.0000041448.22771.48

Rutman, R. J., Cantarow, A., & Paschkis, K. E. (1954). "The catabolism of uracil in vivo and in vitro." J Biol Chem. 1954 Sep;210(1):321-9. - PubMed - NCBI. Abgerufen 26. März 2019, von https://www.ncbi.nlm.nih.gov/pubmed/13201593

Santi, D. V., & Hardy, L. W. (1987, Dezember). "Catalytic mechanism and inhibition of tRNA (uracil-5-)methyltransferase: evidence for convalent catalysis." Biochemistry. 1987 Dec 29;26(26):8599-606. Abgerufen 26. März 2019, von https://www.ncbi.nlm.nih.gov/pubmed/3327525

Taal, W., Bromberg, J. E., & van den Bent, M. J. (2015, Mai 1). „Chemotherapy in glioma." CNS Oncol. 2015 May; 4(3): 179–192. Abgerufen 25. März 2019, von https://www.ncbi.nlm.nih.gov/pmc/articles/PMC6088309/figure/F0001/

Tanaka, F., Fukuse, T., Wada, H., & Fukushima, M. (2000, September). "The history, mechanism and clinical use of oral 5-fluorouracil derivative chemotherapeutic agents." Curr Pharm Biotechnol. 2000 Sep;1(2):137-64. - PubMed - NCBI. Abgerufen 5. August 2019, von https://www.ncbi.nlm.nih.gov/pubmed/11467334

Thermo Fisher Scientific. (2019). Pierce BCA Protein Assay Kit - Thermo Fisher Scientific. Abgerufen 16. April 2019, von https://www.thermofisher.com/order/catalog/product/23225

ThermoFisherScientific. (2019). CellEvent Caspase-3/7 Green Detection Reagent - Thermo Fisher Scientific. Abgerufen 28. März 2019, von https://www.thermofisher.com/order/catalog/product/C10423

Tietze, F. (1969, März). “Enzymic method for quantitative determination of nanogram amounts of total and oxidized glutathione: applications to mammalian blood and other tiss...” Anal Biochem. 1969 Mar;27(3):502-22. - PubMed - NCBI. Abgerufen 6. Juli 2019, von https://www.ncbi.nlm.nih.gov/pubmed/4388022

Tong, D., Poot, M., Hu, D., & Oda, D. (2000, März). “5-Fluorouracil-induced apoptosis in cultured oral cancer cells.” Oral Oncol. 2000 Mar;36(2):236-41. - PubMed - NCBI. Abgerufen 7. August 2019, von https://www.ncbi.nlm.nih.gov/pubmed/10745178

Torsvik, A., Stieber, D., Enger, P., Golebiewska, A., Molven, A., Svendsen, A., … Bjerkvig, R. (2014, August). ”U-251 revisited: genetic drift and phenotypic consequences of long-term cultures of glioblastoma cells.” Cancer Med. 2014 Aug; 3(4): 812–824. Abgerufen 6. September 2019, von https://www.ncbi.nlm.nih.gov/pmc/articles/PMC4303149/

University of Colorado. (o. J.). Differences between necrosis and apoptosis. Abgerufen 28. März 2019, von https://www.uccs.edu/Documents/rmelamed/apoptosis_003_004.pdf

Vigneswaran, K., Neill, S., & Hadjipanayis, C. G. (2015, November 5). “Beyond the World Health Organization grading of infiltrating gliomas: advances in the molecular genetics of glioma classification.” ATM Vol 3, No 7 (May 2015). Abgerufen 25. März 2019, von http://atm.amegroups.com/article/view/6335/7112

Voboril, R., Hochwald, S. N., Li, J., Brank, A., Weberova, J., Wessels, F., … MacKay, S. L. (2004, August). “Inhibition of NF-kappa B augments sensitivity to 5-fluorouracil/folinic acid in colon cancer.” J Surg Res. 2004 Aug;120(2):178-88. - PubMed - NCBI. Abgerufen 9. August 2019, von https://www.ncbi.nlm.nih.gov/pubmed/15234211

Weiss, J. T., Fraser, C., Rubio-Ruiz, B., Myers, S. H., Crispin, R., Dawson, J. C., … Unciti-Broceta, A. (2014, Juli 29). “N-alkynyl derivatives of 5-fluorouracil: susceptibility to palladium-mediated dealkylation and toxigenicity in cancer cell culture.” Front Chem. 2014; 2: 56. Abgerufen 26. März 2019, von https://www.ncbi.nlm.nih.gov/pmc/articles/PMC4114543/

Werz, E., Viere, R., Gassmann, G., Korneev, S., Malecki, E., & Rosemeyer, H. (2013, Mai). „Synthesis of Thymidine, Uridine, and 5-Methyluridine Nucleolipids: Tools for a Tuned Lipophilization of Oligonucleotides.” Helvetica Volume96, Issue5 May 2013 Pages 872-888. Abgerufen 5. August 2019, von https://doi.org/10.1002/hlca.201200573

Westphal, M., Haensel, M., Mueller, D., Laas, R., Kunzmann, R., Rohde, E., … Herrmann, H. (1988, Februar). “Biological and karyotypic characterization of a new cell line derived from human gliosarcoma.” Cancer Res. 1988 Feb 1;48(3):731-40. - PubMed - NCBI. Abgerufen 6. September 2019, von https://www.ncbi.nlm.nih.gov/pubmed/3275500

Westphal, M., Hänsel, M., Hamel , W., Kunzmann, R., & Hölzel, F. (1994). „Karyotype analyses of 20 human glioma cell lines.” Acta Neurochir (Wien). 1994;126(1):17-26. - PubMed - NCBI. Abgerufen 6. September 2019, von https://www.ncbi.nlm.nih.gov/pubmed/8154317

Wettergren, Y., Carlsson, G., Odin, E., & Gustavsson, B. (2011, Oktober). „Pretherapeutic Uracil and DihydrouracilLevels of Colorectal Cancer Patients AreAssociated With Sex and Toxic Side EffectsDuring Adjuvant 5-Fluorouracil–BasedChemotherapy.” Abgerufen 26. März 2019, von https://onlinelibrary.wiley.com/action/cookieAbsent

WHO, World Health Organisation. (2018, September 12). Cancer. Abgerufen 25. März 2019, von https://www.who.int/news-room/fact-sheets/detail/cancer

Wong, R. S. (2001, September). “Apoptosis in cancer: from pathogenesis to treatment.” J Exp Clin Cancer Res. 2011; 30(1): 87. Abgerufen 13. Oktober 2019, von https://www.ncbi.nlm.nih.gov/pmc/articles/PMC3197541/

Xia, L., Tan, S., Zhou, Y., Lin, J., Wang, H., Oyang, L., … Liao, Q. (2018, April). “Role of the NFκB-signaling pathway in cancer.” Onco Targets Ther. 2018; 11: 2063–2073. Abgerufen 13. Oktober 2019, von https://www.ncbi.nlm.nih.gov/pmc/articles/PMC5905465/

Xu, M., McCanna, D. J., & Sivak, J. G. (2015, Februar). “Use of the viability reagent PrestoBlue in comparison with alamarBlue and MTT to assess the viability of human corneal epithelial cells.” J Pharmacol Toxicol Methods. 2015 Jan-Feb;71:1-7. doi: 10.1016/j.vascn.2014.11.003. Epub 2014 Nov 15. - PubMed - NCBI. Abgerufen 28. März 2019, von https://www.ncbi.nlm.nih.gov/pubmed/25464019

Yang, N. J., & Hinner, M. J. (2016, Juli). „Getting Across the Cell Membrane: An Overview for Small Molecules, Peptides, and Proteins.” Methods Mol Biol. 2015; 1266: 29–53. Abgerufen 5. August 2019, von https://www.ncbi.nlm.nih.gov/pmc/articles/PMC4891184/

Yoon, J. H. (2005, Juni 30). “Systemic overview of 5-FU based chemotherapy in breast cancer.” Korean J Clin Oncol. 2005;1(1): 68-73. Abgerufen 5. August 2019, von http://kjco.org/journal/view.php?number=207

Yue, P. Y., Leung, E. P., Mak, N. K., & Wong, R. N. (2010, Mai). “A simplified method for quantifying cell migration/wound healing in 96-well plates.” J Biomol Screen. 2010 Apr;15(4):427-33. doi: 10.1177/1087057110361772. Epub 2010 Mar 5. - PubMed - NCBI. Abgerufen 6. Juli 2019, von https://www.ncbi.nlm.nih.gov/pubmed/20208035

Zitka, O., Skalickova, S., Gumulec, J., Masarik, M., Adam, V., Hubalek, J., … Kitek, R. (2012, Dezember). “Redox status expressed as GSH:GSSG ratio as a marker for oxidative stress in paediatric tumour patients.” Oncol Lett. 2012 Dec; 4(6): 1247–1253. Abgerufen 9. August 2019, von https://www.ncbi.nlm.nih.gov/pmc/articles/PMC3506742/

7.1. Own publications

Master thesis:

1. Knies C, Bonaterra GA, **Hammerbacher** K, Cordes A, Kinscherf R, Rosemeyer H. (2015a). Ameliorated or Acquired Cytostatic/Cytotoxic Properties of Nucleosides by Lipophilization. Chemistry & Biodiversity 12(12):1902–1944.

2. Knies C, **Hammerbacher K**, Bonaterra GA, Kinscherf R, Rosemeyer H. (2015b). Nucleolipids of Canonical Purine ß-d-Ribo-Nucleosides: Synthesis and Cytostatic/Cytotoxic Activities toward Human and Rat Glioblastoma Cells. ChemistryOpen 5 (2):129-141.

3. Knies C, **Hammerbacher K**, Bonaterra GA, Kinscherf R, Rosemeyer H. (2016). Novel Nucleolipids of Pyrimidine β-D-Ribonucleosides: Combinatorial Synthesis, Spectroscopic Characterization, and Cytostatic/Cytotoxic Activities. Chemistry & Biodiversity 13(2):160-80.

Dissertation:

4. **Hammerbacher K**, Görtemaker K, Knies C, Bender E, Bonaterra GA, Rosemeyer H, Kinscherf R. (2018). Combinatorial Synthesis of New Pyrimidine- and Purine-ß-D-Ribonucleoside Nucleolipids: Their Distribution Between Aqueous and Organic Phases and Their in vitro Activity Against Human- and Rat Glioblastoma Cells in vitro. Chem Biodivers. 2018 Jun. 21. doi: 10.1002/cbdv.201800173; PMID: 29928783

5. Knies C, Reuter H, **Hammerbacher K**, Bender E, Bonaterra GA, Kinscherf R, Rosemeyer H. (2019a). Synthesis of New Potential Lipophilic Co-Drugs of 2-Chloro-2'-deoxyadenosine (Cladribine, 2CdA, Mavenclad®, Leustatin®) and 6-Azauridine (z6U) with Valproic Acid. Chem Biodivers. 2018 Dec. 21. doi: 10.1002/cbdv.201800497; PMID: 30614625

6. Rosemeyer H, Knies C, **Hammerbacher K**, Bender E, Bonaterra GA, Hannen R, Bartsch JW, Nimsky C, Kinscherf R. (2019). Nucleolipids of the Nucleoside Antibiotics Formycin A and B: Synthesis and Biomedical Characterization particularly using Glioblastoma Cells. Chem Biodivers Volume16, Issue4 April 2019 doi: https://doi.org/10.1002/cbdv.201900012; PMID: 30773842

7. Reuter H, Van Bodegraven A.M, Bender E, Knies C, Diek N, Beginn U, **Hammerbacher K**, Schneider V, Kinscherf R, Bonaterra GA, Svajda R, Rosemeyer H. (2019). Guanosine Nucleolipids: Synthesis, Characterization, Aggregation and X-Ray Crystallographic Identification of Electricity-Conducting G-ribbons. Chem Biodivers. 2019 Feb. 22. doi: https://doi.org/10.1002/cbdv.201900024; PMID: 30793846

8. Supplements

Verzeichnis der akademischen Lehrer/-innen

1. Bachelorstudiengang molekulare Biomedizin an der Rheinische Friedrich-Wilhelms-Universität Bonn

Meine akademischen Lehrenden waren in Bonn:

- Prof. Becker
- Prof. Bruchhaus
- Prof. Famulok
- Prof. Franz
- Prof. Haas
- Prof. Hoch
- Prof. Kirfeld
- Prof. Koch
- Prof. Lang
- Prof. Mader
- Prof. Maier
- Prof. Mayer
- Prof. Schilling
- Prof. Schilling
- Prof. Völker
- Prof. Weisbart
- Prof. Wittke

2. Masterstudiengang Humanbiologie mit Schwerpunkt Zellbiologie an der Philipps-Universität Marburg

Meine akademischen Lehrenden waren in Marburg:

- B. Greene
- Dr. Bonaterra
- Prof. Timmesfeld
- PD Dr. Buchholz
- PD Dr. J. Hänze
- Prof. Elsässer
- Prof. Jacob
- Prof. Kinscherf
- Prof. Lill

Danksagung

Herrn Prof. Dr. Ralf Kinscherf möchte ich für die Möglichkeit danken, meine Promotion der Vertiefung und Weiterführung dieses interessanten Themas zu widmen. Die Herausforderung eines eigenständigen Projektes hat mir viel Spaß gemacht.

Herrn Prof. Dr. Helmut Rosemeyer und seiner AG möchte ich für die Erweiterung meines Verständnisses für Chemie sowie die Unterstützung bei chemischen Fragestellungen danken.

Mein besonderer Dank gilt vor allem Dr. Gabriel Bonaterra, der mir als kompetenter Betreuer jeder Zeit zur Seite stand. Danke für die hohe Diskussions- und Hilfsbereitschaft sowie die große Geduld bei der Korrektur meiner Dissertation. Die konstruktive Kritik hat mir bei der Strukturierung und Durchführung meiner Arbeit sehr geholfen.

Bei Andrea Cordes und Nadine Heinrich bedanke ich mich ganz herzlich für die stetige Unterstützung in der Zellbiologie und die ermutigenden Worte. Ein großer Dank geht auch an Elke Völck-Badouin und Claudia Keppler für die kompetente Einweisung und Hilfe sowie die nützlichen Ratschläge zur Durchführung der biochemischen Experimente.

Ich möchte mich ganz herzlich bei allen Mitarbeitern der AG Kinscherf für das entspannte Arbeitsklima und die hilfreichen Antworten auf all meine Fragen bedanken.
Es war für mich eine schöne Erfahrung mit Euch zu arbeiten.

Meiner Familie, besonders meinen Eltern, danke ich für ihre dauerhafte Unterstützung und Geduld während meines gesamten Studiums und der Promotion.